Dissertation

submitted to the

Combined Faculties for the Natural Sciences and for Mathematics

of the Ruperto-Carola University of Heidelberg, Germany

for the degree of

Doctor of Natural Sciences

Put forward by

Maqsuda Afroz

Born in Dhaka, Bangladesh

Oral examination: 28.04.2010

Supernovae Observations and Dark Energy Models

Referees:

Prof. Dr. Christof Wetterich

Prof. Dr. Luca Amendola

Supernovae Observations and Dark Energy Models

In this thesis we review data sets available from various SNe groups like SNLS and HSST and utilize them to put constraints the cosmological parameters. We use the software CMBEASY to apply the MCMC method to models like ΛCDM, Constant Equation of State (EoS) w and Quintessence, with our emphasis being on the IPL and Corasaniti model. We do the analysis using the Riess Gold Set, the SNLS sample and the Union Data Set (with and without systematics). We have extended CMBEASY to include the Union Data Set and hence be up-to-date with latest observations. Our results show that Ω_m might be smaller than commonly assumed. Further, we find that irrespective of model or data set chosen we get approximately the same value for Ω_m, whereas this is not the case with w. The work in this thesis indicates that the emphasis in constructing new cosmological models should change from empirical to theoretical motivations.

Supernovae-Beobachtungen und Modelle der Dunklen Energie

In dieser Arbeit untersuchen wir mehrere Datensätze von Supernova-Gruppen wie dem HSST und der SNLS und nutzen diese, um die Werte der kosmologischen Parameter einzuschränken. Wir verwenden die Software CMBEASY, um Modelle wie das der konstanten Bewegunsgleichung w, der Quintessenz sowie das ΛCDM-Modell einer MCMC-Untersuchung zu unterziehen. Schwerpunkte legen wir dabei auf das IPL- und das Corasaniti-Modell. Unsere Analyse basiert auf dem Riess Gold Set, dem SNLS-Datensatz und dem Union Data Set (mit und ohne systematische Fehler). Wir haben CMBEASY um das Union Data Set erweitert und die Software damit auf den neusten Stand der Beobachtungen gebracht. Unsere Ergebnisse zeigen, dass Ω_m kleiner sein könnte als für gewöhnlich angenommen. Desweiteren stellen wir fest, dass wir unabhängig von Modell und Datensatz ungefähr den gleichen Wert für Ω_m erhalten, was für w nicht der Fall ist. Die vorliegende Arbeit legt die Empfehlung nahe, beim Errichten neuer kosmologischer Modelle das Augenmerk weg von emprischen hin zu theoretischen Motivationen zu richten.

Contents

I Basics of Cosmology 8

1 Concepts . . . 8
1.1 Cosmological Principle . . . 8
1.2 Comoving and Physical Coordinates . . . 8
1.3 Hubble's Law/Expansion of the Universe . . . 9
1.4 Dynamics of the Universe . . . 9
1.4.1 Friedmann Equation . . . 10
1.4.2 Fluid Equation . . . 10
1.4.3 Acceleration Equation . . . 10
1.4.4 Equation of State . . . 11
1.5 Density Parameter . . . 11
1.6 Concordance Model of the Universe . . . 11
1.6.1 Historical Development . . . 11
1.6.2 Current Development . . . 12
1.7 Anthropic Principle . . . 13
1.8 General Relativity . . . 14
1.9 Conclusion . . . 14
2 Observational Cosmology . . . 15
2.1 Introduction . . . 15
2.2 FRW Cosmological Models with $\Lambda \neq 0$ . . . 16
2.3 Observational Consequences of a Cosmological Term . . . 16
2.3.1 The Age Issue . . . 16
2.3.2 High Redshift SuperNovae and the Cosmic Microwave Background . . . 17
2.3.3 Structure Formation . . . 18
2.3.4 Baryon Excess in Clusters . . . 18
2.4 SNe Ia Observations . . . 18
2.4.1 Luminosity Distance . . . 18
2.4.2 The Magnitude-Redshift Relation . . . 20
2.5 The Angular Size - Redshift Relation . . . 20
2.6 Conclusion . . . 22

II Dark Energy 23

3 Introduction . . . 23

3.1 Dynamics of Dark Energy 24
3.1.1 The Acceleration Equation 24
3.1.2 Deceleration Parameter 25
3.2 Hubble's Parameter and z 25
4 Dark Energy Task Force Report 26
4.1 Goals and Methodology for Studying Dark Energy 26
4.2 Findings of the Dark Energy Task Force 27
4.3 Recommendations of the Dark Energy Task Force 28
4.4 Dark Energy Primer 29
4.5 Staging stage IV: Ground and Space Options 31
4.6 Technique Performance Projections 31
5 Candidates of Dark Energy 33
5.1 Cosmological Constant 33
5.2 Quiessence 34
5.3 Quintessence 34
6 Conclusion 38

III SuperNovae Observations 39
7 SNe Ia Projects 39
7.1 Reiss Gold Sample 39
7.2 Astier Sample or SNLS 40
7.3 SNAP 40
7.4 Union Data Set 42
8 Different Methods Used for Calculations using SN Ia 43
8.1 SALT 43
8.2 MLCS2k2 Multicolor Light Curve Shape 43
8.3 CMAGIC - Color-MAGnitude Intercept Calibration 44
8.4 Evolution of SNe 44
8.5 Systematics Involved in SNe 45

IV Methodology 46
9 Introduction 46
10 Parametrization 46
11 Numerical Tools and MCMC Calculation: 47
11.1 CMBEASY 47
11.2 MCMC Simulation 48

12 Observational Data 49
12.1 Error Estimations 53
13 Models Chosen 54
13.1 ΛCDM Model 54
13.2 Constant EoS$\neq 0$ 54
13.3 Inverse Power Law Model 55
13.4 Corasaniti Model 55

V Results and Discussion 57
14 Results 57
14.1 Reiss Gold Sample 58
14.1.1 Λ Model 59
14.1.2 Constant Equation of State 60
14.1.3 Inverse Power Law 61
14.1.4 Corasaniti Potential 63
14.2 SNLS/Astier Sample 64
14.2.1 ΛModel 65
14.2.2 Constant Equation of State 65
14.2.3 Inverse Power Law 67
14.2.4 Corasaniti Potential 68
14.3 Union Nosystematics 69
14.3.1 ΛModel 70
14.3.2 Constant Equation of State 71
14.3.3 Inverse Power Law 73
14.3.4 Corasaniti Potential 74
14.4 Union Systematics 75
14.4.1 Λ Model 76
14.4.2 Constant Equation of State 77
14.4.3 Inverse Power Law 78
14.4.4 Corasaniti Potential 79
15 Discussion 82

VI Conclusion 85

VII References 89

Introduction and Outline

Cosmology can probably be considered one of the oldest sciences existing. Even from the era of Hipparchus we have wondered about our universe and its fate. We have come a long way since those days. The advancements in our understanding and technology has allowed us to reach out to the frontiers of science and to challenge old beliefs and accept new ones about our universe. One of these new challenges is Dark Energy and its properties.

Dark Energy is that part of the energy density of the universe which has been introduced to describe the accelerated expansion of the universe. It has found its way into the Standard Model after various observations made us rethink the steady state and other static universe models. It has negative pressure and has been a requirement ever since the dimmer-than-expected observations of the light curves for the Supernovae Ia.

The basis of this thesis is to show how observations specially SNe relate to different theoretical models of our universe. The emphasis is put on trying to figure out what the Dark Enegy component of the universe might be. This thesis is divided into sections which one by one build up the whole case. In the first chapter we recall the basics of cosmology and how some of the important theoretical aspects are derived, which will be crucial in the later stages. In the following chapter we concentrate on trying to explain what is Dark Energy and figure out some of the important eras associated with it as well as the dynamics involved. Before we go into further details about that an overview about observational cosmology is given in the next chapter. In the fifth section we look into a few among the many different models of dark energy existing.

The following chapters are started with a brief summary of the DETF report [85] and then a closer look at the SNe Ia observations [15, 37, 32] and methods like SALT [95] used for calculations is taken. The next chapters deal with methods like MCMC [28] used for calculating the parameters and their constraints, models chosen and the justifcaiton for choosing those models, the results and their intepretation.

Part I. Basics of Cosmology

1 Concepts

Cosmology has come a long way since the early stages and now is a full-fledged science stream on its own. Below are given some of the major concepts of cosmology that are required to further proceed along the way of this thesis.

1.1 Cosmological Principle

The cosmological principle basically says that we are in no way special in the cosmos. This as we understand it, naively leads to isotropy and homogeneity. Let us now see what we mean by a homogeneity and isotropy. A homogeneous isotropic spacetime is one for which the geometry is spherically symmetrical about any one point (isotropy) and the same at any point in space other than that (homogeneity). Homogeneity and isotropy are symmetries of space and not spacetime. The simplest example of a homogeneous, isotropic cosmological geometry is described by the line element

$$ds^2 = dt^2 + a(t)(dx^2 + dy^2 + dz^2) \tag{1}$$

ds^2 is known as the Flat Robertson-Walker metric [115]. Models in which the scale factor a obeys Einstein's laws are known as Friedmann-Robertson-Walker models and the metric for such cases is called the FRW metric.

1.2 Comoving and Physical Coordinates

The distribution of galaxies and radiation in FRW models are smoothened out into a cosmic fluid. In such a case an individual galaxy is thought to be like a particle located by the three coordinates x^i at time t. Since our universe is isotropic, the velocity of each galaxy must vanish, else it would establish a preferred direction, i.e. $\frac{dx^i}{dt} = 0$. The coordinate is, therefore, said to be comoving. Comoving coordinates are carried along with the expansion. This means an individual galaxy has the same coordinate x^i at all times. Now if $a(t)$ increases with time and $(\Delta x + \Delta y + \Delta z)^{1/2}$ describes the coordinate distance between any two points then the actual physical distance is given by $d(t) = a(t)d_{coord}$. We see if the scale factor increases with time

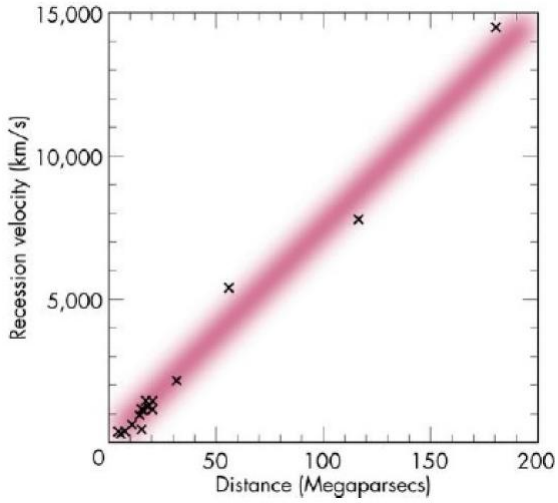

Fig. 1: Hubble's Law

so does the physical distance [116]. Hence, the scale factor describes an expanding universe.

1.3 Hubble's Law/Expansion of the Universe

The most dramatic piece of observational evidence in cosmology is that almost everything in the universe appears to be moving away from us, the further away it is, more rapid is its recession. The velocities of recession are measured using redshifts. Redshift is nothing but the Doppler effect applied to light waves and is given by $1 + z = \frac{\lambda_0}{\lambda_{em}} = \frac{a_0}{a(t)}$. The distance between any pair of galaxies separated by more than $100\,Mpc$ is proportional to a universal scale factor $a(t)$, the same for every pair. The Hubble parameter is then defined by $H = \frac{\dot{a}}{a}$, where dot denotes the time derivative. For an object receding at velocity v, the redshift is $z = v/c$. Hubble used this relation and expressed velocity and distance in a linear way now well known as Hubble's Law [78]. $\overrightarrow{v} = H_0 \overrightarrow{r}$, where H_0 is the present value of Hubble's parameter known as Hubble's Constant. We generally take the present value of $a_0 = 1$ and find that H_0 is at a value of approximately $70 \pm 4\ km/sec/Mpc$.

1.4 Dynamics of the Universe

We know that cosmology is about the structure and evolution of the universe on the largest scales of time and space. On these large scales it is gravity that dominates. So in order to understand the dynamics of the universe we must understand what effects gravity has on it. Gravity is nothing but an attractive force between any

two bodies. If gravity were negligible, $a(t)$ would increase linearly with time and $\dot{a}$ would be constant. In fact, gravity tends to slow down the expansion making $\dot{a}$ a decreasing function of time. But in reality, this is not the case. Below we discuss some important parameters used in the dynamics of the universe.

1.4.1 Friedmann Equation

The Friedmann equation describes the expansion of the universe and is, therefore, probably one of the most important equations in cosmology. To calculate the effect of gravity consider a test particle of unit mass, on the surface of a comoving sphere (one expanding with the universe). If ρ is the mass density of the universe and r is the radius of the sphere, the volume of the sphere is $\frac{4\pi}{3}r^3$ and the potential energy of the particle is $-\frac{GM}{r}$. The kinetic energy of the particle is $\frac{\dot{r}^2}{2}$ and therefore $E = \frac{\dot{r}^2}{2} - \frac{GM}{r}$, where E is the total energy of the particle. From this equation for total energy one can derive the Friedman Equation [43, 116].

$$H^2 \equiv (\frac{\dot{a}}{a})^2 = \frac{8\pi G}{3}\rho - \frac{kc^2}{a^2} \tag{2}$$

The term k is known as the curvature. It tells us about the geometry of the universe. $k = 0, \pm 1$ corresponds to a flat, open or closed universe respectively.

1.4.2 Fluid Equation

Along with the Friedmann equation, we now need some equations to tell us about the density ρ of material and its evolution with time in the universe. We get the fluid equation by using the 1st law of thermodynamics $dE + pdv = ds$ and $E = \frac{4\pi}{3}a^3\rho c^2$ to get

$$\dot{\rho} + 3\frac{\dot{a}}{a}(\rho + \frac{p}{c^2}) = 0 \tag{3}$$

1.4.3 Acceleration Equation

The Friedmann and Fluid equation can be used to derive a third equation, which describes the acceleration of the scale factor. We differentiate eq. (2) with respect to time and then substitute for $\dot{\rho}$ and cancel out the $2\frac{\dot{a}}{a}$ in each term to get

$$\frac{\ddot{a}}{a} = -\frac{4\pi G}{3}(\rho + 3\frac{p}{c^2}) \tag{4}$$

1.4.4 Equation of State

We see that by the use of the three basic equations derived above, we can start to understand the dynamics of the universe. But in order to know how the universe might evolve we need to specify a parameter which allows us to get specific relations. We do this by defining a relation known as Equation of State (EoS) which relates the pressure and the density by $w \equiv {}^{p}/_{\rho}$. Let us find out how density of different materials in the universe vary with a and hence time.

Dust/Matter: Dust exerts negligible pressure so we can take $p = 0$ as Equation of State. We then find, by solving the Fluid equation $\rho \propto 1/a^3$. We see that the density falls of proportional to the volume.

Radiation: Particles of radiation move with the speed of light. Their kinetic energy leads to a pressure force. The Equation of State for radiation is therefore given by $p = \frac{\rho c^2}{3}$. Using this and solving the Fluid equation we find $\rho \propto 1/a^4$.

1.5 Density Parameter

The density parameter gives the geometry of the universe. We have from eq. (2) if $k < 0$, i.e. $E > 0$ [116, 115], the expansion will continue indefinitely, whereas, if $k > 0$, it will eventually give way to contraction leading to a Big Crunch. The critical value separating these possibilities is $k = 0$, which leads to $H^2 = \frac{8\pi G}{3}\rho$. The corresponding mass density is called the critical density given by $\rho_c = 3H^2/8\pi G$. Its present value is $\rho_c(t_o) = 1.88h^2 \times 10^{-26} kg/m^3$. It is common practice to define the density parameter by [44, 45]

$$\Omega(t) \equiv {}^{\rho_i}/_{\rho_c} \tag{5}$$

The Friedmann Equation becomes

$$\Omega - 1 = \frac{k}{a^2 H^2} \tag{6}$$

1.6 Concordance Model of the Universe

1.6.1 Historical Development

Questions about the cosmos and our belonging and role in it can probably be considered one of the oldest scientific questions to have existed. As a first modern physical approach to questions of origin, evolution and fate of the Universe, one

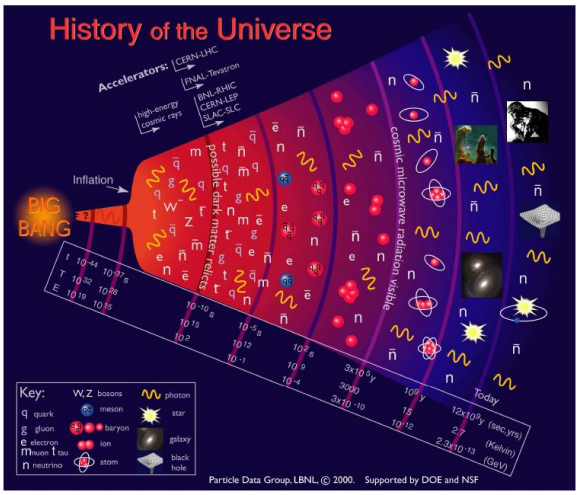

Fig. 2: History of our Universe from Particle Data Group 2000

usually considers Einstein's paper "Cosmological Considerations in the General Theory of Relativity" from 1917 [114]. One might say that high-precision observational cosmology started with the Hubble space mission in 1990. Ever since then the advancements in our understanding and technology have allowed us to reach out to the frontiers of science and to challenge old beliefs and accept new ones about our universe. Various observations have led to one coherent picture of our universe which we call the Concordance Model.

1.6.2 Current Development

The Concordance Model also often referred to as the ΛCDM model is based on six parameters: physical baryon density, physical dark matter density, dark energy density, scalar spectral index, curvature fluctuation amplitude and reionization optical depth. From these the other model values, including the Hubble constant and age of the universe, can be derived. The model assumes a hot big bang, an inflationary period and an accelerated expansion of the universe. It consists not only of baryons but also of an unknown Dark Matter component which has the property of non-relativistic, only gravitationally interacting heavy particles, and a Dark Energy component, in the simplest version described by a cosmological constant Λ.

Looking at figure (2) one can see how the history of the universe tracks. It can

be outlined in the following way from the very early stages to todays present time where t refers to the age of the universe and T to the temperature defined by the photon temperature. The universe history is given below in terms of t.

- *Planck epoch*: $t \approx 10^{-43}$ *seconds*, $T \approx 10^{19}$ GeV, this epoch is not fully understood and is described by quantum gravity.
- *Inflation [24, 72] and Baryogenesis:* $t \approx 10^{-35}$ *seconds*, $T \approx 10^{15}$ GeV, an era of rapid exponential expansion and production of matter antimatter symmetry.
- *Quark-hadron transition*: 10^{-6} *seconds* $\leq t \leq 10^{-2}$ *seconds*, $T \approx 0.1$ GeV, an era during which neutrons and protons were formed.
- *Nucleosynthesis*: 1 *second* $\leq t \leq 3$ *minutes*, $T \approx 1$ MeV, $z \approx 10^{10}$, during this time light elements like D, He, Li etc started to form.
- *Matter Domination*: $t \approx 70,000$ *years*, $T \approx 1$ eV, $z \approx 5000$, the matter dominated era began.
- *Recombination*: $t \approx 300,000$ *years*, $T \approx 0.25$ eV, $z \approx 1100$, recombination occured and Cosmic Microwave Background formed making the universe transparent.
- *Galaxy/star formation*: $z \geq 1100$, structures started to form and stars and early galaxies are seen.

1.7 Anthropic Principle

It is important to note that Dark Energy models with an unevolving equation of state need to have their initial conditions properly tuned in order to dominate the universe at precisely the present epoch. This problem, which is most acute for the cosmological constant, is known as the fine tuning problem. The fine tuning problem affects almost all models of Dark Energy. A combined analysis of CMB, galaxy clustering and supernovae data indicates that a constant equation of state for dark energy must satisfy $w < 0.82$ at the 95% confidence level [46, 47] and it is easy to show that for these models the fine tuning (and cosmic coincidence) problems are almost as acute as they are for the cosmological constant. Though there are models which assume the cosmological constant to be zero and avoid the fine tuning to a large extent it still runs into problems of trying to explain

why the cosmological constant should be zero. Hence we see that the nature of dark energy is very elusive to us yet observations suggest it has to be there. A large set of observational values of the fundamental constants of nature and the fine tunings involved that suggest exactly those values which support life on earth the way we know and hence allows life to emerge, has led some cosmologists to propose anthropic arguments for the existence of a small cosmological constant [52, 113]. The anthropic principle states that the universe which we observe has to be capable to develop intelligent life like us. Otherwise we would not be here and could not ask the question why the universe has exactly the laws of nature which it has.

1.8 General Relativity

No discussion on cosmology is complete without a few words on general relativity. General relativity is an extension of the theory of special relativity, which states that gravity is a purely geometric effect, generated by the curvature of spacetime. The relation between the curvature of space-time and the stress-energy tensor is given by the Einstein field equation

$$R_{\mu\nu} - \frac{1}{2}Rg_{\mu\nu} = \frac{8\pi G}{c^4}T_{\mu\nu} \tag{7}$$

where $R_{\mu\nu}$ is the Ricci tensor, R the Ricci scalar, $g_{\mu\nu}$ the metric tensor and $T_{\mu\nu}$ the stress-energy tensor. Equation (7) is a complicated differential equation which can in general only be solved if one makes simplifying assumptions and/or uses numeric techniques [48].

1.9 Conclusion

We have seen in brief what is the basic physics involved in cosmology. We have moved from the simple FRW metric and worked our way through to the Dark Matter and Dark Energy situation. Though observations do indeed suggest their presence, they are yet to shed light on their nature. In the case of Dark Energy, one of the most debatable issues is the form of this energy. Is a cosmological constant enough to explain all observations, i.e. is $w = -1$? If so, we are faced with the challenge of explaining the cosmological coincidence and why Λ has such a small value. On the other hand, if we neglect it then we must come up with an explanation in light of high energy physics or gravitational theory. Overall,

we see the key in determining the properties of Dark Energy and Dark Matter to great precision clearly lies with ongoing and future astrophysical experiments and observations.

2 Observational Cosmology

2.1 Introduction

Recent years have witnessed a great amount of interest in the possibility that a positive Λ-term (a cosmological constant) may dominate the total energy density in the universe. Interest in the cosmological constant stems from several observatonal directions:

- Observations of high redshift Type Ia supernovae appear to suggest that our universe may be accelerating [49] with a large fraction of the cosmological density in the form of a cosmological constant term.
- Most dynamical estimates of the amount of clustered matter yield a conservative upper limit $\Omega_m < 0.3$. In addition, theoretical modeling of structure formation based on the Cold Dark Matter model (CDM) with $\Omega_m = 1$ has failed to match observations at a quantitative level.

In contrast, a flat low density $CDM + \Lambda$ universe with $\Omega_m = 0.3$ and $\Omega_x = 0.7$ agrees remarkably well with a wide range of observational data ranging from large and intermediate angle CMB anisotropies to observations of galaxy clustering on large scales. Although none of the above arguments can be regarded as conclusive evidence for a cosmological constant on their own, the growing amount of work on the subject, combined with a possible relationship between a small cosmological constant today and a large cosmological term driving inflation at an early epoch, suggests that the case for Λ[1] should be taken seriously.

[1] From the physical point of view, Λ represents a new type of dark non-baryonic matter, completely unknown from laboratory experiments. Its difference from other type of dark non-baryonic matter observed by gravitational lensing is essentially that matter described by Λ is, (a) not gravitationally clustered at all scales where ae we see clustering of baryons and dustlike dark matter, and (b) has a strongly negative effective pressure. Thus, remarkably, by investigating the behavior of the present universe, we are studying novel fundamental physics [116].

2.2 FRW Cosmological Models with $\Lambda \neq 0$

A homogeneous and isotropic universe is characterized by the Friedmann-Robertson-Walker line element

$$ds^2 = c^2dt^2 - a^2t[\frac{dr^2}{1-kr^2} + r^2d\theta^2 + r^2sin^2\theta d\phi^2] \tag{8}$$

In this metric the Einstein equation with matter in the form of a perfect fluid acquires the following simple form

$$3H^2 = \frac{8\pi G}{3}\rho + \Lambda c^2 - \frac{kc^2}{a^2} \tag{9}$$

Eq (13) can be rewritten to look like the equation of motion of a point particle on the surface of a sphere of radius $R = a$ and mass M. Setting $c = 1$, we obtain $R^2 = -\frac{\ddot{G}M}{R^2} + \frac{\Lambda}{3}R$ and the total gravitating mass is $M = \frac{4\pi}{3}R^3(\rho+3p)$. This reflects that pressure carries weight in Einstein's Theory of Gravity. Hence we see that a particle on the sphere feels both attractive and repulsive forces. The force of repulsion $F_{rep} = \frac{\Lambda}{3}R$ is caused by the cosmological constant and increases with distance if $\Lambda > 0$.

2.3 Observational Consequences of a Cosmological Term

Arguments favoring $\Lambda > 0$ at the present epoch essentially arise from four sets of observations.

2.3.1 The Age Issue

A running debate over the previous decade or so has centered around whether or not the universe even has an age problem, i.e. on whether matter dominated cosmological models predict a substantially younger age for the universe than their oldest constituents [71] (which happen to be metal poor old globular cluster stars). A key role in this controversy is played by the Hubble parameter , whose present value though known is still debatable in many circles . Higher values of H_0 clearly give rise to a younger universe whereas lower values lead to an older one as age is related to the inverse of H_0. The age of the universe is given by

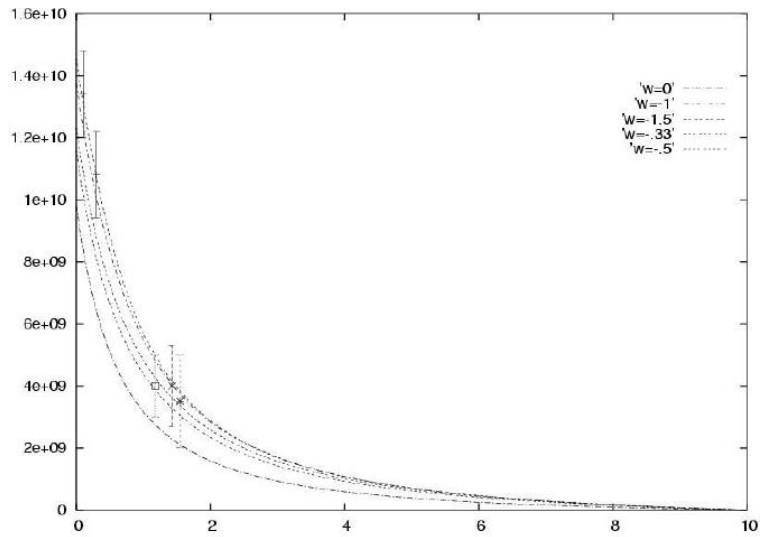

Fig. 3: Age of the Universe vs Equation of State w

$$t(z) = H_0^{-1} \int \frac{dz}{(1+z)h(z)} \tag{10}$$

A high value of the Hubble constant $H_0 > 80\,km/sec/Mpc$ predicts a short age of the universe which is incompatible with the ages of the oldest stars ($12-16\ Gyr$), unless the universe is open, where $\Omega_m < 0.1$. The appeal of this argument has somewhat decreased following recent Hipparcos parallax measurements indicating a lower value $H_0 = 67\,km/sec/Mpc$ and also a lower age for globular clusters at $11.5 \pm 1.5\ Gyr$. Still, recent observations of old galaxies at high redshifts are extremely difficult to accommodate within the framework of a matter-dominated universe. New estimates about the age of the universe has been predicted can be obtained by using the deceleration parameter [70].

2.3.2 High Redshift SuperNovae and the Cosmic Microwave Background

Preliminary results from this rapidly advancing field of cosmology suggest that the universe may be an accelerating universe with a dominant contribution to its energy density coming in the form of a cosmological constant. These results, when combined with CMB anisotropy observations on intermediate angular scales,

strongly support a flat universe $\Omega_x \simeq 0.7$.

2.3.3 Structure Formation

The standard COBE normalized Cold Dark Matter model of structure formation with $\Omega_m = 1$ appears to be in serious conflict with observations. The situation may be fixed if the universe is flat, with most of the matter being smoothly distributed in the form of a cosmological constant and only a small fraction $\Omega_m h \simeq 0.2$ in clustered matter. (Here h is the Hubble constant in units of $100\,km/s/Mpc$). Studies of the abundance and evolution of clusters of galaxies and of lensing by clusters also favor a low density universe. With today's observational precision in structure formation by studying large scale structures [79] we have a much better understanding of the cosmological paramters involved.

2.3.4 Baryon Excess in Clusters

In a spatially flat universe with $\Omega_m = 1$, the mass fraction in baryons, $\Omega_{baryons}$, in the Coma cluster is expected to greatly exceed nucleosynthesis bounds [81] leading to what has been called the baryon catastrophe. The mass fraction in baryons can be kept in agreement with nucleosynthesis constraints only if $\Omega_m h \simeq 0.16$ (Ω_m includes contribution from baryons and clustered dark matter). In agreement with the inflationary scenario which strongly favors a spatially flat universe this then suggests that the remaining mass might be in the form of Dark Energy.

2.4 SNe Ia Observations

In this section we will take a closer look at the SNe observations and their development in brief and later on it will be discussed in detail. The SNe observations and its future is the main object and topic of discussion for the thesis.

2.4.1 Luminosity Distance

Consider an object of absolute luminosity L, located at a coordinate distance r from an observer at $r = 0$. Light emitted by the object at a time t is received by the observer at $t = t_0$, t and t_0 being related by the cosmological redshift $(1 + z) = {}^{a_0}/_{a(t)}$. The luminosity flux reaching the observer is $F = L(4\pi d_L^2)^{-1}$, where d_L is the luminosity distance [82, 89] given by $dL = a(t_0)r(1 + z)$.

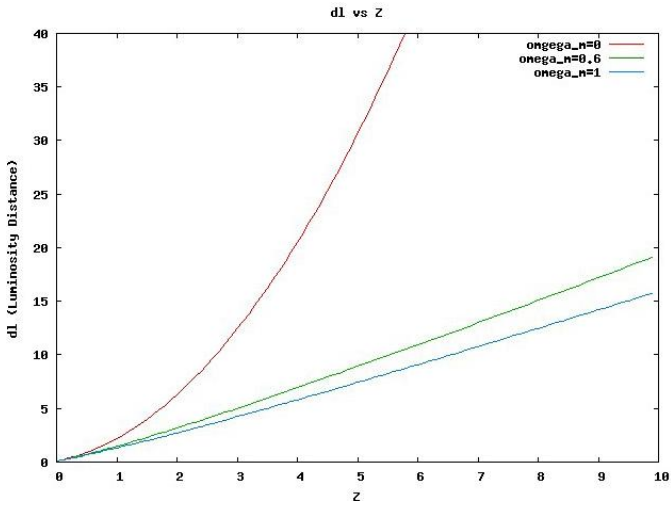

Fig. 4: Luminosity Distance vs Redshift. The luminosity distance d_L (in units of $1/H_0$) is shown as a function of cosmological redshift z for flat cosmological models with a cosmological constant.

The luminosity distance d_L depends sensitively upon both the spatial curvature and the expansion dynamics of the universe. Furthermore, since $dz/dt = (1+z)H(z)$, we get

$$d_L = (1+z)\int \frac{dz}{H(z)} \tag{11}$$

Now that we have a relation between the luminosity distance and redshift let us find out why and how it is useful to us and what role it plays in cosmology. Since recent observations allow us to take a spatially flat universe we see that the situation becomes simpler. Let us consider the two extreme cases : A matter dominated universe, i.e. $\Omega_m = 1$ and a deSitter universe, i.e. $\Omega_x = 1$ we respectively get the luminosity distances as

$$d_L^{MD} = \frac{[2(1+z) - (1+z)^{1/2}]}{H_0}\ ; \quad d_L^{dS} = \frac{z(1+z)}{H_0}$$

We can appreciate that the supernoave will appear brighter in an Einstein-deSitter universe than it will in a deSitter universe. This is also true for a two component universe consisting of matter and a cosmological constant as demonstrated in fig (4). We can see by a simple example that if an object has a redshift of say $z = 3$, then it will appear 9 times fainter in a deSitter universe than in a Einstein-deSitter or matter dominated universe.

2.4.2 The Magnitude-Redshift Relation

The relation which relates the apparent magnitude m of an object to its absolute magnitude M is given by

$$\mu \equiv m - M = 5log\frac{d_L}{Mpc} + 25 \tag{12}$$

where μ is known as the distance modulus. Since d_L depends upon the geometry of space and its material content, the magnitude-redshift relation can in principle be used to determine Ω_{tot} and Ω_m if both m and M are known within reasonable limits. The results obtained by both the Supernova Cosmology Project [37] and the High-Z Supernova Search Team present the strongest direct evidence for a non-zero cosmological constant. Though one major concern in using this is the fact that we have assumed the faintness in the observation to be due to the presence of Λ. If there are evolutionary and extinction processes that go on before the light from the SNe reaches us, then all models based on this assumption are in serious trouble. But by using the CMB observations, we also put tight constraints on the cosmological parameters which do agree with those obtained from SNe observations.

2.5 The Angular Size - Redshift Relation

The suggestion that angular sizes of galaxies could be used to discriminate between cosmological models was made some time back [43]. Hence it is yet another potentially sensitive probe for dark energy. It helps test different models due to the fact that the angular size of an extended object D located at a redshift z depends rather sensitively on the properties of the cosmological model in which it is being measured. Knowing the absolute size of an object (e.g. galaxy or radio source) and the angle subtended by a distribution of such objects in the universe, it may be possible (after correcting for projection and evolution effects) to say something about the geometry of space and the matter content of the universe. Let us now derive a relation between $\Delta\theta$ and D [82]. Consider an object of proper length D at a coordinate distance r, and assume for simplicity that the object is aligned along the axis. The proper length of the object can be obtained by setting $t = constant$ in the FRW line element eq. (1) as follows $ds^2 = -D^2 = -a^2(t)r^2\Delta\theta^2$. The angle

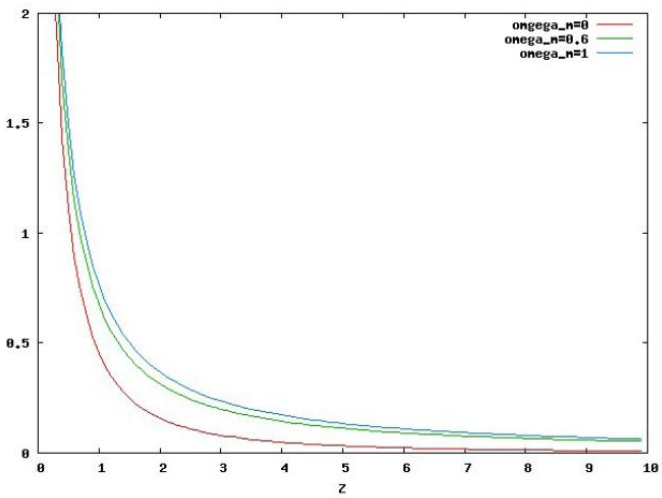

Fig. 5: $\Delta\theta$ vs z for different values of Ω_m

subtended by the object then becomes $\Delta\theta = {}^{D}/_{d_A}$, where d_A is given by

$$d_{A=}a(t)r = d_L(1+z)^{-2}$$

Hence we see there is a straight forward relation between the observable d_L and $\Delta\theta$.

The appearance of a minimum angular size at a given redshift z_{min} is a generic feature of cosmological models with $\Omega_{m>0}$. We see that for a matter dominated universe z_{min} is at 1.25 and it moves to higher values as the cosmological constant term becomes larger. For the extreme case of a deSitter universe there is no minimum point.

Curiously, the angular size of a typical galaxy at a redshift $z < 1$ is roughly 1" which is close to the limiting value of the angular resolution (seeing) allowed by the Earth's atmosphere [104]. Beyond $z > 1$ the angular size of an object increases, and if one is confident that galaxies of a given class at higher redshifts are similar in form to their lower redshift counterparts, then this test can in principle provide a powerful means of discriminating between world models especially with the use of satellite data which can get around the seeing limit. Other objects which can be used to probe the angular- size-redshift relation include clusters of galaxies and both extended and compact radio galaxies [87, 52]. However in order to use this method of testing cosmological models we must first have comprehensive knowledge about the evolutionary processes that the radio galaxies go through.

2.6 Conclusion

Since the original discovery of an accelerating universe [17, 21, 55] the SNe data base has grown considerably and are available in the literature [41, 15, 42]. Although affects due to gravitational lensing, evolution etc. might be able to nullify Dark Energy hypothesis it is reassuring that recent observations of CMB anisotropies and estimates of galaxy clustering in the 2dF [83] and SDSS [84] surveys make a strong and independent case for dark energy. Therefore, in order to prove the existence and nature of dark energy on a stronger footing we need observations from all sectors to come up along with SNe data.

Part II. Dark Energy

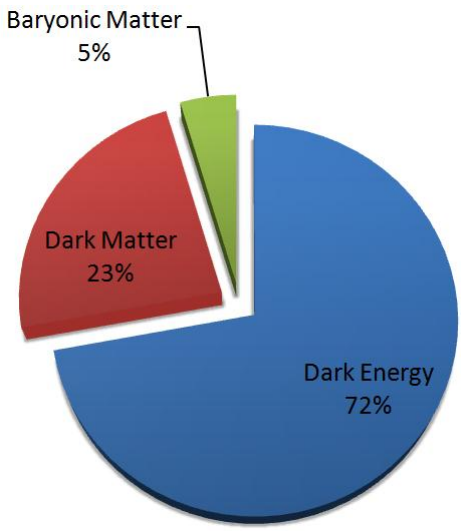

Fig. 6: Pie Chart of the Universe Constituents

3 Introduction

Now that we have discussed some of the basics of cosmology let us discuss in a little more detail about its constituents. Observational evidence suggests that the universe is made up of more than just the luminous matter that we see. We find that the total energy density of the universe is estimated at about $\Omega_{tot} \equiv \frac{8\pi G}{H^2}\rho_{tot} \simeq 1.02 \pm 0.02$. This value is much larger than the value we know for luminous matter or even baryons, which is only approximately 0.04. The remaining is unknown. Both Dark Matter and Dark Energy [80, 22] are considered essential missing pieces in the cosmic jigsaw puzzle.

$$\Omega_{tot} - \Omega_{baryons} = ?$$

While there are now multiple lines of evidence indicating that 70% of the critical density of the universe is in the form of a negative-pressure component termed Dark Energy we have no real clues about its origin and nature. Theoretical studies operate in the shadow of the cosmological constant problem [56], considered one of the most embarrassing hierarchy problems in particle physics. Experiments to be carried out over the next decade should shed considerable light on the matter by constraining the Dark Energy Equation of State and determining whether it

is consistent with vacuum energy or something else. Recent observations of type Ia supernovae (SNe Ia) at high redshift indicate that the expansion of the universe is accelerating [63, 64]. Though concerns about systematic errors remain, these calibrated standard candles seem to appear fainter than would be expected if the expansion were slowing down due to gravity. According to general relativity, accelerated expansion requires a dominant component with effective negative pressure. Such a negative-pressure component with $w = {}^{p}/_{\rho} < 0$ is now generically termed Dark Energy; a cosmological constant with $p = -\rho$, is the simplest but not the only possibility. Recent results for the CMB anisotropy, favoring a nearly flat universe, $\Omega_{tot} = 1$, coupled with a variety of observations pointing unambiguously to low values for the matter density parameter, $\Omega_m = 0.3$, provide independent evidence for a dark energy component with $\Omega_{DE} = 0.7$.

3.1 Dynamics of Dark Energy

In a homogeneous and isotropic Friedmann-Robertson-Walker (FRW) universe consisting of pressureless dust (Dark Matter) and Λ, the Raychaudhury equation takes the form $\frac{\ddot{a}}{a} = -\frac{4\pi G}{3}(\rho_m + \frac{\Lambda}{3})$. This can be rewritten in the form of a force law $F = -{}^{GM}/_{R^2} + \frac{\Lambda}{3}$, which demonstrates that the cosmological constant gives rise to a repulsive force whose value increases with distance. The repulsive nature of Λ could be responsible for the acceleration of the universe. Let us now look at the the dynamics of dark energy.

3.1.1 The Acceleration Equation

The acceleration equation is easily generalized to

$$\frac{\ddot{a}}{a} = -\frac{4\pi G}{3}\sum_i \rho_i(1 + 3w_i) \tag{13}$$

where $w_i = {}^{p_i}/_{\rho_i}$ gives the Equation of State and the summation is over all forms of matter present in the universe. Eq. (13) along with the eq. (2) can completely describe the dynamics of the FRW universe. For conveniences sake let us write the Hubble's equation here once more assuming a flat universe

$$H^2 \equiv (\frac{\dot{a}}{a})^2 = \sum_i \frac{8\pi G}{3}\rho_i \tag{14}$$

We see from eq. (13) and eq. (14) that if the universe has only one component, it will accelerate if $w < -1/3$. At $w = -1/3$ the universe will be in a perfect balance of neither acceleration nor deceleration. In both the cases above the strong energy condition which states that $w \geq 0$ is violated. We can have a case where the weak energy condition $w = -1$ [105, 87, 102, 106] can also be violated but it leads to exotic situations which I will not touch upon here. Now let us find out some conditions and constraints using eq. (13) and eq. (14).

3.1.2 Deceleration Parameter

It is convenient to express accelaration in terms of the so-called deceleration parameter [117]. It is given by

$$q \equiv \frac{\ddot{a}}{aH^2} = -\frac{4\pi G}{3H^2}\sum_i \rho_i(1+3w_i) = 1 + 3\Omega_x w_x \tag{15}$$

where

$$\Omega_x = -\frac{8\pi G}{3H^2}\sum_i \rho_i \tag{16}$$

and $\Omega_m + \Omega_x = 1$. For acceleration we need $q < 0$. Applying this to eq. (15) we can easily see that $w_x \leq \frac{1}{3}(1-\Omega_m)^{-1}$. It is clearly dependent on Ω_m.

3.2 Hubble's Parameter and z

Let us try and get a relation between Hubble's parameter and the cosmological redshift in order to have a formula based on a quantity that we can observe using $(1+z) = {}^{a_0}/_{a(t)}$ and eq. (16) we get

$$H(z) = H_0[\Omega_m(1+z)^3 + \Omega_x(1+z)^{3(1+w)}]^{1/2} \tag{17}$$

whereas, in a ΛCDM model with $w = -1$, we get

$$H(z) = H_0[\Omega_m(1+z)^3 + \Omega_x]^{1/2} \tag{18}$$

Now that we have certain tools in hand to work with, let us look at a few important epochs in the history of the universe. If Dark Energy is described by an unevolving equation of state $w = {}^{p_x}/_{w_x}$, then the transition between deceleration and acceleration $\ddot{a} = 0$ occurs at redshift $(1+z_{trans})^{-3w} = (1+3w)\frac{\Omega_m}{\Omega_x}$.

Another epoch of importance is when the densities of the Dark Matter and Dark Energy become equal. This happens at redshift $(1+z_{eq}) = \frac{\Omega_m}{\Omega_x}$.

Solving these for $w = -1$, and $\Omega_m = 0.3$ and $\Omega_x = 0.7$ we get $z_{trans} \simeq 0.67$ and $z_{eq} \simeq 0.32$ which we see are fairly recent eras. The fact that the acceleration of the universe is a relatively recent phenomenon illustrates the cosmic coincidence puzzle according to which we appear to live during a special epoch when the densities inDark Energy and Dark Matter are almost equal. A recent origin for the acceleration epoch is supported by supernova observations which suggest a decelerating universe at $z > 0.5$ [107].

4 Dark Energy Task Force Report

Conclusive evidence from SNe as well as other independent observational evidences show that the universe is expanding at a much faster rate than expected for only a matter dominated universe, leading to the beginning of a new world of cosmological theories and predictions. Within the cosmological framework this expansion is thought to arise from a substance which has negative pressure. This substance has been coined the term Dark Energy. It makes up almost two-thirds of our universe yet almost nothing is known about it. Hence Dark Energy became a pressing concern and interest in the scientific community to get a better understanding of how things work in the universe. Dark Energy Task Force (DETF) [85] was formed to help in this endeavor. Below we briefly review the main points of DETF primarily focusing on SNe.

4.1 Goals and Methodology for Studying Dark Energy

- The goal is to determine the fundamental nature of dark energy, the laws that govern it etc. In the process the EoS and Ω_ϕ will play a vital role. So methods to observe these with as much precision as possible is needed. Parametrization of $w(a)$ [102] will serve as a robust, quantitative guide to distinguish between the different models.

- A DETF figure of merit is used to quantify the precision and progress that will be reached by future projects[2].

- Development is broken down into four stages. Stage I represents knowledge that is already known , Stage II represents the knowledge that will come upon completion of the ongoing experiments and observations, Stage III represents

[2] The DETF figure of merit is the reciprocal of the area of the error ellipse enclosing the 95% confidence limit in the $\omega_0 - \omega_a$ plane. Larger figure of merit indicates greater accuracy.

near-term medium-cost currently proposed projects and Stage IV represents large ambitious projects for the future like SKA (Square Kilometer Array), JDEM (Joint Dark Energy Mission) etc.

4.2 Findings of the Dark Energy Task Force

- Four experimental techniques are in primary focus so far. They are BAO, Galaxy Cluster, Supernovae, and Weak Lensing. Among them SN will be discussed in greater detail as it is by far the most robust of all methods so far. Maybe with further work and investigation other methods may provide better and more precise measurements for explaining and detecting Dark Energy and also be able to explain its properties. BAO is less affected by astrophysical uncertainties but is in its infancy, GL has statistical potential to exceed SN and BAO but is plagued by very large systematics, WL is also just an emerging technique and will be limited by systematics that are difficult to predict at this stage.

- SN as mentioned above is by far the most tested method so far. But this method too has its problems. If redshifts are determined using multiband photometry than the accuracy achieved for photo-z's is of importance.[3] On the other hand if spectroscopically measured redshifts are used the power of the experiments is much better but depends on the uncertainties in the evolution of the SNe and also on the flux calibration.

- Though increased precision in a particular cosmological parameter might improve Dark Energy constraints from a single technique, it does not affect the overall DETF figure of merit obtained from a multiple technique. However using a multiple technique may provide new constraints on the cosmological parameters themselves. A good example of this is the spatial curvature of the universe. When set to zero, it largely affects the constraints obtained on dark energy from SNe but has little impact on other techniques. Hence when combined setting the spatial curvature to zero has very little impact on the over all result.

- Understanding systematic errors is the biggest step in making future projects a success. A way in which this can be achieved or better assessed for SNe would be to study at least 500 nearby ones both spectroscopically as well as

[3] Multiband photometry measures the intensity of the object in several colors. A redshift determined by multiband photometry is called photometric redshift or photo-z.

photometrically resulting in being able to look for evolutionary tendencies, metalliicity, reddening etc. and improvements in the system of photometric calibration.

- For stage III projects it is assumed that a modest increase in Dark Energy parameters is likely to result from the SN technique using photo-z's. This would be of immense value if it could give an idea about the success and capability of photometric determination of supernova redshifts, types and evolutionary effects.

- For stage IV projects JDEM and LST might be of equal risk though the JDEM would incur more costs and due to it being space based whilst the success of the LST would largely depend on how well the photo-z uncertainties are mitigated and made small on very large samples of galaxies. As it will only be effective if the systematics are made far smaller than what they are to date.

4.3 Recommendations of the Dark Energy Task Force

- High priority should be given to projects that improve our understanding of the dominant systematic effects in dark energy measurements and whenever possible reduce them even if this does not increase the overall DETF figure of merit for the time being. Understanding the systematic errors will be the key to better and more precise results in the future allowing more detailed study and understanding of the very nature of Dark Energy.

- Priority should be given to establishing a high precision photometric and spectroscopic calibration in as many wavelengths as possible. Precise photo-z's, K-correction, luminosity distances etc cannot be obtained without a fundamentally improved calibration system which is as error free as possible.

- Once a proper system for calibration is obtained, a large ensemble of high precision spectra and light curves for SNe Ia in different light bands to be able to better constrain systematic effects due to reddening, metallicity, evolution etc. should be obtained.

- For stage III and IV projects, the systematic uncertainties will ultimately determine the accuracy of our knowledge. So critical assessment of the potential systematics is very crucial.

- There should be a method devised such as to be able to quantify and monitor our progress of the understanding of Dark Energy.
- Further theory work on deviations from our common understanding using general relativity as a reference point should be encouraged and kept in mind when developing projects to test and try to crack down on our understanding of Dark Energy.

4.4 Dark Energy Primer

- In general relativity, the growth of the universe is described by a scale factor $a(t)$, and the time evolution of the expansion obeys

$$\frac{\ddot{a}}{a} = -\frac{4\pi G}{3}(\rho + 3P) + \frac{\Lambda}{3}$$

  where P is the pressure and ρ is the density of the contents of the universe and Λ is the cosmological constant. Present day experiments have all pointed to $\ddot{a} > 0$ signifying an accelerated expansion and hence implying the universe has more to it than just ordinary matter or that GR stands incorrect.

- Observational consequences of Dark Energy can be realized using the following equations and arguments. If general relativity is assumed to hold then one can write from the expansion history and other factors

$$\dot{\rho} = -3H(\rho + P)$$

  which now holds separately for each density contributor. Using this and introducing Ω as a density parameter one can now write the following

$$H^2(a) \equiv (\frac{\dot{a}}{a})^2 = H_0^2[\Omega_R a^{-4} + \Omega_M a^{-3} + \Omega_k a^{-2} + \Omega_x a^{-3(1+w)}] \qquad (19)$$

  Here the term Ω_x represents the cosmological constant if $w = -1$ else it represents Dark Energy with a constant w and can easily be generalized for a non-constant w. The Cosmic Microwave Background can give very good constraints on $H_0^2\Omega_m$ and $H_0^2\Omega_r$, so it would seem like one can determine the time history of the Dark Energy density if one could determine $H(a)$.

- It is straightforward to determine the scale factor a at the time of emission of light as all photons stretch during the expansion and this is quantified

in the redshift z. But one also needs the derivative of a to determine $H(a)$ which is more difficult as time is not measured directly. In order to avoid this problem most cosmological observations involve measuring the distance to a given source of a known redshift z which is closely related to the expansion history.

- All photons on the radial path must satisfy the following

$$ds^2 = -dt^2 + a^2(t)(\frac{dr^2}{1-kr^2}) = 0$$

This allows us to define $D(z)$, a distance to a redshift of z as the following

$$D(z) = \int_0^r \frac{dr'}{1-kr'^2} = \int_t^{t_0} \frac{dt'}{a(t')} = \int_0^z \frac{dz'}{H(z')} \tag{20}$$

This allows one to now express the coordinate r in terms of the redshift z. $r(z)$ has many measurable consequences through itself or closely related functions. The one of interest here is the luminosity distance which is given by

$$d_L(z) = r(z)(1+z)$$

Other than this it also has close relations with proper distance, angular diameter distance, volume element etc.

- One of the major astronomical approaches to measure dark energy is SNe Ia. They are thought to be the explosions caused by disintegration of white dwarf stars that accreted material from its binary partner to exceed the limit of $1.4_\odot$ known as the Chandrasekhar limit. They are considered as standard candles whose luminosity is well established and known. Hence the relation

$$f = L/4\pi d_L^2$$

can be used to find the luminosity distance. Spectral lines in the SNe and also of the host galaxy can be used to determine redshift.

- Theoretical modeling of SNe explosions are extremely difficult and it is not expected that this theory will ever deduce the absolute magnitude nor the standardization that is required for precise Dark Energy studies. Hence the standardization must be empirical and its ultimate accuracy or cosmic

evolution with time is very difficult to predict. Knowing this fact one should look at alternate methods in which the modeling of the physics behind the event is more likely to be fundamental than empirical.

4.5 Staging stage IV: Ground and Space Options

- *Strength and weakness*: It is by far the most established method of observation and contributes most to the present day constraints. But the fact that the physics of there nature is not well understood leaves us plagued with not being able to understand the systematics to the fullest.

- *Advantages for LST*: A very large number of SNe can be detected in a short span of time increasing the statistical precision. Also a large number of high signal-to-noise ratio events will allow search for more parameters and help in maybe understanding the evolutionary effects caused by them.

- *Advantages of Space Mission*: NIR coverage offers light curves less affected by extinction. Being carried out in space, these missions allow for a larger wavelength band to be studied for low and high redshifts. In the long run it will help contain extinction and understand evolution better.

- *Steps to sharpen Forecast*: A large low-z SNe Ia survey is needed for the primary calibration and understanding of the variety of spectra probed in the rest frame before moving to high-z surveys.

- *Advantages of Ground Based Dark Energy Experiments*: The huge number of SNe Ia that will be detected, hopefully tens of thousands per year will allow us to get a better demography of the SNe in a way that are complimentary to a JDEM SNe survey.

- The primary advantage of space based observations is the drastically reduced systematics. Hence a less down-side risk in a space based mission as compared to a ground based one. So JDEM might be a lower risk stage IV experiment as it will provide richer data with less systematics which will be the key to better understanding.

4.6 Technique Performance Projections

- The DETF has modeled Dark Energy constraints that will be useful in the future to determine which experiments will benefit from it the most. They

have based the modeling on the four most known and established techniques so far. Below is a discussion of the SNe model with the basic points.

- Since to first approximation all SNe Ia have the same intrinsic luminosity, by measuring their redshift and apparent peak flux one gets a direct measurement of their luminosity distance.

- In practice though the peak luminosities are not all identical it is possible to find a strong correlation between peak luminosities and the rate at which the SNe decline in brightness. This correlation can be used to make corrective measures before using the SNe Ia as standard candles.

- When spectroscopic followup will be used in the SNe technique the statistical uncertainties in $D(z)$ and hence dark energy will be determined by the number of observed SN Ia, their redshift distribution and the standard deviation σ_D in the absolute magnitude after all required corrections are made.

- One needs to be able to put lower end constraints on the Hubble diagram for low redshift z's as they will be the primary basis for a good and fundamental calibration for future high-z SNe's. So a sample of 500 low-z's should be observed and studied.

- An alternative to spectroscopic observations is to rely upon photometry. Though the statistical sample would be much larger, the price to pay would be loss of resolution and hence important information is lost which might have allowed us a better understanding of dispersion, contamination etc. This would result in systematics creeping in. Once the statistical error bars reach those of systematics, one will have to rely on full spectroscopic analysis for each SNe, though this might prove difficult as the number of SNe steadily rises.

- Systematic errors in $D(z)$ arise predominantly from two sources. The wavelength dependent errors in the astronomical flux propagate into the luminosity distance as observed wavelength of the SNe redshifts through the visible and NIR spectrum. Any shift with redshift in the properties of the supernovae or its host galaxy propagates into $D(z)$ without being detected. This can lead to a biased interpretation of the observational data received or studied unless and until this shift can be attributed to its real physical reasons.

Dark Energy Model	State Parameter	Energy Density
Cosmological Constant	$w = -1$	$\Lambda/8\pi G$
Constant EoS	$w \neq -1$ but $w = constant$	$\rho_0(1+z)^{3(1+w)}$
Kinessence	$w \neq constant$	$\rho_0 exp[\int_0^z dz \frac{1+w(z)}{1+z}]$

Tab. 1: Candidates for Dark Energy

5 Candidates of Dark Energy

Supernovae observations when combined with those of the cosmic microwave background, gravitational clustering and LSS suggest that our universe is (approximately) spatially flat and that an exotic form of negative-pressure matter called Dark Energy (DE) causes it to accelerate by contributing as much as three-quarters to the closure density of the universe. The remaining quarter consists of non-relativistic Dark Matter and baryons. The simplest example of dark energy is the cosmological constant Λ. Though the concordance model ΛCDM provides an excellent explanation for the acceleration phenomenon and other existing observational data, it remains entirely plausible that the dark energy density is weakly time dependent [18, 19, 58] and maybe even coupled [59, 60]. Moreover, it is natural to suggest that the dark energy which we observe today might really be dynamical in nature and origin. This means that a completely new form of matter might be responsible. Table 1 gives a broad catagory of candidates plausible as a Dark Energy Model. The list is by no means complete and many models, even yours, may be missing.

5.1 Cosmological Constant

A physical basis for the cosmological constant had to wait until 1968, when Y. B. Zel'dovich puzzling over cosmological observations which appeared to require Λ (the quasar excess at $z \sim 2$ alluded to earlier) realized that one loop quantum vacuum fluctuations gave rise to an energy momentum tensor which, after being suitably regularized for infinities, had exactly the same form as a cosmological constant $\langle T_{ik} \rangle_{vac} = \Lambda_{gik}/8\pi G$. Theoretical interest in Λ remained on the increase during the 1970's and early 1980's with the construction of inflationary models, in which matter[4] behaved precisely like a weakly time-dependent Λ-term. The current interest in Λ stems mainly from observations of Type Ia high redshift

[4] Matter was in the form of a false vacuum, as vacuum polarization or as a minimally coupled scalar-field

supernovae which indicate that the universe is accelerating fueled perhaps by a small cosmological Λ-term [86, 43, 45].

In spite of the theoretical glitches perhaps the simplest model for Dark Energy is the cosmological constant, whose energy density remains constant with time and is defined as $\rho_\Lambda \equiv {}^{\Lambda}/_{8\pi G} = 6.44 \times 10^{-30}({}^{\Omega_\Lambda}/_{0.7})({}^{h}/_{0.7})^2\, gcm^{-3}$ where h is the Hubble constant H_0 in in terms of $100\, kms^{-1}Mpc^{-1}$. Its equation of state is $w = -1$ and has the following form for the value of H from eq. (18) for a flat two component universe.

$$H(z) = H_0[\Omega_m(1+z)^3 + \Omega_m - 1]^{1/2}$$

5.2 Quiessence

The next simplest form of dark energy after the cosmological constant is provided by models for which the equation of state is given by $w = constant \neq -1$. For this form of dark energy, which we call quiessence [22]

$$H(z) = H_0[\Omega_m(1+z)^3 + \Omega_x(1+z)^{3(1+w)}]^{1/2}$$

The cosmological constant then becomes a limiting case of quiessence. Important examples of quiessence include a network of non-interacting cosmic strings with $w = -{}^1/_3$ or domain walls with $w = -{}^2/_3$. Quiessence in a FRW universe can also be produced by a scalar field which has the potential

$$V(\phi) \propto sinh({}^{-2(1+w)}/_{w})(C\phi + D) \tag{21}$$

with appropriately chosen values of C and D.

5.3 Quintessence

The simplest example of kinessence is provided by quintessence [19, 23, 18], a self-interacting scalar field which couples minimally to gravity. Its density, pressure and Equation of State are given by

$$\rho_\phi = \dot{\phi}^2 + V(\phi) \quad , \quad p_\phi = \dot{\phi}^2 - V(\phi)$$

$$w_\phi \equiv \frac{p_\phi}{\rho_\phi} = \frac{\dot{\phi}^2 - V(\phi)}{\dot{\phi}^2 + V(\phi)} \tag{22}$$

The action for the quintessence is given by:

$$S = \int d^4x\sqrt{-g}(-\frac{1}{2}(\nabla\phi)^2 - V(\phi)) \tag{23}$$

with $(\nabla\phi)^2 = g^{\mu\nu}\partial_\mu\phi\partial_\nu\phi$ and $V(\phi)$ being the potential of the field, depending on the particular choice of the model. The variation with respect to the metric tensor $g_{\mu\nu}$ gives us the energy-momentum tensor

$$T_{\mu\nu} = \partial_\mu\phi\partial_\nu\phi - g_{\mu\nu}(\frac{1}{2}g^{\alpha\beta}\partial_\alpha\phi\partial_\beta\phi + V(\phi)) \tag{24}$$

Scalar field evolution is governed by the equation of motion given by the modified Klein-Gordon equation which is obtained by the variation of eq. (23)

$$\ddot{\phi} + 3H\dot{\phi} + \frac{dv}{d\phi} = 0 \tag{25}$$

where H becomes the following

$$H(z) = \frac{8\pi G}{3}[\rho_{0m}(1+z)^{3+}\dot{\phi}^2 + V(\phi)] \tag{26}$$

Models with this property can lead to an accelerating universe at late times. DETF has carried out an extensive approach to see how certain quintessence models will behave to future generation of experiments [111].

Trackers

An important subclass of quintessence models displays the so-called tracker behavior during which the ratio of the scalar field energy density to that of the matter/radiation background changes very slowly over a substantial period of time. Models belonging to this class satisfy $V^{"}V/(V')^2 \geq 1$ [36] and approach a common evolutionary tracker path from a wide range of initial conditions. The tracker solution is an attractor in the sense that a very wide range of initial conditions for ϕ and $\dot{\phi}$ rapidly approaches a common evolutionary track, so that the cosmology is insensitive to the initial conditions. Tracking has an advantage similar to inflation insofar a wide range of initial conditions is funneled into the same final condition [50]. As a result, the present value of dark energy in tracker models is to a large extent, though not entirely, independent of initial conditions and is determined by parameters residing only in its potential [80].

For all quintessence models, $w \geq -1$ and the inequality is saturated only if $\dot{\phi} = {}^{dV}/_{d\phi}$.

Quintessence Potentials

The literature describing phenomenological forms of matter violating the SEC is vast. Nevertheless two kinds of matter have been singled out in recent times as being of special interest:

- Cosmological constant $P_X = \rho_X \Rightarrow (w_X = 1), \Lambda \equiv {}^{\rho_X}/_{8\pi G}$
- A scalar field rolling down a potential $V(\phi)$

Though both of the above seem appealing they both run into some problems. If one assumes a very simplistic potential like $V \propto m^2\phi^2$ [80], we see that the over-damping of the potential requires a very precise level of accuracy of the two density ratios, in order for it to be just about one at the present epoch. This is the classic fine tuning problem that plagues almost all models of Dark Energy. On the other hand, if we assume that the energy density in the field were comparable to that of radiation at very early times, it cannot arise from a polynomial potential $V \propto \phi^m$ as ϕ will not remain sub-dominate long enough to get a epoch of matter dominance. It will rapidly dominate the density of the universe resulting in a very large Λ for the present. Hence for the ϕ-field energy density to dominate only at recent times it must have fallen of rapidly earlier. But its fall must ultimately be less then that of matter or radiation for it to be seen in the present epoch. Fortunately, there do exist families of potentials for which the behavior of ϕ is as desired. This family is termed Quintessence. By Quintessence [87, 88, 117] we mean a slow rolling scalar field which, for a large values of initial conditions, converges towards a tracker field obeying an effective equation of state $w_\phi = {}^{P}/_{\rho_\phi}$, where $P \equiv p_\phi(\rho_\phi, a)$ which tracks the background field equation of state given by

$$w_B(a) = P_{rad}/(\rho_{rad} + \rho_{mat}) = {}^{1}/_{3} \tag{27}$$

The condition for a tracker solution to exist is that ${}^{V'}/_{V}$ be a slowly decreasing function of ϕ, where $V' \equiv {}^{dV}/_{d\phi}$ [112].

Inverse Power Law

The famous pioneering work of Ratra and Peebles [18] has been taken into consideration for this section. We have considered an inverse potential of the form $V = V_o/\phi^\alpha$. We see a scalar field with such a potential serves as a good candidate [51] for Dark Energy. Although it stays almost dormant during most of the evolution of the universe as seen fig. (7), it emerges to dominate at later times almost

around the present epoch of $a = 1$. Here depending on the value of α the steepness of the potential changes. The larger α is, the steeper will be the potential. Hence it will fall off much faster at initial stages before freezing until later times to come back and dominate.

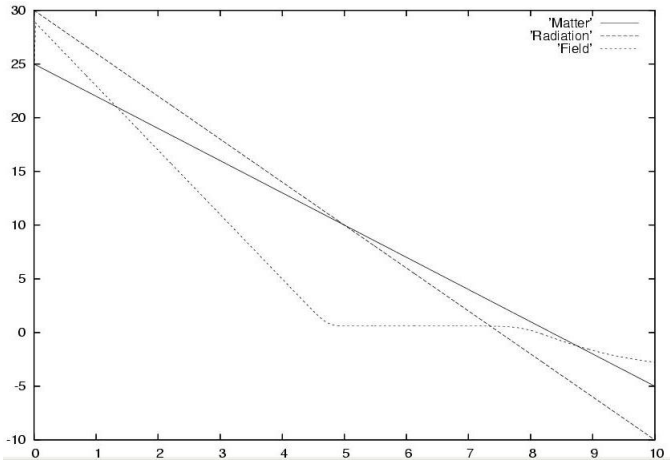

Fig. 7: Density vs Redshift for an Inverse Power Law potential

Exponential Potential

The Exponential potential given by $V = V_0 e^{-\lambda\phi/M}$, is one of the simplest and most motivated of the various quintessence potentials [51], where λ is an unknown coefficient and M is the reduced Planck mass. This potential and its cosmological behavior has been studied by various authors at various times as it works as a good starting point due to its tracking behavior.

This potential works as an attractor, i.e. there exists an attractive fixed point trajectory where ρ_b and ρ_ϕ are constant over all time and the density parameter is given by $\Omega_\phi = {}^3/\lambda^2(1 + w_b)$. This results in the solution not being dependent on V_o, alleviating the initial condition or fine tuning problem. But the very fact that the potential is an attractor, there is no mechanism to trigger its deviation from a tracking solution. Hence, it can never give rise to the acceleration of the universe. We see that if we take an exponentially positive potential it will rip the universe apart as it will no longer mimic a slowly rolling down potential, where as an exponentially negative potential cannot accelerate the universe under the normal constraints set at the present epoch, since no matter what initial condition we start with it ultimately tracks the background equation of state.

Other than the problem of having no mechanism to jump out of this attractor pool, if it were to be that ϕ dominates today over ρ it would also dominate through out the history of the universe, which is in contradiction to BBN.

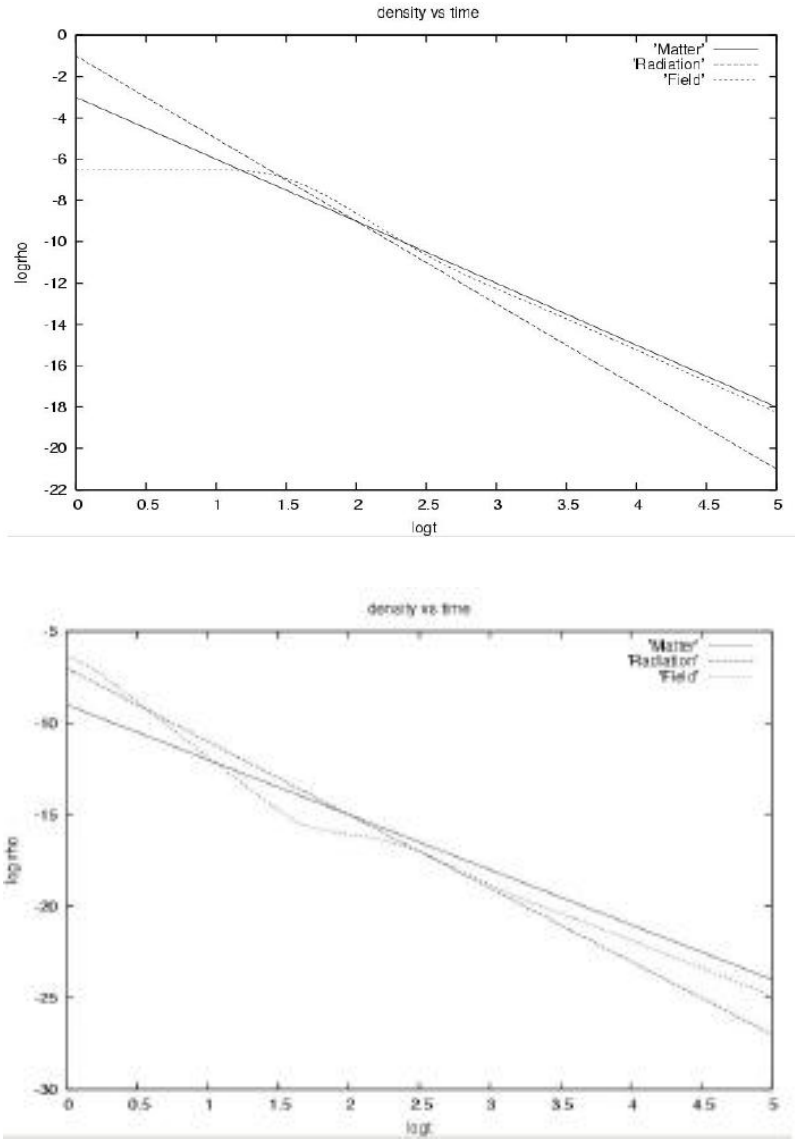

Fig. 8: Background Density for an Exponential potential

6 Conclusion

In this section we have tried to get an idea of what dark energy is and what the dynamics behind it maybe. We have also looked at the possible candidates for dark energy starting from the very simplest cosmological constant to qunitessence.Yet due to the huge challenges involved with the fine tuning and why now problem, many alternatives remain. Also challenges of how to scale cosmologies also arise [73]. Other than the ones mentioned above, many alternative theories are also being explored as a viable alternative to dark energy [74, 75, 76, 77, 59].

Part III. SuperNovae Observations

7 SNe Ia Projects

SNe Ia are considered standard candles in cosmology and have been the corner stone for the present day concordance model. The relations stated in eq. (11) and eq. (12) are crucial to understand. They are a way of directly relating observations to the theoretical models. As we see the L.H.S. of the equations can be determined by observations while the R.H.S. is determined by theory. It is exactly this correlation that historically lead Reiss and Perlmutter to the discovery of an accelerated expansion of the universe. Since then observations in this line have come along way. It started with observations of only a few dozen SNe light curves and spectra which is now a few hundred and will become a few thousand with future generation experiments. Some of the surveys are listed in table 2.

Name of Survey	Number of estimated SNe	Redshift Range
SuperNovae Legacy Survey	~ 450	$0.1 < z < 0.9$
ESSENCE	~ 200	$0.1 < z < 0.8$
HST+GOODS	43	$z \simeq 1.4$
SN Factory	300	$0.03 < z < 0.08$
SDSS	~ 500	$0.05 < z < 0.3$
JWST+ELTS	$> 10^3$	$up\ to\ z \sim 4$
Pan-Starrs	$> 10^4$	$up\ to\ z \sim 3$
KAIT	$\sim 50/yr$	$z < 0.03$

Tab. 2: Some current and upcoming SNe surveys [39, 32, 40, 41, 42]

7.1 Reiss Gold Sample

As recently as 2003, the entire supernova data set from the two different surveys – Supernova Cosmology Project (SCP) [15] and High-Z Supernova Search Team (HZT) [90], along with low redshift supernovae from the Calan-Tololo Supernova Search (CTSS) comprised of a meager 92 supernovae with very few at high redshifts, $z > 0.7$. The method of data reduction for the different teams was also somewhat different, so that it was not possible to use the supernovae from the two data sets concurrently. The picture changed somewhat dramatically during 2003-2004, when the two teams jointly presented a data set of 194 supernovae using the same data reduction method [90, 91, 92]. This new data resulted in doubling the data at $z > 0.7$. Not all these supernovae could be identified beyond doubt as

Type Ia supernovae however, since in many cases complete spectral data was not available. In early 2004, Riess *et al.* [37] reanalyzed the data with more rigorous standards, excluding several supernovae for uncertain classification or inaccurate color measurements. They also added 14 new high redshift supernovae observed by the Hubble Space Telescope (HST) to this sample. This resulted in a sample known as the Gold data set. The latest publication from the same team adds ten more SNe from HST to the data set, and excludes data below $cz = 7000\,{}^{km}/_{sec}$ or $z = 0.0233$ to avoid the influence of a possible local Hubble Bubble. It also rejects those SNe which were not identified as a confirmed SNeIa beyond the 95% confidence level. The separation led to two groups of data. The clean and crisp ones were called the Gold sample while the others were called the Silver sample. We use the Gold sample as one of our data sets to carry out the analysis for the different models.

7.2 Astier Sample or SNLS

The cosmological analysis requires assembling a sample of nearby and distant SNe Ia. Though for the SNLS data [32] objects with redshift $z < 0.015$ were rejected. This was because at such low redshifts, one enters the local Hubble Bubble and the non linear regime comes into play. Hence, rejection of the SNe having redshifts below the cut-off value made sure that peculiar velocity was not a reason for the dimming and reddening effects. Also only those objects were kept whose photometric point was no more than five days after maximum though it was seen that distance measurements are not affected even if the photometric point was seven days after maximum. A sample of 44 nearby SNe Ia matched these requirements. This data set considers only distant SNe Ia that were discovered and followed during the first year of SNLS, since this data set was at one stage the largest well controlled homogeneous sample of distant SN Ia. Other than the 44 nearby SNe, 91 more were also spectroscopically analyzed and those that were identified as SNe Ia were included in the data set.

7.3 SNAP

Probing Dark Energy With SNAP [52, 53, 54]: The apparent magnitude or intensity of the supernova is a measure of its distance and redshift, which in term is a measure of the expansion history of the universe. Supernovae observation was one of the first probes which resulted in the prediction of a component other than

matter being present, which this acceleration is riding on. A sample of several thousand type Ia supernovae with redshifts $z > 1.7$, as might be gathered by the proposed SNAP satellite, would serve as a powerful probe of dark energy. SNAP will constrain the equation of state to about 5%, independently of other cosmological probes and assuming only a flat universe.

Several other observations will help to further tighten these constraints [2]. Among them are the CMB and the location of the acoustic peaks. These also give hints about the age of the universe being 14.0 billion years which is more than predicted in a only matter dominated universe. This value only holds if the conventional Hubble value is taken, the universe is flat and the matter density perturbations are assumed to be adiabatic.

From the large scale galaxy redshift surveys such as 2dF, the power spectrums for matter density fluctuations also suggest a component with a very large negative pressure through the shape it obtains.

These two separate observational signatures which are completely independent of each other or SNe observations work as a very good cross-reference to indicate the existence of the expansion of our universe.

This mapping of the expansion history allows one to investigate new physics. For example luminosity distances allow us to explore the dynamics involved in cosmology which in turn leads us to high energy field theory:

$$D(z) \rightarrow a(t) \rightarrow V(\phi(a(t)))$$

where $V(\phi)$ is the potential of the dark energy field.

The major thing that future experiments will be plagued by is systematic uncertainties rather than mere imprecision in the observations. The CMB is insensitive to time variation and can only provide a rough estimate of an averaged value of the EoS, except for a small impact on the late-time Sachs-Wolfe effect buried in cosmic invariance. While Gravitational Lensing (GL) and growth rate of Large Scale Structure (LSS) are promising but will have a problem with the complex non-linear astrophysical effects that need to be taken into consideration. SNAP's primary aim will be to deal with these systematic uncertainties head-on. It will benefit from the the fact that, it is a space based mission.

To be able to investigate and distinguish between the different classes of physical models, we need to be able to probe the universe at the transition point from matter dominated deceleration to an accelerated era of the universe.

7.4 Union Data Set

Time finally comes to combine all these data sets to get a better understanding and fuller picture of SNe data and what can be done with it. The Union Data set is an attempt at this. It includes the recent large samples of SNe Ia from the Supernova Legacy Survey and ESSENCE Survey, the older data sets, as well as the recently extended data set of distant supernovae observed with HST. This allows it to try and plug in the gaps that exist in each of these different data sets for some of these work only with high redshift while others work for nearby supernovae. The Union Data set [15, 16] uses the SALT [32] method for both old and new SNe data points, though some points have been ignored as they do not converge. Salt is based on a spectral index [33] and light curves. The SNe used for the calibration is obtained from nearby samples so that it does not interfere with the cosmological sampling and data and results. The union data set consists of 307 SNe Ia samples which can be trusted. It excludes the ones that are below a certain confidence level hence making its results reliable.

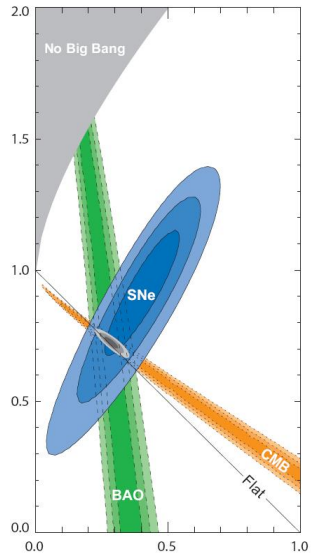

Fig. 9: Confidence level contours of 68.3%, 95.4% and 99.7% in the $\Omega_\Lambda - \Omega_m$ plane from the Cosmic Microwave Background, Baryonic Acoustic Oscillations and the Union SNe Ia set, as well as their combination (assuming $w = -1$). Courtesy of Kowalski *et al.* [15].

The union data set also uses a covariance matrix format to calculate its systematic errors. So two different covariance matrices are created. One which includes the list of systematics involved while the other involves only the statistical errors. It also uses cuts and priors so as to be able to filter out even more unwanted data

points. It uses three cuts for this purpose.

8 Different Methods Used for Calculations using SN Ia

As SNe physics grew in understanding, many groups started observing in this field and with time better and more precise experiments and observations were conducted. This also resulted in different methods of analysis. Hence some ambiguity exists and also some room for questioning as to which is the most effective method used for calculating.

8.1 SALT

Spectral Adaptive Light curve Template is new method to parametrize Type Ia Supernovae (SNe Ia) multi-color light curves [33, 93]. The method was developed in order to analyze the large number of SNe Ia multi-color light curves measured in current high-redshift projects. The technique is based on empirically modeling SNe Ia luminosity variations as a function of phase, wavelength, a shape parameter, and a color parameter. The model is trained with a sample of well-measured nearby SNe Ia and then tested with an independent set of supernovae by building an optimal luminosity distance estimator that combines the supernova rest-frame luminosity, shape parameter, and color reconstructed with the model. It allows us to determine simultaneously the SN Ia rest-frame B magnitude at maximum, stretch and color excess (or deficit) using any measured multi-color light curve within the wavelength range of rest-frame UBV bands.

8.2 MLCS2k2 Multicolor Light Curve Shape

This is the method used by the High-Z Supernovae Team [94, 95] and keeps in mind that dust and evolution can play a part in the evaluation of the brightness of the supernovae. The MLCS method is used to determine the distance moduli from light curve shapes in at least two wavelengths. A training set of well observed SNe is used to establish a light curve shape template of a typical type Ia SN, along with a set of corrections to this light curve shape depending on the parameter $\triangle$, defined as the difference in magnitudes at B band maximum between an individual supernova and the template SN [95, 17]. These corrections measure the linear and quadratic modifications to the light curve shape as a function of $\triangle$. The MLCS templates are then used to fit curves of V and B-V, for example to measure the distance modulus μ, extinction A_v, and the MLCS offset parameter $\triangle$.

The way this has been done in the past is to shift two of the light curves to B and V applying the proper cross-filter K-corrections [96] whose uncertainties can be quite large. To avoid large K-corrections, special filters designed to correspond to B and V at high redshifts have been utilized for some searches [97].

From the light curves at multiple wavelengths, one can determine the luminosity distance to these objects, e.g. via the MLCS method, and with the redshift from the spectra, place Type Ia SNe on the cosmological diagram which can be used to see constraints for various models of Dark Energy.

8.3 CMAGIC - Color-MAGnitude Intercept Calibration

CMAGIC [98] is based on the behavior of SNe Ia in color-magnitude diagrams. Starting approximately one week after B_{max} and lasting approximately three weeks, the relation between the B magnitude and $B-V$ color is strikingly linear [1]. This holds true for other colors as well. The temporal extent of this linear region is a function of stretch, with slower and higher stretch light-curves starting and ending their linear behavior later. The slope of the linear region has a narrow distribution. Currently very few rest frame R and I observations are available for high redshift SNe Ia, so here we consider only $B\ vs\ B-V$. The simplicity of this behavior is so far not completely explained by theory, which gives it a status similar to the empirical width-luminosity relation. Prior to the linear region, the majority of SNe Ia are less luminous than the linear extrapolation. However, a minority, typically those with high stretch display excess luminosity, which is referred to as a bump. Standard light-curve template fitting techniques do not adequately reproduce the results obtained via CMAGIC.

8.4 Evolution of SNe

The possibility that the average properties of SNe Ia have evolved between the current epoch and a redshift of one is of considerable concern for supernova cosmologists. So far it has been impossible to demonstrate conclusively that evolution is not the cause of the claimed cosmological results. The best that can be done is to continue to quantitatively add to the list of ways in which they are similar while failing to discern any way in which they are different [17]. One method to approach this problem is to compare high and low redshift SNe in similar environments, as done in [3], where no evidence for evolutionary biases was found. Since all measured dependencies of SNe Ia properties on local environment disappear

after stretch correction, and because the diversity of environments in which local SNe Ia occur, concerns about evolution can be usefully restricted to mechanisms which affect the luminosity-width relationship.

8.5 Systematics Involved in SNe

Systematic errors have plagued the study and analysis of SNe observations from its infancy. While some errors are common to all groups like contamination, evolution, Malmquist bias, gravitational lensing etc., there are some that are observer specific, like light curve fitting, k-correction etc [52, 32, 30, 25, 20, 40, 94, 15]. Those that are common to all observations are handled pretty much in the same manner by most groups whereas the handling of the individual observations can differ greatly and hence often give very diversified results. Table. 3 gives a list of systematic errors[5] for various groups.

Systematic	SNLS	ESSENCE	SDSS
Flux reference	0.053	0.02	0.037
Experiment zero points	0.01	0.04	0.014
Low-z photometry	0.02	0.005	...
Landolt bandpasses	0.01	...	0.019
Local flows	0.014	...	0.04
Experiment bandpasses	0.01	...	0.014
Malmquist bias model	0.01	0.02	0.017
Dust/Color-luminosity (β)	0.02	0.08	0.017
SN Ia Evolution	...	0.02	...
Restframe U band	...	...	0.08

Tab. 3: Current estimates on the systematic errors of $\langle w \rangle$ as measured by the major groups doing work in SNe Physics (courtesy [41])

[5] Systematic error estimates on $\langle w \rangle$ from Conley et al. (2009), Wood-Vasey et al. (2007), and Kessler et al. (2009). Hicken et al. (2009) CfA3 systematics are similar to those for Wood-Vasey et al., though they are not separately tabulated. The SDSS errors are for their MLCS2k2 fit. Errors for each survey use their largest sample. For the SNLS 3rd year results the total systematic error is ~ 0.06, comparable to the statistical error, and the total (statistical + systematic) error is ~ 0.09. The other studies find that systematic errors are dominant.

Part IV. Methodology

9 Introduction

Now that we have a good handle on the basics of cosmology and also on the various dynamics involved I start to look at different models for the above mentioned data sets for the SNe Ia, i.e. the Gold, the SNLS and the Union set [37, 32, 15]. We describe the method used to compute the best fit model as well as to compute the likelihoods.

10 Parametrization

Parametrization is the process of defining the parameters necessary for a complete or relevant specification of a model or geometric object. It is a powerful tool used in cosmology when a more fundamental theory is not at hand. This way one can try and study the physical properties in more details and hope that the observations along with the parametrization will help lead to more fundamental theories. One of the most common parametrizations done is of the equation of state given by w [99, 100, 101, 102] for a more complex system if we assume the ΛCDM is wrong. The most common assumption made is that w is a variable and varies with time. Then, w becomes $w_0 + w_a(1-a)$ in its simplest form.

Table 10 shows the values of the parameters for the Standard Model. There are many more parameters and as the models get more complex the number of parameters also rise. It is important to remember to try and keep the number of parameters as minimal as possible.

Parameter	Symbol	Value
Hubble Parameter	h	0.72 ± 0.03
Baryon Density	$\Omega_b \equiv \rho_b/\rho_c$	0.0462 ± 0.0015
Dark Matter Density	$\Omega_{dm} \equiv \rho_{dm}/\rho_c$	0.233 ± 0.013
Matter Density	$\Omega_m = \Omega_b + \Omega_{dm}$	0.279 ± 0.013
Dark Energy Density	$\Omega_\Lambda \equiv \rho_\Lambda/\rho_c$	0.721 ± 0.015
Radiation Density	$\Omega_r \equiv \rho_r/\rho_c$	$(5.0 \pm 0.2)10^{-5}$
Neutrino Density	$\Omega_\nu \equiv \rho_\nu/\rho_c$	$< 0.013(95\%CL)$
Baryon to Photon Ratio	$\eta \equiv \eta_b/\eta_\gamma$	$(6.21 \pm 0.16)10^{-10}$
CMB Temperature	T	$2.275K$

Tab. 4: Parameters describing our Universe. WMAP recommended parameter values [65] from WMAP5, BAO and SNe for a ΛCDM cosmology

Parameter	Symbol	Value
Equation of State	w	-0.992 ± 0.061
Tensor-to-scalar ratio	r	$< 0.22,\ k_{0=}0.002\ Mpc^{-1}\ 2\sigma$
Spectral Index	α	$0.028 \pm 0.020,\ k_{0=}0.002\ Mpc^{-1}$
Neutrino Mass	m_ν	$< 0.67\ eV\ (2\sigma)$

Tab. 5: Other Parameters for Non-concordance models

11 Numerical Tools and MCMC Calculation:

11.1 CMBEASY

With the amount of observation available to cosmology we have entered a regime that we like to call precision cosmology. As the vast data keeps pouring in we need better and better numerical tools to keep up with it. Tools such as CAMB, CMBEASY, CMBFAST etc. allow us to calculate the predictions of a given model on the basis of the observational data.

CMBEASY is a C++ based code using CMBFAST as its base code. As CMBFAST is written using FORTRAN90 it is not very modular and user friendly. C++ allowed for modularity in the code and hence implementation of new data sets became easier without having to make changes to the whole code. It utilizes the presence of objects, classes and inheritance to the fullest. It allows for keeping each section and data set as separate segments which may then be individually compiled and worked on, a characteristic property of C++ that comes in very handy when dealing with lengthy codes like CMBEASY. This makes sure that time is saved during compilation and also debugging is easier.

While the CMBEASY or any of the other numerical tools mentioned are relatively fast, the amount of computing and time required to evaluate models on an n-dimensional grid in parameter space increases exponentially with the increase in the number of parameters. The Markov chain Monte Carlo (MCMC) method scales linearly with the increase in the number of parameters, as a result of which it is much more useful and less stressful in terms of computing power and time needed. The MCMC method has been used to constrain several parameters already [27, 29, 30, 31].

The CMBEASY uses the package AnalyzeThis [28] which includes a parallel MCMC driver and a routine to calculate the likelihood with respect to various data sets available.

11.2 MCMC Simulation

In the following section we will assume that the reader is familiar with the basic ideas of Markov chain Monte Carlo simulation and the Metropolis algorithm.

The global Metropolis algorithm [9] chooses new steps for a Markov Chain via a symmetric proposal distribution. In our implementation, [26] we assume flat priors P on the parameters, and we assign likelihood zero to any parameter set that has at least one point outside the prior.

A very important aspect of MCMC is to test when the chains are sampling from the underlying distribution. Since at the beginning the chain migrates from its random starting point to regions of higher likelihood, there is a burn-in associated with each chain that must be eliminated prior to parameter estimation. In principle, it may be difficult to tell from a single chain if it has converged. In MCMC one therefore uses several chains with random starting points and monitors mixing and convergence. Our implementation employs the convergence test of [7]. The key ingredient for this test is a parameter R which can be computed from previous chain points. This parameter is a comparison of the variance within the chains compared to the variance between different chains. A value of $\mathrm{R} < 1.2$ for each parameter indicates the chains have converged and all previous points should be removed. If one uses the GUI for chain analysis, the burn-in is automatically removed.

Since there is no generally accepted procedure to determine when one has generated enough chain points for reliable estimates, the algorithm just runs indefinitely in our implementation. However, any breaking-criterion [8] may be implemented easily. The chains may be monitored with external programs during the run.

The number of steps needed for good convergence and mixing depends strongly on the step proposal distribution. If the proposed steps are too large, the algorithm will frequently reject steps, giving slow convergence of the chain. If on the other hand, the proposed steps are too small, it will take a long time for the chain to explore the likelihood surface, resulting in slow mixing. In the ideal case, the proposal distribution should be as close to the posterior distribution as possible which unfortunately is not known a priori. While a simple Gaussian proposal distribution with step sizes σ_k is sufficient, it is not optimal in terms of computing costs if cosmological parameters are degenerate. Instead of using a naive Gaussian proposal distribution, we sample from a multivariate Gaussian distribution [10] with the covariance matrix estimated from the previous points in the chains. By taking into account the covariances among the parameters, we effectively approx-

imate the likelihood contour in extent and orientation. The Gaussian samples are taken along the principal axis of the likelihood contour.

The convergence can be further improved by scaling the covariance matrix with a variable factor α. Using α, we can cope better in situations where the projected likelihood takes on banana shapes. It also improves the convergence during the early stages when the low number of points available limits the estimate of the covariance matrix. We dynamically increase if a chain takes steps too often, while we decrease if the acceptance rate is too low. By this procedure the convergence is sped up by a factor of about four compared to naive Gaussian sampling.

One can show that modifying the proposal distribution based on previous chain data during the run may lead to a wrong stationary distribution. Therefore, we only apply the dynamical strategy of finding an optimal step proposal during the early stages of the simulation i.e. we allow the step size to vary until it starts to converge. When the convergence is better than R = 1.2 and the chain has calculated a certain number of points, at least 500 points, we freeze-in the step proposal distribution.

12 Observational Data

Observations are the cornerstone of good science. After a theory or hypothesis has been made some form of experiment or observation must follow to test the predictions made by it. Cosmology is no different, though in this field more observations then experimetation is still going on. Specially, lab tests are far from being realistic, though the LHC might change the outlook on that. Data and its analysis are vital to the understanding the cosmological parameters and their values. Below is a brief discussion about the observations that have been used to carry out the work conducted in this thesis. For the combined analysis observations from WMAP, SDSS, BAO and SNe are used.

SNe Ia In the previous sections it was discussed in detail how the supernovae data are used. In the case of the SNe union data set the covariant metric is also calculated and used to calculate the systematic errors involved. We start our analysis by using only the SNe Union data set. Then we test for the other sets mentioned, i.e. the Gold and SNLS data sets.

All three sets are used to be able to make a meaningful analysis and comparison of how the number of SNe observed has helped reduce the statistical errors for these observations and also how systematics have been dealt with. Here we see

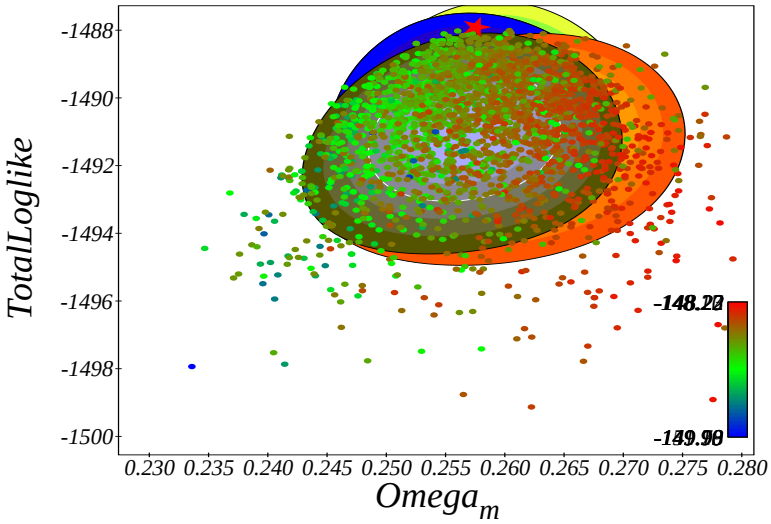

Fig. 10: The likelihood of Ω_m for different combined data sets of various models. The specks indicate the SNe Union data likelihood.

the orange represents the Corasiniti model, blue is the constant EoS, yellow at the back is the ΛCDM and in front we have the IPL model. We see that most of the points for the SNe Union data set do fall within a close range to the likelihood for a combined case.

WMAP 5-Year Data No combined data set is complete without the WMAP data. We compute using the WMAP 5-year [65] data which enables us to determine the background power spectrum and so forth. It gives us parameters which we work around to formulate the concordance model. The new data now allows us to put stringent constraints on the amount of Dark Energy present independent of previous SNe data. It also allows us to be more confident in using a numerical solution which only allows for a flat universe, since data from WMAP suggests a flat universe at the 95% confidence level. It allows us to take a peak at the universe back in time as early as possible, right back to the surface of last scattering. These measurements aim at giving a detailed map of the tiny temperature anisotropies, as small as 10^{-4} in the Cosmic Microwave Background (CMB) radiation, whose frequency distribution is that of a perfect black body at $T = 2.75K$. The observed intensity and location of the different anisotropy peaks provide fundamental information on the physical properties of the universe, in particular, on those related to the time it becomes optically thin.

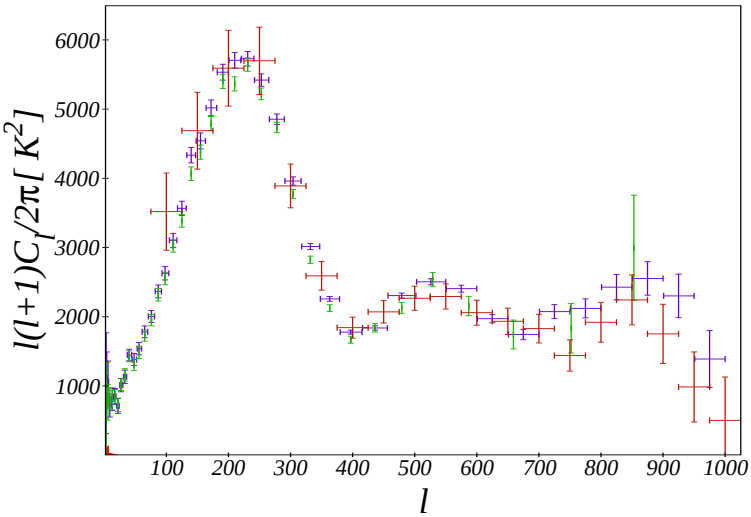

Fig. 11: Temperature angular power spectrum corresponding to the best-fit ΛCDM model

Observations of the cosmic microwave background provide us with very accurate measurements, which may be used to gain insight about dark energy . We see in fig. 11 a comparative analysis of the WMAP 3-year [34] marked in green, WMAP 5-year, in purple and the Boomerang [103] data marked in red along with their error bars. It is clear how the errors involved are steadily decreasing and hence the constraints are also getting tighter. But inspite the increase in precision the data still fits the cosmological constant model best. We may use the WMAP 5-year results to get [65, 66]

$$R = \sqrt{\Omega_{0m}} \int_0^{z_{ls}} \frac{dz}{h(z)} \tag{28}$$

where $h(z) = {}^{H(z)}/_{H_0}$, and z_{ls} is given by the fitting function

$$z_{ls} = 1048[1 + 0.00124(\Omega_b h^2)^{-0.738}][1 + g_1(\Omega_{0m} h^2)^{g_2}] \tag{29}$$

Baryon Acoustic Oscillations Another way of measuring distances are by measuring the Baryon Acoustic Oscillations [14], which we mention here as one example of the many other cosmological probes that have confirmed the picture of the accelerating universe. When measuring the large-scale correlation function of galaxies, one finds a peak at a separation of about $100h^{-1}$ Mpc. This peak is a remnant of the sound waves in the photon-baryon fluid in the early universe, the acoustic

oscillations. In the coupled photon-baryon fluid, these waves can propagate, until at recombination, the wave propagation effectively stops. The comoving distance that a sound wave can travel from the initial seed of a perturbation to the time of recombination has a characteristic length scale, known as the sound horizon and is denoted by s.[6] It is this scale that is responsible for the observed peak. Its size depends both on the expansion history, and the properties of the photon-baryon plasma, encoded in its speed of sound c_s, and is given by

$$s = \int_{z_{dec}}^{\infty} dz \frac{c_s}{H(z)} \tag{30}$$

where $z_{dec} \sim 1100$ is the redshift of decoupling between the photons and the baryons. Measuring this scale in the clustering of galaxies in the transverse and line-of-sight directions yields a determination of $\chi(z)/s$ and of $sH(z)$, respectively. The power of measurements of the baryon acoustic oscillations [61] now lies in the fact that we can observe the imprint of the acoustic oscillations in the CMB, thereby calibrating the sound horizon at a very high redshift, and then measure this length scale at different redshifts in the large-scale baryon power spectrum. The ratios of these distances determine the angular-diameter-distance to redshift relation, yielding a powerful geometric measurement of the expansion history of the universe. This angular diameter distance which is nothing but the the distance to the surface of last scattering, corresponding to its angular size also has a simple relation to the luminosity distance d_L given by

$$d_{ls} = \frac{d_L(z_{dec}, \Omega_m, \Omega_\Lambda)}{(1 + z_{dec})^2} \tag{31}$$

The main observational obstacle for BAO is the weakness of the acoustic feature in the correlation function [67], so the first detection at z $\approx$ 0.35 was only reported a few years ago, by [68, 69]. A crucial ingredient for the correct interpretation of these distance ratios is obviously the precise determination of the size of the sound horizon from the CMB.

SDSS The Sloan Digital Sky Survey plays an important part mapping out the large scale structures of the universe. The distribution of matter is probed by comparing the linear matter power spectra with data from the Sloan Digital Sky

[6] The distance sound waves could have traveled in the time before recombination is called the sound horizon s. It is a fixed physical scale at the surface of last scattering. The size of the sound horizon depends on the values of cosmological parameters.

Survey [11] and the 2dF Galaxy Redshift Survey [12]. Data from the SDSS [62] allows us to measure a variety of observables and use them to determine the parameters and put constraints on them. It uses gravitational lensing to measure distant objects to get a better picture and idea of the halos surrounding galaxies and hence allowing a more precise matter power spectrum [13] to be obtained since now the amount of Dark Matter can be better inferred.

12.1 Error Estimations

Error estimation is a major part of being able to decide and say with confidence which model is a best fit. Errors creep into observational values in mainly two distinct ways, statistical and systematic. Errors are calculated using the standard Fisher information[7]. A short description is given below. A Fisher matrix can be used to calculate the covariance matrix that is essential in error measurements as a covariance matrix is nothing but the variance measured in higher dimensions. Since we know that the variance of a parameter is obtained from the matrix, let us now assume we have a data set defined as $O = \{O_1, O_2, O_3, ..., O_n\}$. Then the probability distribution function f depends on the parameters $P = \{p_1, p_2, p_3, p_4, ..., p_n\}$ which we want to estimate. Then the Fisher matrix F_{ij} becomes

$$F_{ij} = -\left\langle \frac{\partial^2 ln f(O;P)}{\partial p_i \partial_j} \right\rangle \tag{32}$$

The inverse of this matrix F_{ij}^{-1} gives the best possible covariance matrix which measures the errors of the parameters P. This information matrix comes in specifically handy when comparing two methods of observing. As by doing a comparative analysis of the two different matrices obtained for the different parameter sets, one can determine which has a better likelihood of the two methods. As mentioned above even for the new SNe Ia data set the Fisher information and hence the covariant matrix has been calculated for both statistical as well as systematic purposes. It can be particularly handy for systematics as we can then calculate how a systematic error in O_i propagates into the expected value of the parameter p_j through the following

$$\delta p_j = (F^{-1})_{ij} \sum_k \Delta O_i \frac{\partial O_i}{\partial p_k} \frac{1}{\sigma^2(O_i)} \tag{33}$$

[7] The Fisher information is a way of measuring the amount of information that an observable random variable X carries about an unknown parameter θ upon which the likelihood function of θ, $L(\theta) = f(X, \theta)$ depends.

13 Models Chosen

For testing the code and also the data sets ability to put better and tighter constraints, we have decided to pick up some cosmological models and see how it affects the constraints on them as compared to previous data sets. For this purpose we have decided to use some classes of Quintessence models.

13.1 ΛCDM Model

Vacuum fluctuations contributing to Λ, generate a very large value of the cosmological constant given by

$$\langle T_{oo}\rangle_{vac} \propto \int_0^\infty \sqrt{k^2+m^2}k^2 dk \tag{34}$$

The integral diverges as k^4 resulting in an infinite value for $\langle T_{oo}\rangle_{vac}$ and hence also for the cosmological constant $\Lambda = \langle T_{00}\rangle_{vac} 8\pi G$ [86]. Since each form of energy gravitates and therefore reacts back on the space-time geometry, an infinite value of Λ is expected to generate an infinitely large space-time curvature through the semi-classical Einstein equations $G_{00} = \langle T_{00}\rangle_{vac} {}^{8\pi G}/_{c^4}$. One way to avoid this is to assume that the Planck scale provides a natural ultraviolet cutoff to all field theoretic processes, this results in $\langle T_{00}\rangle_{vac} \sim 10^{76} GeV^4$ which is 123 orders of magnitude larger than the currently observed value ρ_Λ. A cutoff at the much lower QCD scale does not fare much better since it generates a cosmological constant of still 40 orders of magnitude larger than observed.

We first see how the data behaved for a cosmological constant and saw that the results were consistent with what others [15, 16] had and were also sensible. The reason for choosing this model as the starting point is due to the fact that till date it remains by far the best fit model and has made its mark in cosmology so far as to be considered the standard model. We use this as our reference model for further comparisons among the different models and see how far they may deviate from this picture, since with more precise observations the window for deviation from this model gets narrower.

13.2 Constant EoS$\neq 0$

Models with constant equation of state w [49, 87, 102] within 20%, say, of the cosmological constant value $w = -1$, but not equal to -1, do not have much

physical motivation [37]. To achieve a constant equation of state requires fine tuning of both the kinetic and potential energies of a scalar field throughout its evolution. It is not clear that a constant $w \neq -1$ is a good approximation to any reasonable dynamical scalar field, where w varies, and certainly does not capture the key physics. However, since current data cannot rule out EoS variation on time scales less than or of the order of the Hubble time, traditionally one phrases constraints in terms of a constant w. For a constant equation of state there are various ways to parametrize it. The most popular being

$$H^2(a) = H_0^2[\Omega_R a^{-4} + \Omega_M a^{-3} + \Omega_x a^{-3(1+w)}] \tag{35}$$

where if $w = -1$ it reduces back to a cosmoloical constant.

13.3 Inverse Power Law Model

There are various reasons for studying the IPL model. One being it is a classic and a point of reference till date for most quintessence models. Here we will focus our attention on the tracker potential $V(\phi) \propto \phi^{-\alpha}$ where $\alpha > 1$. which was originally proposed in by Ratra and Peebles and Wetterich [18, 19] way back in the early 80's. For this potential, the region of initial conditions for ϕ which the tracker regime has been reached before the end of the matter-dominated stage is $\phi_{in} << M_P \equiv 1/\sqrt{G}$, and the present value of the quintessence potential is $\phi(t_0) \sim M_P$. Work on this potential is being carried out till today [111].

For the inverse power-law potential, ϕ has a tracker solution which maintains the condition

$$V" = \frac{9}{2}(1 - w_\phi^2)(\frac{1+\alpha}{\alpha})H^2 \tag{36}$$

The condition that ρ_ϕ is beginning to dominate today means that ϕ must be $\mathcal{O}(M_p)$ today, since $V" \approx \rho_\phi/\phi^2$ and $H^2 \approx \rho_\phi/M_p^2$. The one free parameter M is determined by the observational constraint on Ω_ϕ calculated today. Here is where the fine-tuning issue must be considered. To get the current observed value of $\Omega_\phi \simeq 0.7$ today, we need to impose the constraint $M \approx (\rho_m M_p^\alpha)^{1/\alpha+4}$ [36].

13.4 Corasaniti Model

The next model chosen was the one proposed by Corasaniti and Copeland [108]. It is of particular interest as it allows for a large number of scenarois to be accom-

modated in this particular case by choosing $\alpha$and β carefully. The potential for this quintessence model is given by

$$V(\phi) = \frac{M^{4+\alpha}}{\phi^{\alpha}} e^{\frac{1}{2}(\kappa\phi)^{\beta}} \tag{37}$$

where $\kappa\sqrt{8\pi G}$ and M are fixed such that the ratio of the energy densities $\rho_{\phi}$and ρ_c give the dimensionless density parameter as defined in eq. (5). For $\beta = 0$, eq. (37) becomes the Inverse Power Law case whereas for $\beta = 2$ we can obtain the SUGRA model [110]. For this very property the model is desirable to use during testing and also to try and find a generic class of potentials for Quintessence. This is due to the fact that if the Quintessence field rolls down a very flat region the equation of state varies in the region of $-1 < w_{\phi}^{0} < -0.8$, whereas it has to be larger for an Inverse Power Law. Other than these two classes of models by choosing $\alpha = 0$ and $\beta = 1$ we can also arrive at an Exponential potential [20]. So it can be summarized by saying that if $\alpha, \beta \neq 0$ then the potential has a minimum and the dynamics depends on these two parameters. Although for small values of β and large initial conditions without fine tuning, minimum is not reached for the present epoch, it is possible to set both α, β large so as to avoid this. So by setting a relatively small ϕ we can mimic IPL and hence BBN conditions are not violated at any stage and no unwanted affects on the evolution of density perturbation is seen. Another major plus point of this model is that for different values of w_{ϕ}^{0} the universe starts to accelerate at different redshifts which would have a direct consequence on the observables [109]. So different values of α and β give rise to different luminosity distances which can be measured and hence we could constrain the EoS through this and hence maybe the shape of the potential.

Since for $\beta = 0$ the Corasaniti model boils back to the Inverse Power Law model it also allows us to double check the code CMBEASY. Both IPL and Corasaniti model when implented in to the code should essentially draw the same results and constraints for the cosmological parameters if β is chosen accordingly. We did this cross-check and found that it was indeed the case. This increased our confidence in using CMBEASY for the complete analysis for the remaining models and data.

Part V. Results and Discussion

14 Results

A conventional way to determine how well a dark energy model can fit the observational data is the model-based approach, in which one optimizes the parameters of each dark energy model based on the observational data and then statistically assesses the goodness of the fit by using the likelihood method and also plotting and analyzing the best fit model to the best likelihood. In such an approach one has to obtain the best fit for each set of parameters specific to the particular dark energy model, which might be time consuming yet effective in analyzing the models bit by bit. In particular, in order to optimize the parameters of a Quintessence model the field equations are solved numerically for each point in the parameter space, which is computationally very intensive and tedious [35]. This resulted in significant time being needed to investigate the chosen models.

The vast array of models proposed for Dark Energy makes comparison of every model in the literature to the data a Herculean task. Hence here we selected only four models and have tried to analyze these as intensively as possible. This list is by no means complete and further work can be carried out on this front. Each model was chosen based on the value it adds when analyzed. The starting point is as always the concordance model. Then the constant EoS, though not theoretically motivating if w is close to minus one, is still used as the next conventional point to start and analyze Dark Energy models that deviate from the Standard Model. After that we see what happens if one considers Quintessence models. For this we have chosen the classic pioneering work of Ratra and Peebles first and as a last case we have chosen the model proposed by Corasaniti and Copeland. The last model was chosen because it allows a large class of quintessence models to be analyzed by varying its coefficients and it also allows a cross check of the numerical method being used.

The results for each model and the consequences of the different data sets and the constraints that come out of them are discussed in the subsequent sections. During the analysis we not only checked for the SNe data sets but also what would happen if this were to be combined with other data. These data include BAO, WMAP 5-year data and SDSS.

14.1 Reiss Gold Sample

Based on theoretical motivation from inflation as well as observational evidences from the angular size scale of the CMB fluctuations [34] we start from the assumption that the universe is flat, i.e. $k = 0$ and $\Omega_m + \Omega_x = 1$, where x will denote the different models [17, 21]. Here instead of starting with the assumption that Dark Energy exists they start with the distance independent information to justify the cosmological interpretation of SNe and subsequently combines it other data [37]. Quantitatively,the adopted limit on systematics is defined to be 5% per z at $z > 0.1$ as per the original sample. We see that the results obtained here are indeed consistent with previous values and as seen before they best fit a ΛCDM model at the 95% confidence level. We also see that even for only SNe data we still need $w < -0.5$ suggesting an accelerated universe.

Joint constraints on both the recent equation of state of dark energy and its time evolution are a factor of ~ 8 more precise than its first estimate and twice as more precise than those derived without the SNe Ia discovered by HST. Both of these dark energy properties are consistent with a cosmological constant and are inconsistent with very rapid evolution of Dark Energy. The absence of rapid evolution places constraints on the time in which a simple scalar field could evolve to recollapse the universe. Specifically, the timescale to a potential recollapse is larger than ~ 30 Gyr. If Dark Energy is evolving towards larger negative w, we cannot place any meaningful limit on the minimum time to a Big Rip.

Here we see what happens to the different models we are trying to examine. We have plotted the likelihood for the different models with the orange contour showing the Corasaniti model, the green-yellow signifying the IPL and the purple contour being the Constant EOS. We see the IPL is already very constrained and with more precise observations expected in the future, it might even be possible to rule it out though till date it fits the data almost as well as the concordance model. We see that all of the models prefer a universe where Ω_m lies between 0.24 to 0.28 with the best fit being $0.250 < \Omega_m < 0.265$.

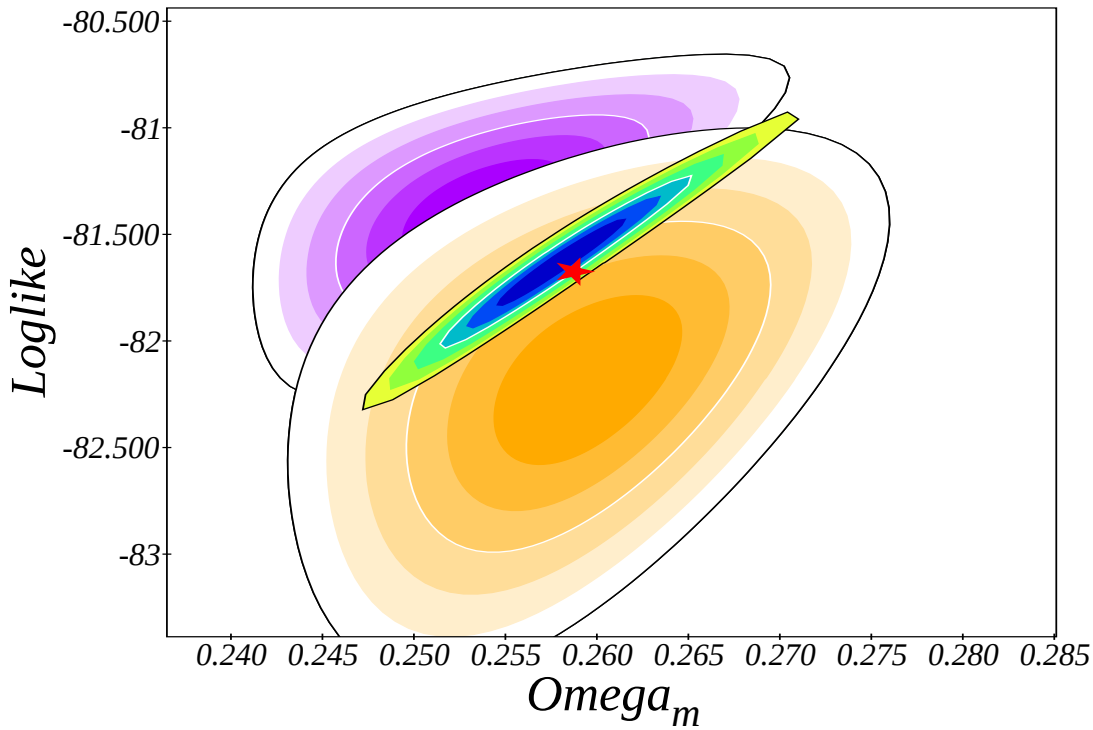

Fig. 12: Total likelihood for Ω_m for different models using the Gold Sample

14.1.1 Λ Model

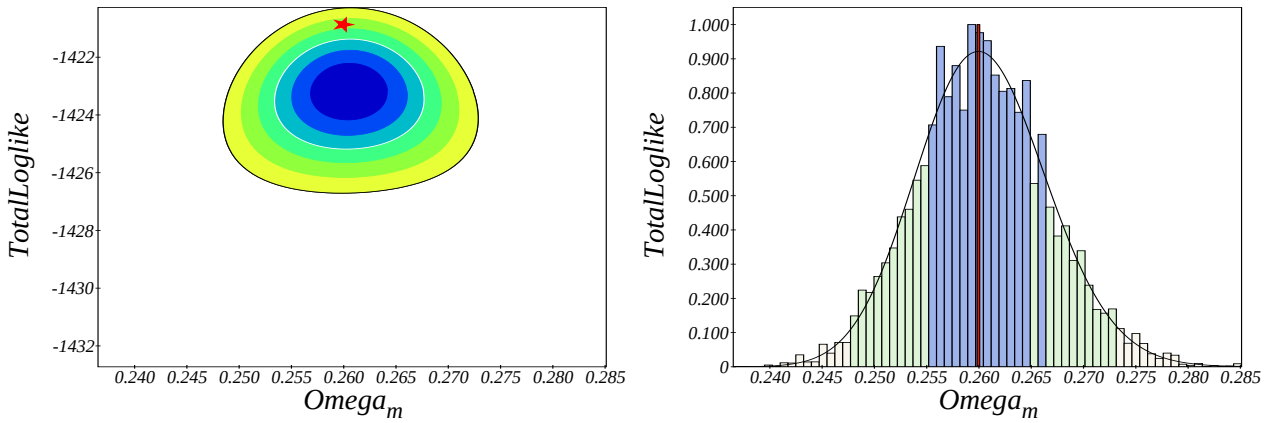

Fig. 13: TotalLikelihood of Ω_m

We see here that the likelihood in the case of SNe data alone is very close to that for a combined data set which is given by $\Omega_m = 0.2600^{+0.0063}_{-0.0061}$. Yet there is a substantial difference in their best fits with $\Omega_{m_{reiss}} = 0.2851$ and $\Omega_{m_{combined}} = 0.2598$ while the best fit for Ω_b^2 is 0.1345. We see that the Gaussian curve fitting the total likelihood for Ω_m is very close to the best fit model in this case - another clear indicator that

it is indeed the concordance model or a model with a cosmological constant that best fits data. We see that the fractional analysis of the matter component into baryons and Dark Matter also fits well.

14.1.2 Constant Equation of State

Now we check for a more generalized case of Constant Equation of State. For this case we have the luminosity distance given by

$$d_L = cH_0^{-1} \int dz[\Omega_m(1+z)^3 + \Omega_x(1+z)^{3(1+w)}]^{1/2} \tag{38}$$

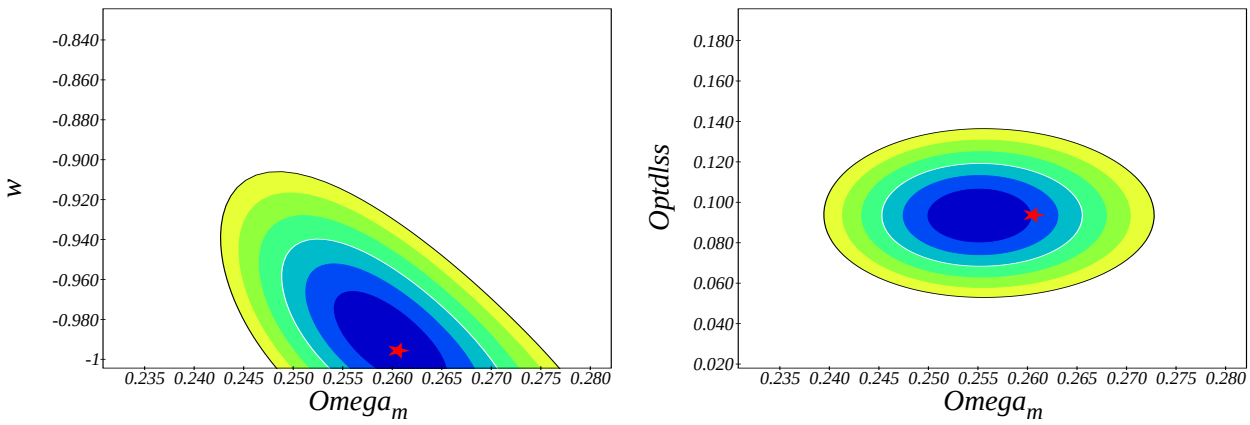

Fig. 14: Ω_m vs w and $\Omega_m$vs $Optdlss$

We look at the likelihood for Ω_m first and we see that $\Omega_m = 0.2572^{+0.0068}_{-0.0072}$ while the best fit models are very close to each other at $\Omega_{m_{reiss}} = 0.2687$ and $\Omega_{m_{combined}} = 0.2603$. We also see that $w = -0.9964$ and is < -0.91 at a 95% confidence level. The best fit model has the value of $w = 0.9059$ for Reiss data[8] alone and when combined with flat universe constraints including CMB and LSS we find the Dark Energy Equation of State to be consistent with previous results for an assumed static EoS of Dark Energy given by $p = wc^2$. But our window of allowed values narrows down even more as the other data now used is more up-to-date as compared to when the original data set was published. Whereas the claim in [37] is $w < -0.76$ we now claim that $w < -0.92$ at the 95% confidence level. This could be due to the fact that there is a strong degeneracy between Ω_m and w in the $\Omega_m - w$ plane.

[8] We have called the Gold Sample Reiss06 throughout our analysis in the plots.

We have also tried to see how and what type of constraints we can get on the optical depth and we see that the bounds start to tighten on the $\Omega_m - optdlss$ plane where we get well defined contours at the 2σ level.

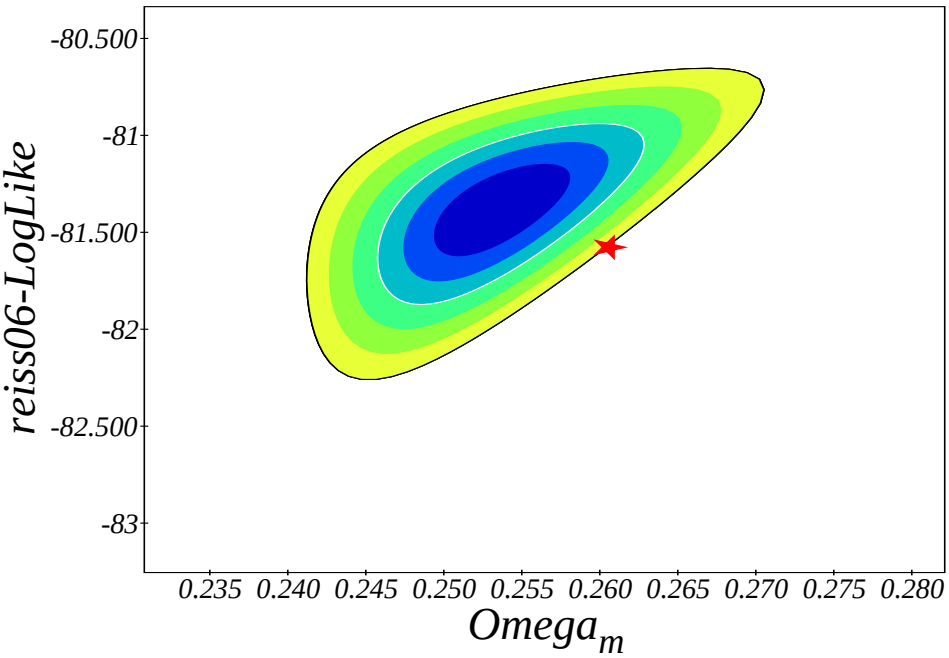

Fig. 15: Likelihood for Ω_m

14.1.3 Inverse Power Law

Though a popular potential for theorists little attention has been paid to this potential. Due to this factor we thought it may be beneficial to invest a little time on this model.

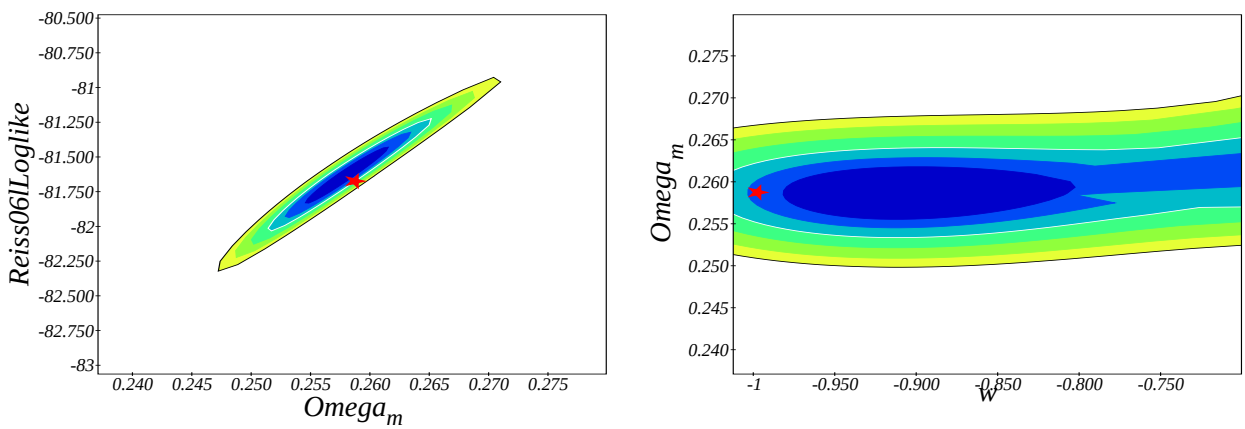

Fig. 16: Likelihood shown for Ω_m for the Riess data set and $\Omega_m$vs w

Here we have decided to show only the consequences of the Reiss data set alone though similar simulations were carried out for the combined data sets too. We have shown only the SNe data set alone because we find it to be of more significance and feel the results derived are interesting. For the $\Omega_m - w$ plane there are almost no bounds on w and all values of it seem to be allowed for $\Omega_m \in [0.265, 0.250]$ with the best fit $w = -0.99$, still very close to the cosmological constant. This could be due to the choice of α whereas we see that the contour for the likelihood of Ω_m is indeed very narrow and almost sharp. Maybe more and better SNe data may be able to make the situation such there is a 1:1 relation between the two factors. That would be an easy way in that case to be able to rule out this model in the future. We see the values as $\Omega_m = 0.2590^{+0.0062}_{-0.0062}$ with the best fit model being $\Omega_m = 0.2800$.

We also look at the shape and contour for the optical depth and see that it agrees very well with the present constraints achieved by the WMAP 5-year data.

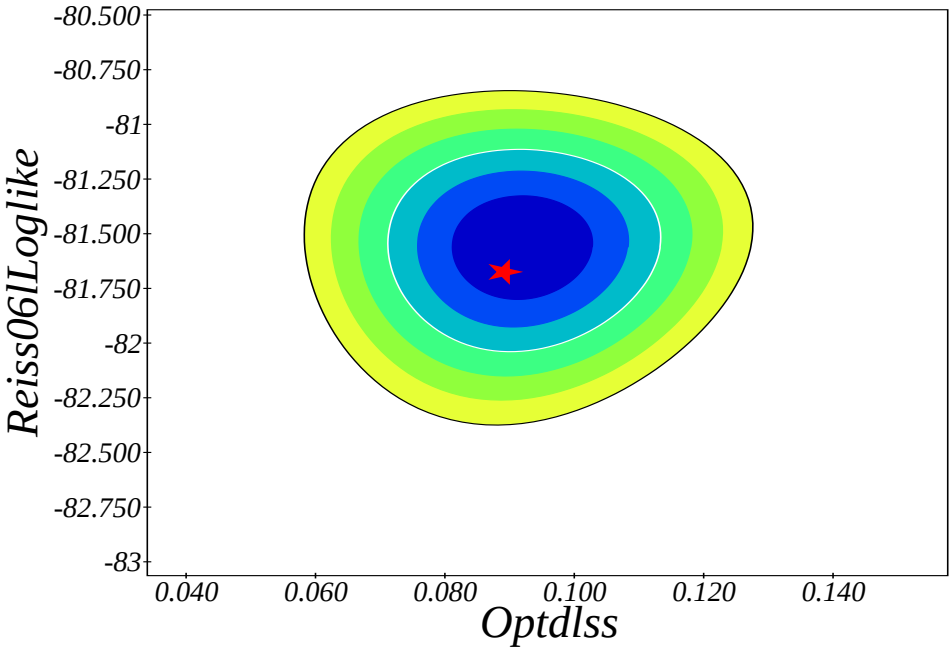

Fig. 17: The Likelihood shown for the Optical depth using only Reiss data

14.1.4 Corasaniti Potential

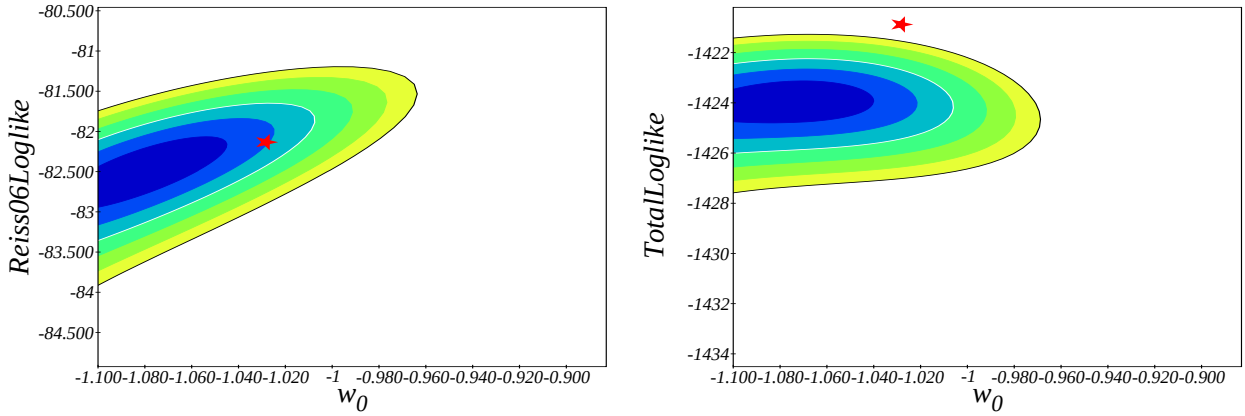

Fig. 18: Likelihood for w_0 for combined data sets as well as only for Reiss data

Though there are many interesting features to address about this model we have kept our concentration in this part mainly on the amount of matter allowed and the EoS. As can be seen we have plotted for both combined as well as only Reiss data to get $\Omega_m = 0.2599^{+0.0083}_{-0.0083}$ with the best fit model having the value $\Omega_{m_{best\,fit}} = 0.2713$. We see that though the overall value of w is given by $w_{reiss} = -0.96$ and $w_{combined} = -0.94$ the value of w_0 for the combined data set tends to marginally prefer $w < -1$ [57] with the best fit being $w_{0_{combined}} = -1.02$. It will be interesting to carry out a full MCMC including perturbations to see how the presence of a potential of this type will affect the amount of Dark Energy present and hence the structure formation overall.

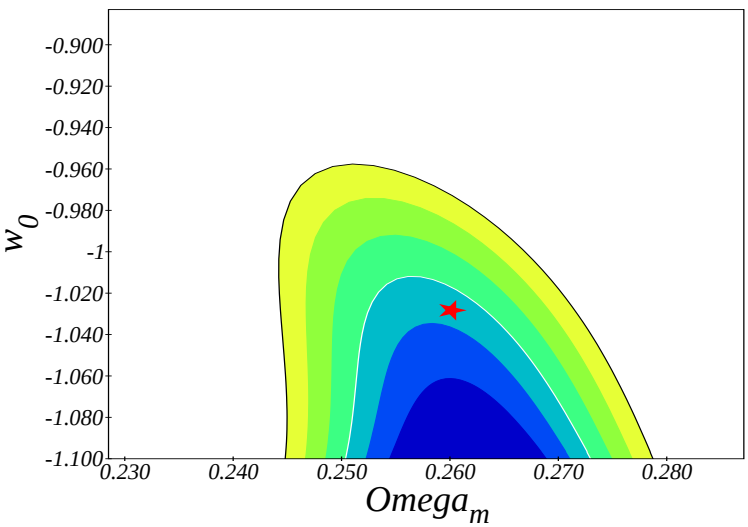

Fig. 19: Ω_m vs w_0

14.2 SNLS/Astier Sample

Firstly, each of the various samples strongly supports the SCP/HZT conclusions for the presence of a cosmological constant. Almost all samples exclude an Einstein-deSitter (EdS) universe at greater than the 99% confidence level and favor cosmological models with $\Lambda > 0$ at $> 97\%$ confidence level. If we restrict ourselves to flat $k = 0$ models, this confidence increases to $> 99\%$ for all SN samples.

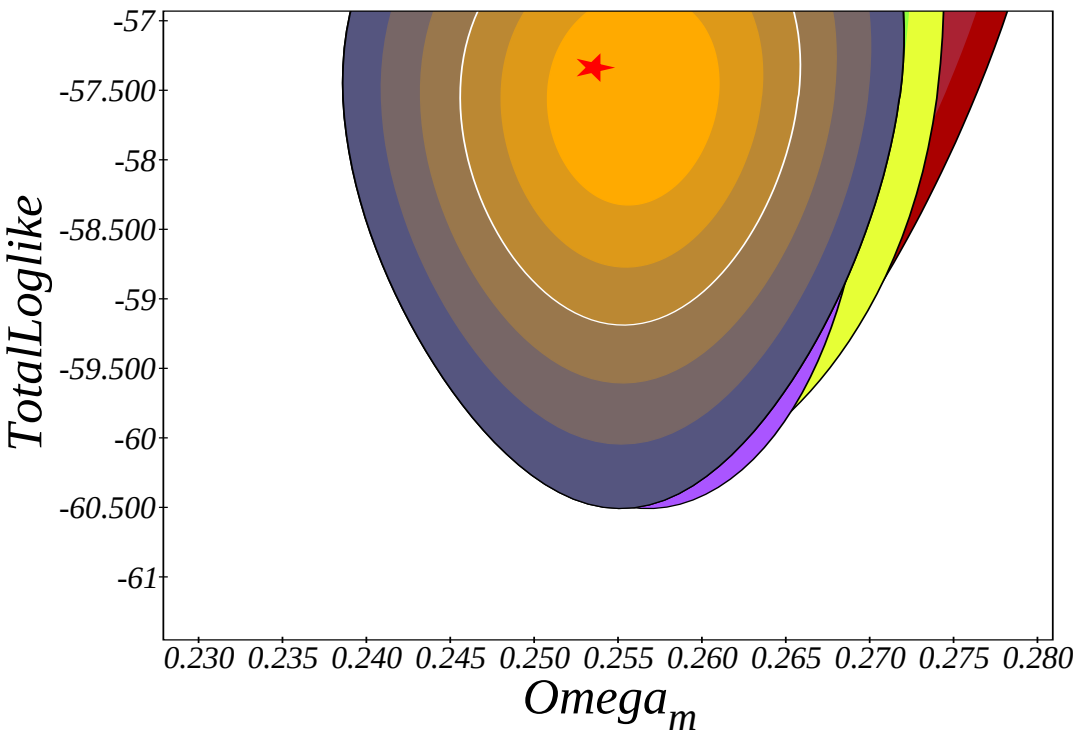

Fig. 20: Ω_m *vs* $TotalLikelihood$ for different models using the Astier Data set for the SNe

Here once again we have plotted the total likelihood for Ω_m and see how the different models fair. We see that in comparison to the Reiss data it is more difficult to tell the differences between the models. This can be due the differences in rhe methods used to calculate likelihoods. Here the yellow colored part is the Λ model, the purple is the IPL, while the front one is the constant EoS and the red at the back is the Corasaniti model. We find that the Corasaniti model has the largest contour.

14.2.1 ΛModel

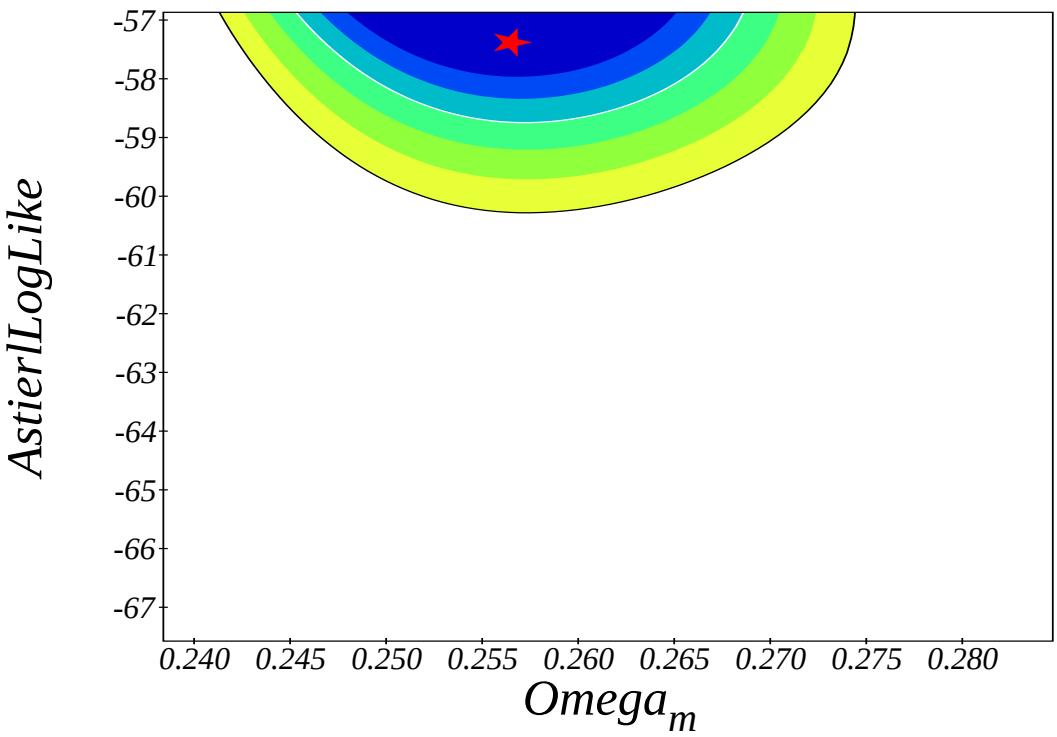

Fig. 21: Likelihood of Ω_m using the Astier data

We first start with the analysis of the standard model. We find the results are in excellent agreement with previously presented values and we get the following constraints as $\Omega_m = 0.2575^{+0.0064}_{-0.0064}$ with the best fit being $\Omega_{m_{astier}} = 0.2490$ and $\Omega_{m_{combined}} = 0.2565$. We notice here that the difference between the best fit model and the maximum likelihood once again almost coincides as would be expected. The values for the coefficients α_{ast} and β_{ast} are 1.60 and 1.81 respectively.

14.2.2 Constant Equation of State

The constraints on Ω_m for the combined data set fairs much better than that of only the SNe data set. But though the likelihood contour is better we also see that the fudicial model falls out of the 68% confidence region.

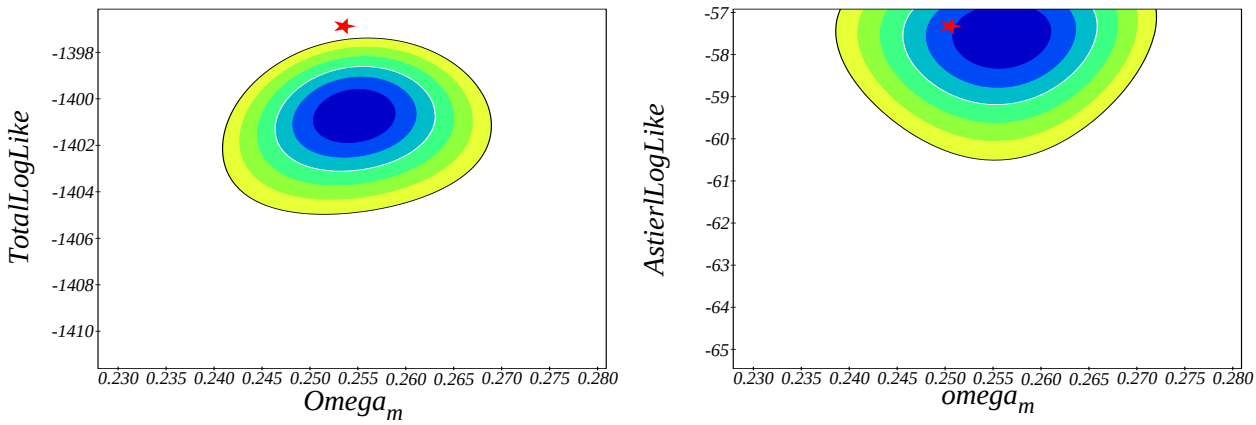

Fig. 22: Likelihoods for Ω_m for the combined data sets of CMB+SDSS+BAO+SNe and also for the SNe data set of Astier *et al.* or SNLS

The value for we obtain is $\Omega_m = 0.2547^{+0.0067}_{-0.0064}$ while the best fit value is given by 0.2504. Since the fudicial model falls well within the confidence region for the SNe data but not the combined data sets we can make the assumption that the other data sets cause a shift of the likelihood of Ω_m away from the chosen fudicial model.

The values for w for both the combined data as well as the SNe alone are given as $w_{Astier} = 0.9846^{+0.0179}_{-0.0160}$ and $w_{combined} = 0.9845^{+0.0176}_{-0.0176}$.

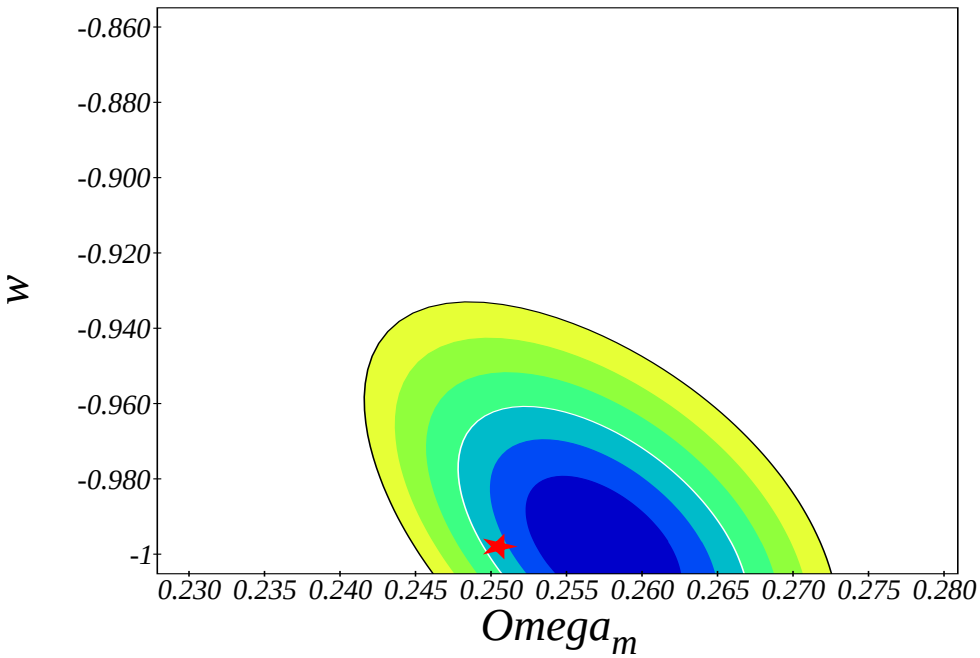

Fig. 23: $\Omega_m$vs w for the combined data sets.

14.2.3 Inverse Power Law

We once again see the same phenomena here as we did for the previous model. That is the contour for the total likelihood is better defined than that of the SNe data alone, yet the fudicial model seems to support the SNe data better. Since this is being seen in two very different models, it is possible there was a certain bias introduced in the measurements for the SNe calculations.

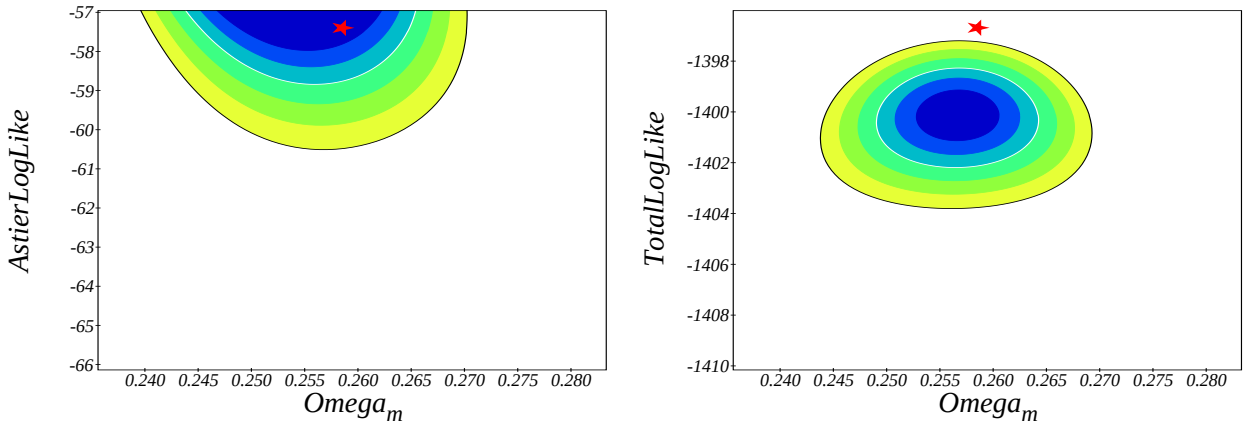

Fig. 24: Likelihoods of Ω_m for Astier data and the combined data sets

The best fit models are respectively given by $\Omega_{m_{Astier}} = 0.2502$ and $\Omega_{m_{Combined}} = 0.2585$, while $\alpha = 0.013$ although it seems to have alot of spread.

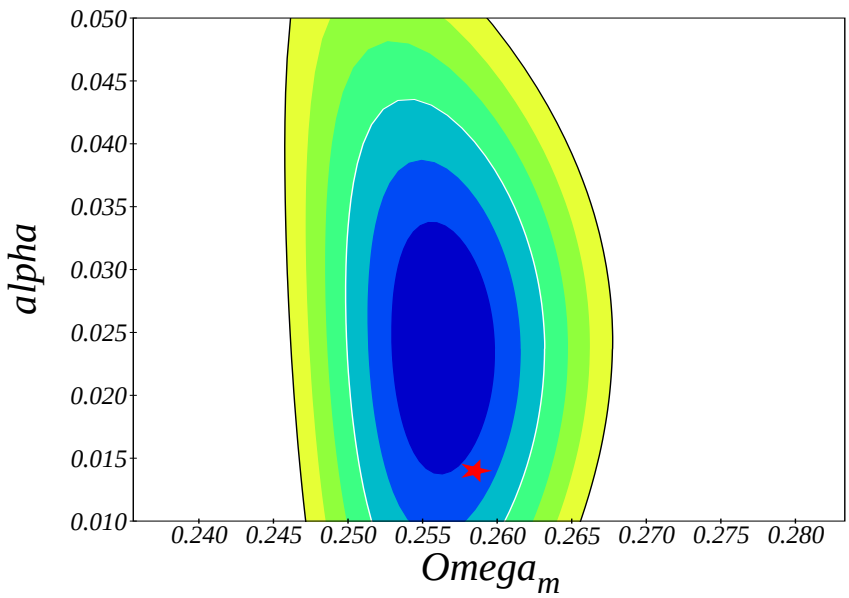

Fig. 25: Likelihood region of $\alpha$for an Inverse Power Law potential at the 2σ level

14.2.4 Corasaniti Potential

Once again the same situation persists for the combined data set. But we also see additionally that the same happens in the case of w_0 where the fudicial model is barely within the confidence region.

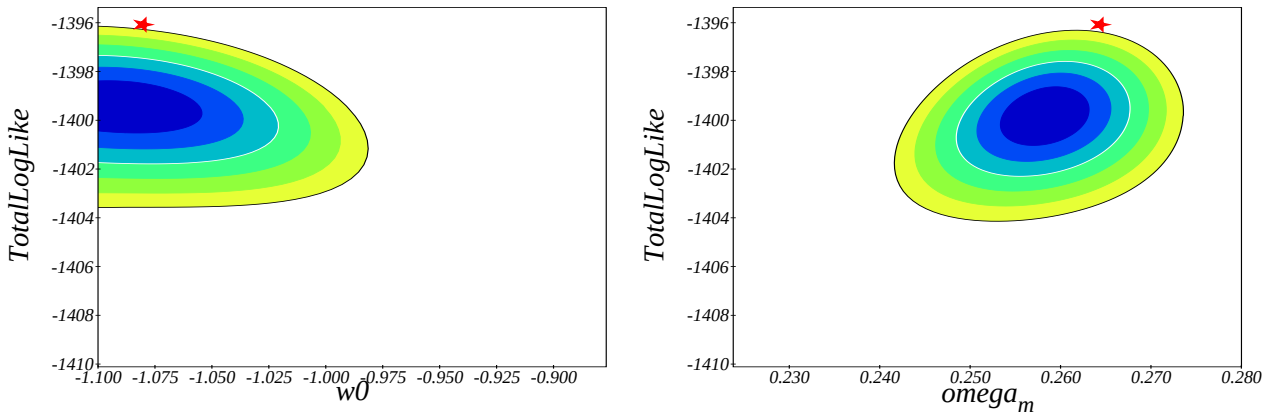

Fig. 26: TotalLogLikelihood for Ω_m and w

We get $\Omega_{m_{Astier}} = 0.2483$, $\Omega_{m_{combined}} = 0.2462$, $w_{o_{Astier}} = -1.02$ and $w_{0_{combined}} = -1.08$. We observe a shift towards the phantom region being present. This is clearly seen from the fact that there are no bounds in that direction.

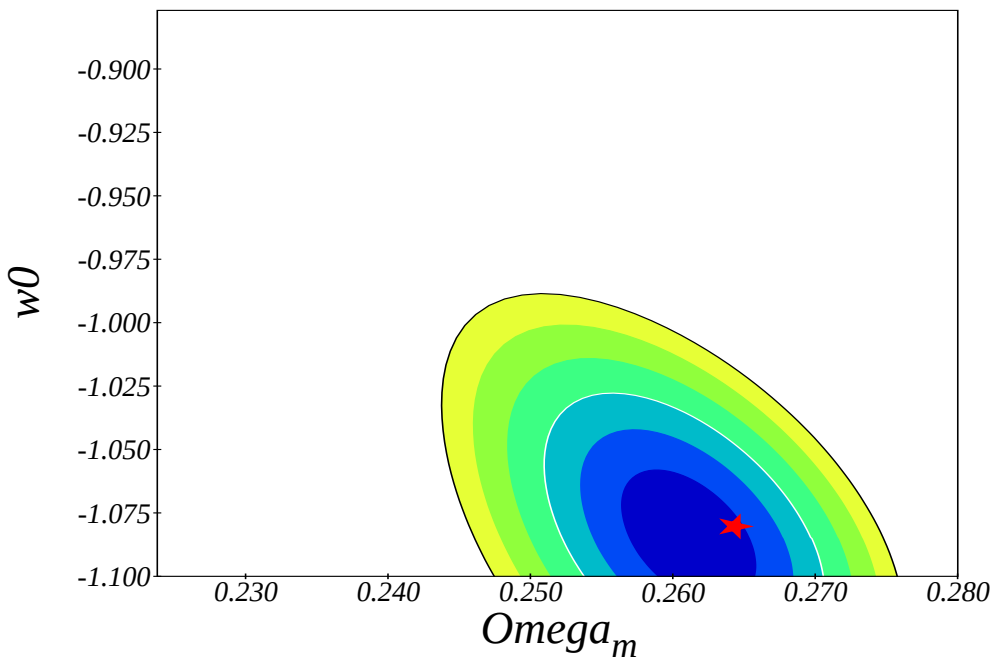

Fig. 27: $\Omega_m$vs w

14.3 Union Nosystematics

Since we are trying to do a thorough systematic analysis and check-up of different models it is critical to employ robust data that is clearly interpretable. It is equally important to get a handle on the confidence in the error estimates for both systematic and statistical uncertainties. This has been done in the unified analysis of the world's heterogeneous SNe data set- the Union Compilation08 [15].

This SNe compilation includes both the large data samples from the SNLS and ESSENCE survey, the compiled high redshift SNe observed with the Hubble Space Telescope, a new sample of nearby SNe, as well as several other, small data sets. All the SNe chosen for this sample had to go through a series of test before being qualified as up to the mark in quality. They had to be available in two bands to measure color, have sufficient light curves to make a meaningful fit, have observations starting well before the maxima is reached. The affects of the local Hubble Bubble, peculiar velocities etc were also taken into account. The samples were then tested blind for any inconsistencies in their calculations before being combined into one complete single file. The final data set consists of 307 SNe which is the basis for the analysis of the next sections.

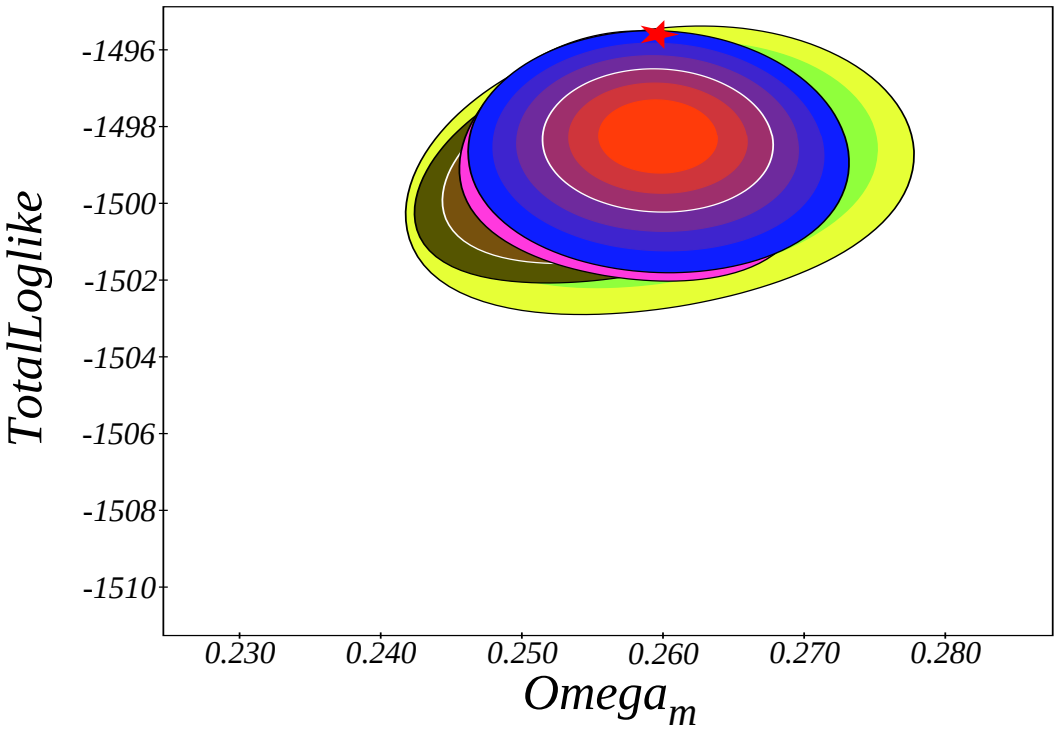

Fig. 28: TotalLIkelihood for Ω_m for different models taking the Union Data set into account but calculated without systematics

Here, like in the previous cases, we have plotted the likelihood of Ω_m for all four models chosen and their color correlations are in the following order of yellow for the corasiniti model, green-brown for IPL, pink for the constant EoS and blue for the ΛCDM. We see that though the constant EoS and concordance model in this case have almost the same value the other two models are at a tilt to these and also have a larger area. The fact that both the constant EoS and the Λ model are almost identical could be attributed to the fact that w for the constant EoS is close to that of Λ. Hence it is difficult to differentiate, but also means there is no significant gain by studying the constant w model so close to the concordance model.

14.3.1 ΛModel

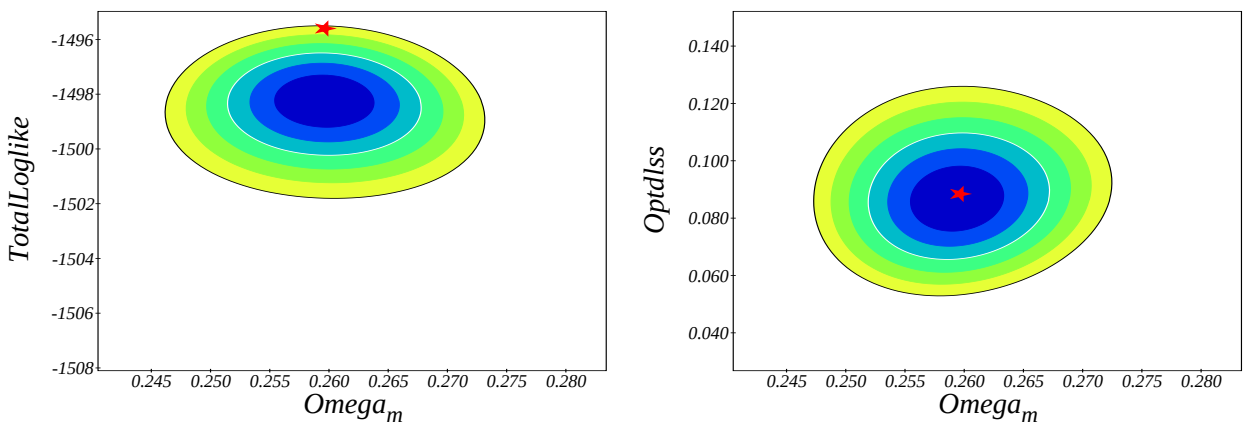

Fig. 29: ΛCDM

Achieving informative constraints on the nature of dark energy requires restricting the degrees of freedom of the theory and the resulting degeneracies in the cosmological model being tested. One degree of freedom entering the model is the present matter density Ω_m. For the case of the spatially flat cosmological constant Λ model, this is the sole cosmological parameter determining the distances entering the SNe magnitude-redshift. Using the Union data we get $\Omega_{m_{union}} = 0.2575^{+0.0064}_{-0.0064}$, the best fit value is $\Omega_{m_{union}} = 0.249$, and the best fit value for combined data is $\Omega_{m_{combined}} = 0.2565$. We have also tried to see how the optical depth looks for a combined data set and see very good agreements with the fudicial model sitting almost at the center of the confidence region. We also did a comparative analysis

of the χ^2 published by [15] and found our results to be in good agreement with theirs.

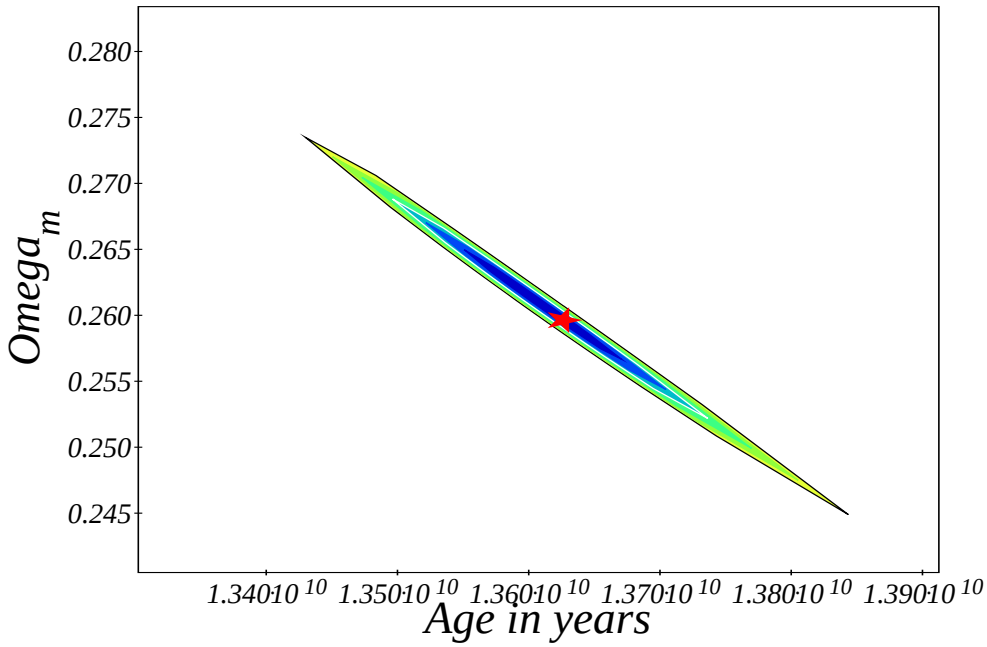

Fig. 30: Age of the Universe given in years.

Last but not least we try and take a look at how the age of the universe is affected by all this as there is a direct relation between the age of the universe and the redshift-luminosity relation which can be obtained using (11) and (10). It can easily be appreciated that at least a cosmological constant term is required to have the age of the universe the way we know it from recent observations of old globular clusters and other things. Using the value of H_0 got from HST we find that the age is given by ~ 13 billion years.

14.3.2 Constant Equation of State

Generally, further degrees of freedom to describe the nature of Dark Energy, i.e. its Equation of State (EoS), or pressure to density ratio is needed. In a few cases the EoS is a free parameter or is determined by the matter density Our next way to parametrize the EoS is to allow it to deviate from -1 but still be constant.

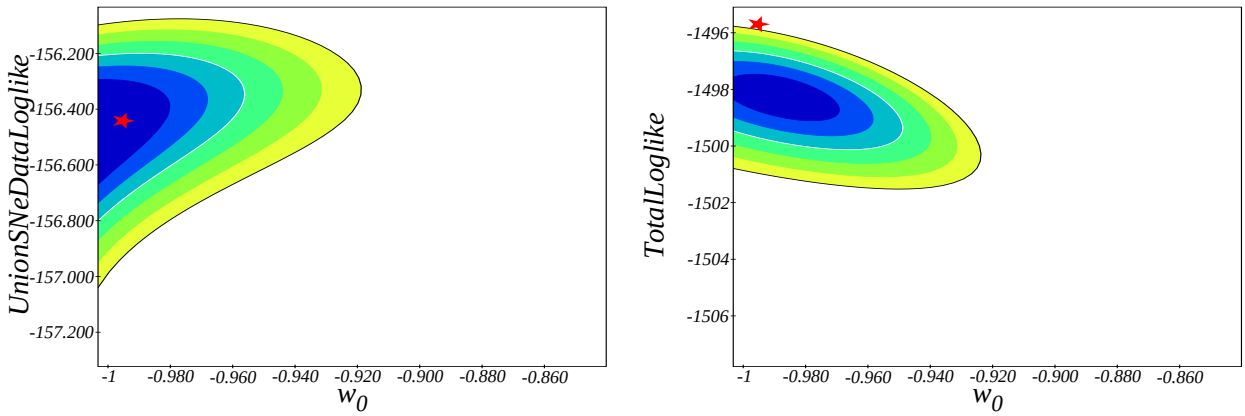

Fig. 31: Likelihoods for w_0

In this section we investigate various parameters for a constant EoS model, and the observational constraints that can be placed upon them using the Union data set. It is to be noted that throughout this section that only statistical errors are being taken into account. We get $\Omega_{m_{Union}} = 0.2561^{+0.0067}_{-0.0068}$ at the 68% confidence level where as it is $0.2561^{+0.0130}_{-0.0133}$ at the 95% level. The best fit models for the SNe data alone and the combined data are $\Omega_{m_{union}} = 0.2769$ and $\Omega_{m_{combined}} = 0.2592$. We see that the amount of matter present changes on a few percent level as soon as there is a combination of data sets, the value of w is $0.9827^{+0.0266}_{-0.0198}$ and is < -0.92 on a 95% confidence level. The best fit models are very close to the -1 mark at $w_{combined} = -0.989$ and $w_{union} = -0.99$.

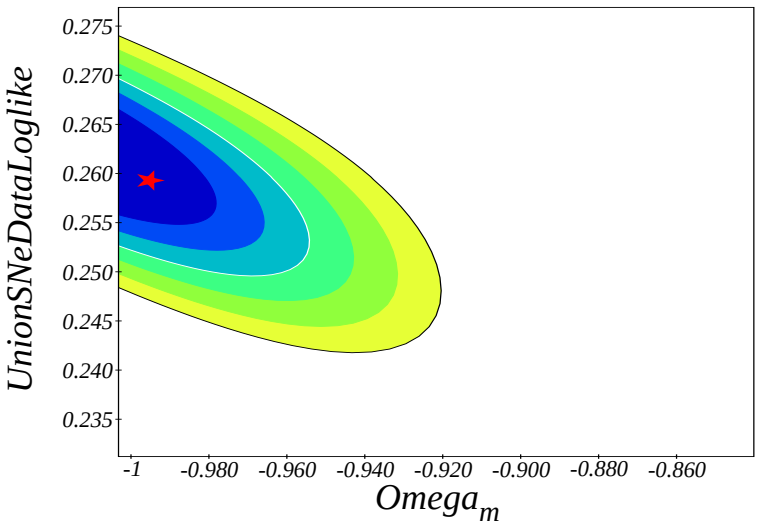

Fig. 32: Likelihood for Ω_m

14.3.3 Inverse Power Law

We again see that the $\Omega_m - w$ plane cannot break the degeneracy to be able to determine w for a well defined value of Ω_m. Ω_m is better constrained for the SNe data alone as compared to combined data sets of SDSS+WAP+BAO with its value being 0.2800. and 0.2591 for SNe alone and combined respectively.

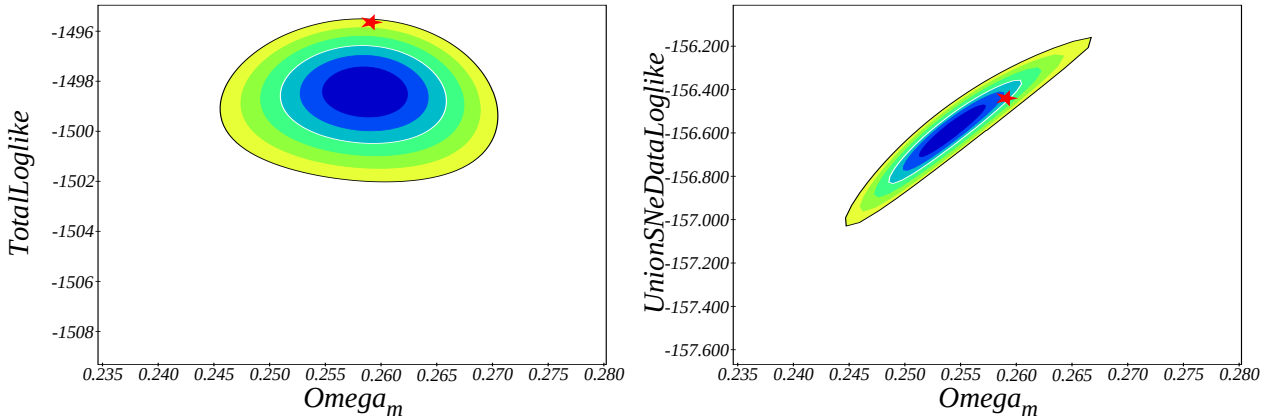

Fig. 33: Likelihoods for Ω_m for combined data sets as well as for Union data set alone without systematics

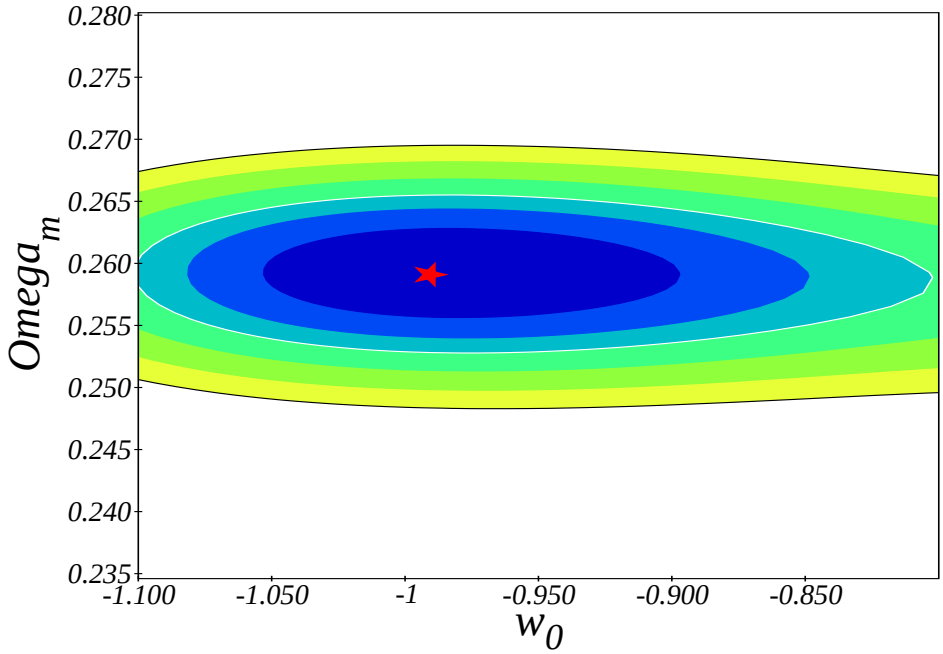

Fig. 34: Ω_m *vs* w for an IPL model using the Union SNe data set

$w < -0.86$ for the union data alone and < -0.80 for the combined case. with

the best fit value being at -0.88 , whereas the best fit value of α differs quite a bit for the two different scenarios. We find $\alpha_{union} = 0.035$ whereas $\alpha_{combined} = 0.014$.

14.3.4 Corasaniti Potential

We again do the same analysis for the Corasaniti model and get $\Omega_{m_{union}} = 0.2604^{+0.0079}_{-0.0079}$ with best fit being 0.2792. For the combined data set the best fit is 0.2626. We also find that w lies at < -0.70 at the 95% confidence level.

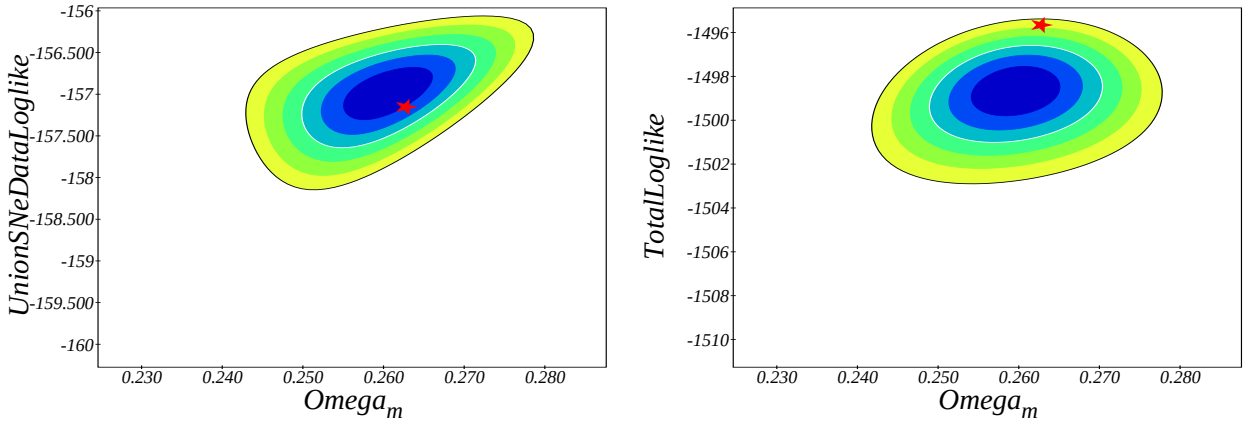

Fig. 35: Likelihoods for Ω_m

We once again see that the w_0 parameter crosses over the phantom line of -1 with $w_0 = 1.07$ at the 68% level and the best fit is -1.025 and -1.015 for union and combined data respectively.

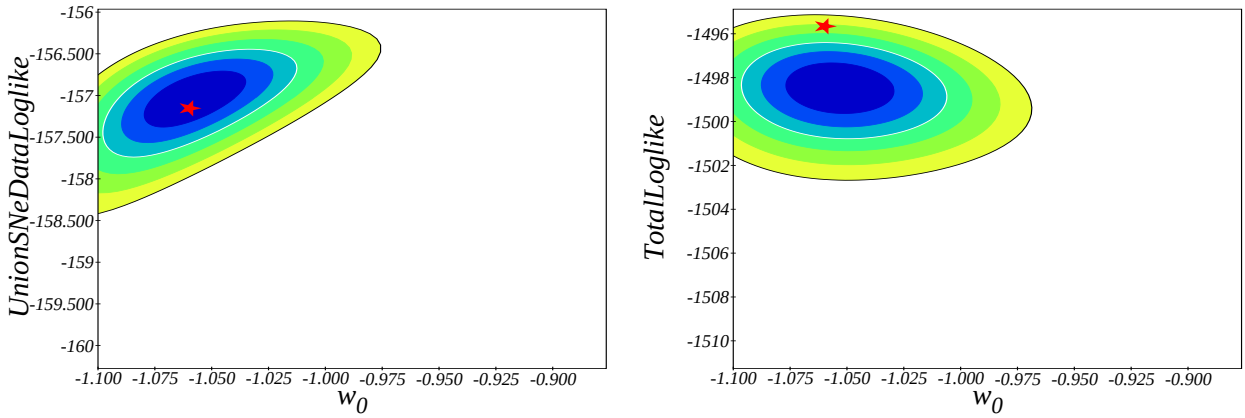

Fig. 36: Likelihoods for w_o

14.4 Union Systematics

Since it is of utmost importance to make sure the systematics are taken into account we discuss here abit about how the χ^2 is calculated for this data set before going into the actual values obtained. The corrections of Tripp [38, 32] were adopted given by

$$\mu_B = m_B^{max} - M + \alpha(s-1) - \beta c \tag{39}$$

It is clear that β is purely empirical as it accounts for dust and intrinsic color-magnitude relation. The χ^2 for eq. (39) is given by

$$\chi^2 = \sum_{SNe} \frac{(\mu_B - \mu(\Omega_m, \Omega_x, z, w))^2}{\sigma_{tot}^2 + \sigma_{sys}^2 + \sum_{i,j} c_i c_j C_{ij}} \tag{40}$$

Here C_{ij} represents the covariance matrix of the fit parameters and the sum in the denominator represents the total statistical error. Of importance here is the term σ_{sys}^2 which is linked to the systematic errors. This σ_{sys}^2 has two basic parts to it, the common irreducible one and one that is observer dependent. The systematic dispersion is calculated by starting from a value of $\sigma_{sys} = 0.15$ magnitude and then calculating the best fit model for that value. All models which have $\sigma > \sigma_{cuts}$ are first removed. Then iterations for σ_{sys} are continued until a unity in χ^2 is reached. Once unity in χ^2 is reached regular χ^2 statistics is used. A covariance matrix of the best fit parameters taking systematics into account is also produced and used for calculations of the total error estimation later. The systematic effect propagates into eq. (40) by adding a nuisance parameter ΔM_i to μ_B.

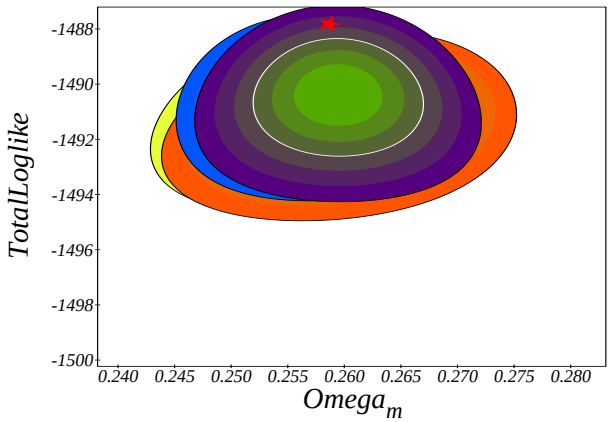

Fig. 37: Ω_m likelihoods for different models now including systematic errors

We see the result for a superimposed set of models for a SNe union data set. We

see that purple signifies the Corasaniti model, yellow corresponds to the constant EoS, dark purple is the IPL while in the front we have the concordance model.

14.4.1 Λ Model

After having analyzed the union data without systematics for the Λ model it is only natural we do the same for it here. We once again see that our results are in agreement with the SCP group and also that we get the exact χ^2 as they do for our value of Ω_m.

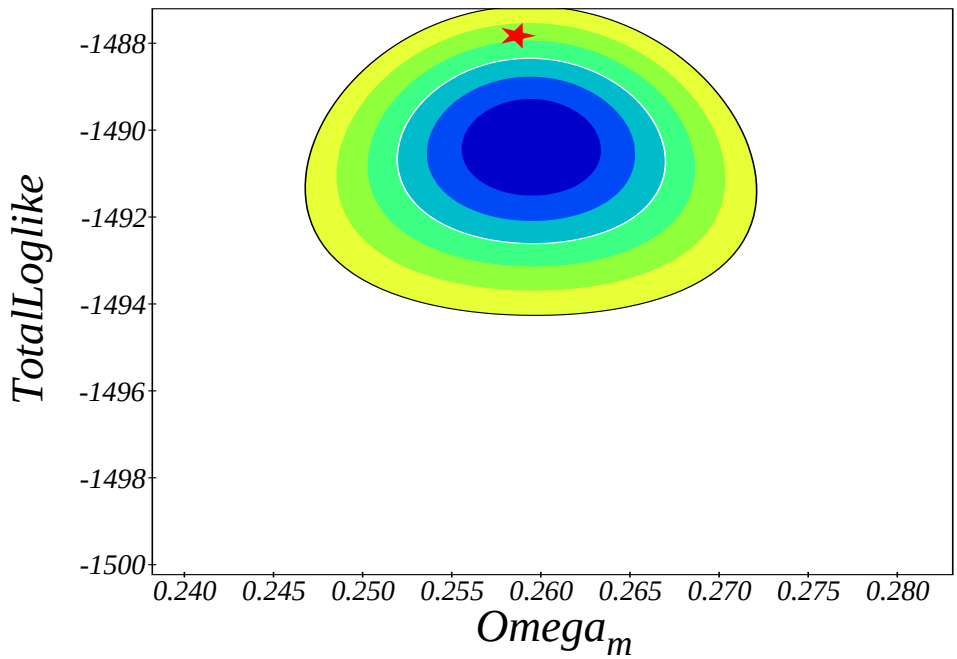

Fig. 38: Likelihood for Ω_m

We get the value of Ω_m to be $0.259^{+0.0120}_{-0.0120}$ at the 95% confidence level. We have also tried to see how adding systematics has any effect on the age of the universe and we see there is not a very large change there. But this could be due to the fact that the error bars associated with it are larger. We also plot the optical depth and once again see a perfect agreement with previous results and also that the fudicial ΛCDM model seems to fit fine and is in fact supported.

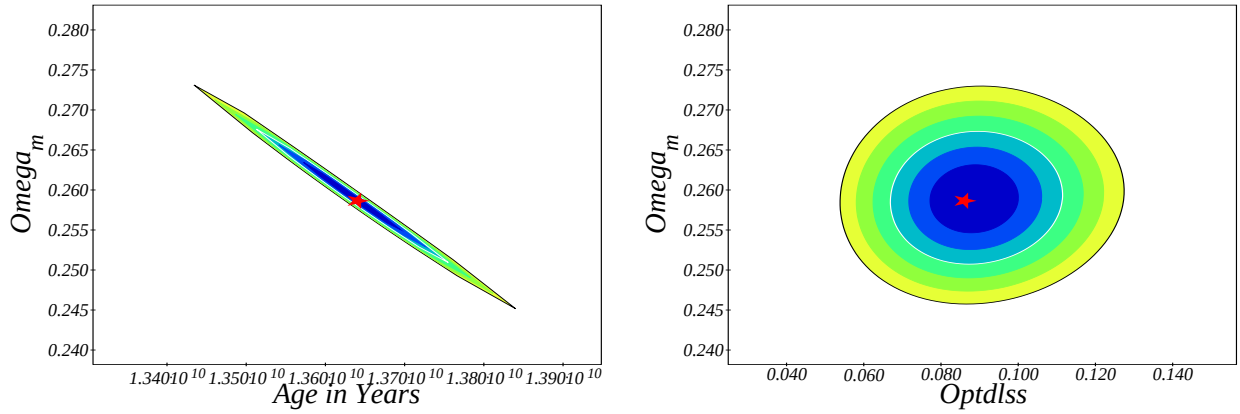

Fig. 39: Age of the universe vs Ω_m and optical depth vs Ω_m

As expected the age is very well bound assuming the HST value of H_0 to be the correct. We also assume, it is indeed Dark Energy that drives the acceleration of the universe.

14.4.2 Constant Equation of State

We see here a clear indicator for maybe a crossover EoS being preferred over one where $w > -1$.

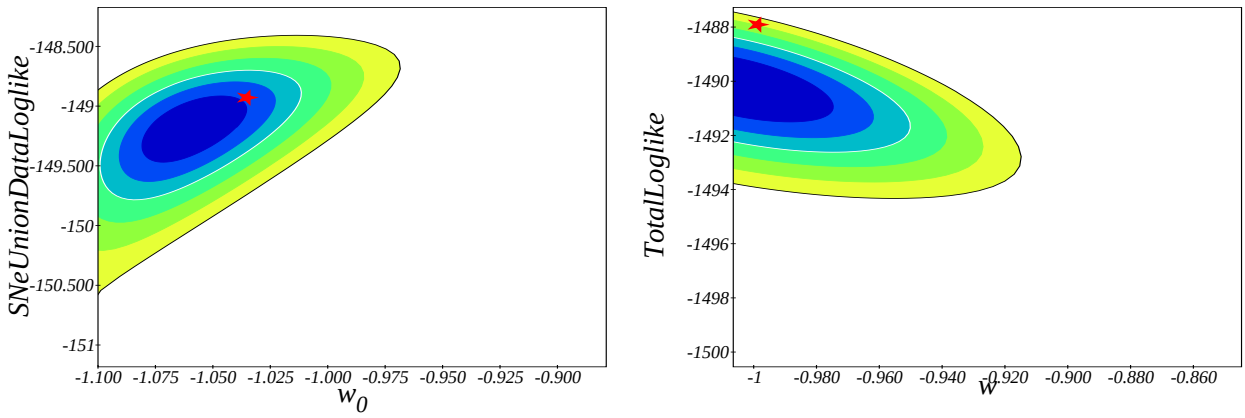

Fig. 40: Likelihood for w

We see the plots for the Likelihoods for w for both the SNe data as well as the Total data sets which as recalled included the BAO+CMB+SDSS. We see that $\Omega_m = 0.2561^{+0.0070}_{-0.0070}$ at the χ^2 level and $\Omega_m = 0.2561^{+0.0140}_{-0.0130}$ at the 95% confidence. Once again there is a very marked shift in the fudicial model values with them being 0.2804 and 0.2577 respectively. We see that $w = 0.9822^{+0.1217}_{-0.0802}$ at the 95% confidence level.

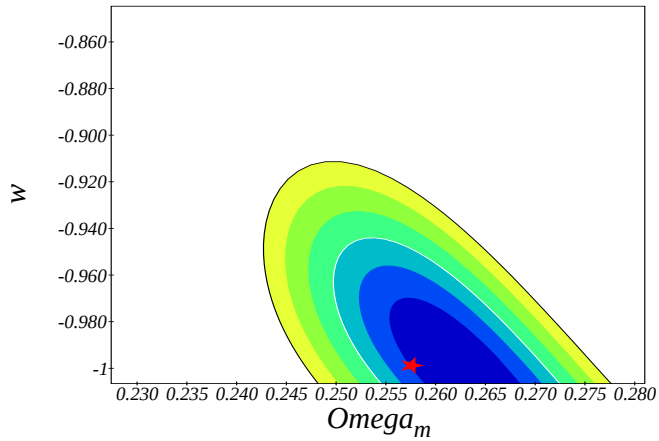

Fig. 41: $\Omega_m - w$ plane

14.4.3 Inverse Power Law

Inverse Power Law has not been studied for the Union data set before so we thought it makes sense to see if this improved more unified data set has any effect on this particular model. From table 6 we find that $\Omega_m \sim 0.26$ which is by no means a way of saying this model can be ruled out and it favors a $w = -0.700$.

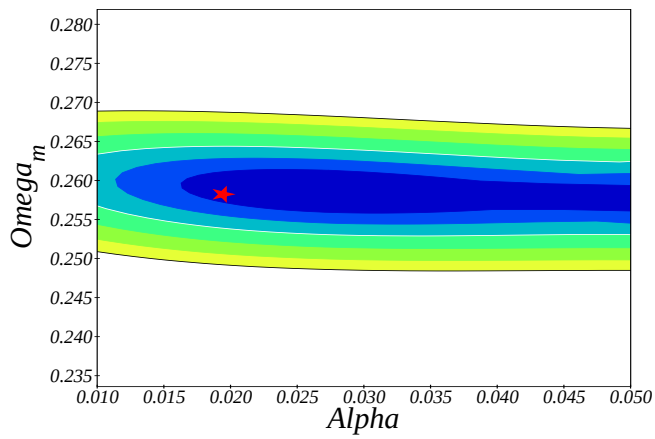

Fig. 42: Ω_m vs α

In this section, however, we have tried to see how the value of α behaves in a $\Omega_m - \alpha$ plane and we find that it is very difficult to break any form of degeneracy here. Hence there is a smear right across the α axis. The values obtained for α from χ^2 statistics were $\alpha_{combined} = 0.030$ and $\alpha_{union} = 0.019$. We also took a look at the baryonic fraction present to see how it fits with the current standings and it agrees very well.

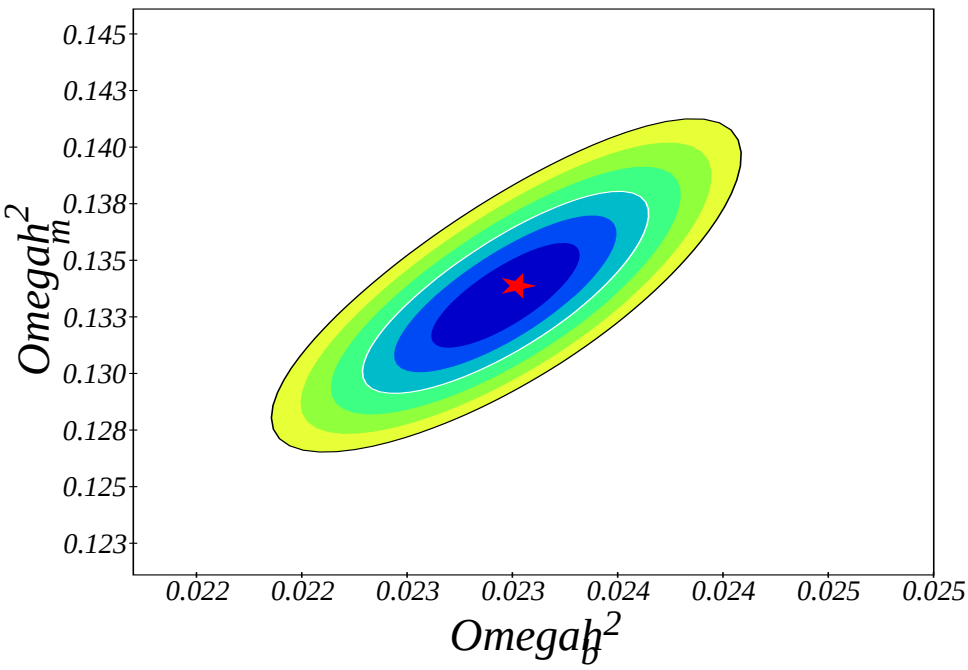

Fig. 43: $\Omega_m h^2$ vs $\Omega_b h^2$

14.4.4 Corasaniti Potential

Last but not least we take a look at how the union data set including systematics effects the parameter constraints on the Corasaniti model because as mentioned above though a very nice and handy model little attention has been paid to it. The value of Ω_m for the combined data sets is $0.2595^{+0.008395}_{-0.008395}$ with the best fit value being 0.02628.

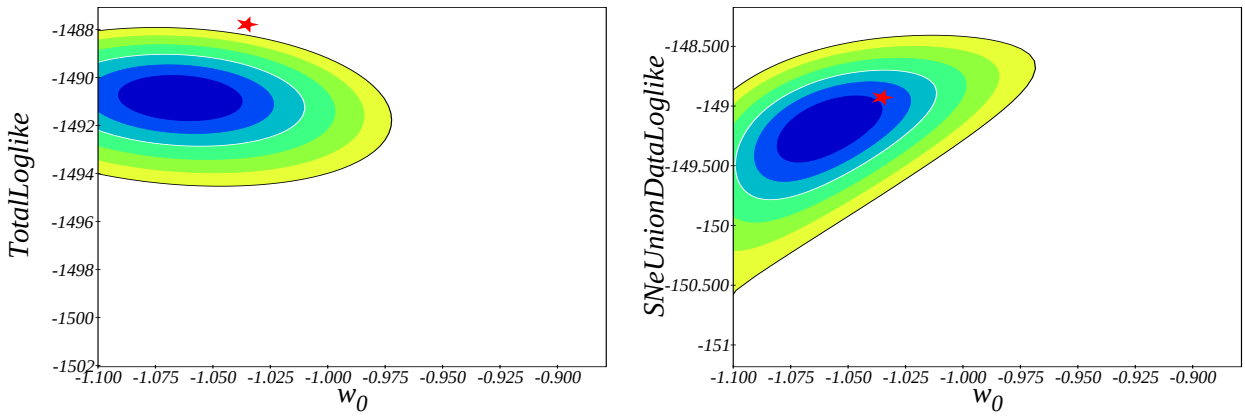

Fig. 44: Likelihoods for w_0

We see here the total likelihoods for the combined as well as for the SNe data

alone in fig 44. The values we get are $\Omega_m = 0.2595^{+0.01640}_{-0.01640}$ at the 95% confidence level while $w < -0.974$ at that same level. ac has the value of 0.18. Once again we see that all these values are well within the range allowed by observations, so more attention needs to be paid to this model before ruling it out.

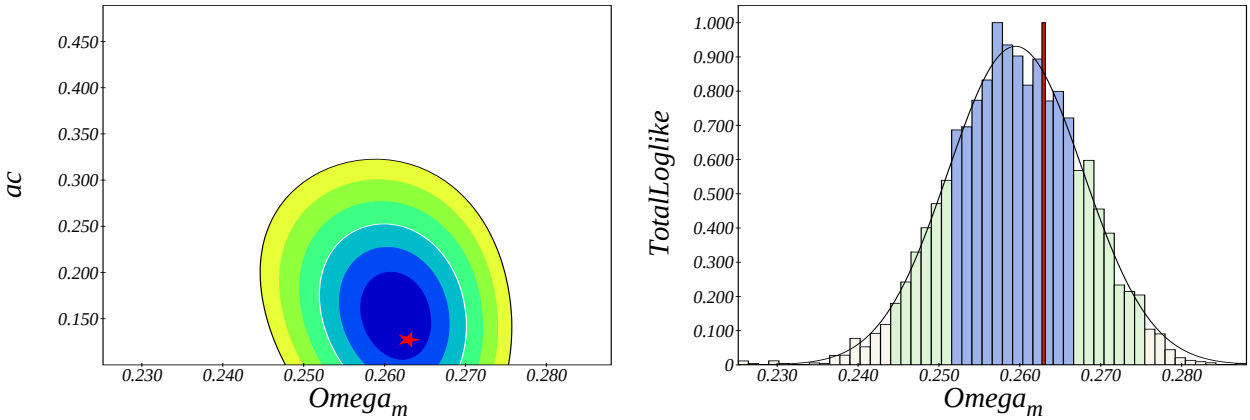

Fig. 45: Ω_m vs ac and Ω_m vs Totallikelihood

Corasiniti	Ω_m			w			w_0			w_m		
	Likelihood		Best Fit	Likelihood		Best Fit	Likelihood		Best Fit	Likelihood		Best Fit
	χ²	95%		χ²	95%		χ²	95%		χ²	95%	
Astier			0.2483			-0.895			-1.02			-0.21
CMB+LSS+BAO+Astier			0.2462			-0.709			-1.08			-0.29
Reiss06	0.2599+/-0.0083		0.2713			-0.96			-0.947			-0.264
CMB+LSS+BAO+Reiss06	0.2599+/-0.0083					-0.94			-1.02			-0.30
Union NoSys	0.2604+/-0.0079		0.272	-0.7		-0.88	-1.07		-1.025	-0.299		-0.271
CMB+LSS+BAO+Union NoSys	0.2604+/-0.0079		0.2626	-0-7		-0.85	-1.07		-1.05	-0.299		-0.137
Union Sys	0.2595+/-0.0083	0.2595+/-0.0164	0.2828	-0.8		-0.827	-1.07	<-0.974	-1.032	-0.290		-0.253
CMB+LSS+BAO+Union Sys	0.2595+/-0.0083	0.2595+/-0.0164	0.2628	-0.8		-0.933	-1.07	<-0.974	-1.030	-0.290		-0.210

IPL	Ω_m			w			α		
	Likelihood		Best Fit	Likelihood		Best Fit	Likelihood		Best Fit
	χ²	95%		χ²	95%		χ²	95%	
Astier			0.2502			-0.883			0.013
CMB+LSS+BAO+Astier			0.2585			-0.716			0.013
Reiss06	0.2590+/-0.0062		0.2800			-0.8832			0.048
CMB+LSS+BAO+Reiss06	0.2590+/-0.0062					-0.99			0.013
Union NoSys	0.2582+0.0064/-0.0061		0.2800	-0.86		-0.80	0.018		0.035
CMB+LSS+BAO+Union NoSys	0.2582+0.0064/-0.0061		0.2591	-0.86		-0.88	0.018		0.014
Union Sys	0.2579+/-0.0063	0.2579+/-0.0125	0.2815	-0.700		-0.921	0.019		0.016
CMB+LSS+BAO+Union Sys	0.2579+/-0.0063	0.2579+/-0.0125	0.2581	-0.700		-0.960	0.019		0.030

Constant EQS	Ω_m			w		
	Likelihood		Best Fit	Likelihood		Best Fit
	χ²	95%		χ²	95%	
Astier	0.2547+0.0067/-0.0064	0.2547	0.2504	-0.9846+0.0179 /-0.0160		
CMB+LSS+BAO+Astier	0.2547+0.0067/-0.0064			-0.9845+/-0.0176		
Reiss06	0.2572+0.0068/-0.0072	0.2572	0.2687	-0.9964	<-0.91	-0.9059
CMB+LSS+BAO+Reiss06	0.2572+0.0068/-0.0072	0.2572	0.2603	-0.9964	<-0.92	-0.9954
Union NoSys	0.2561+0.0067/-0.0068	0.2561+0.130/-0.0133	0.2769	-0.9980	<-0.92	-0.9890
CMB+LSS+BAO+Union NoSys	0.2561+0.0067/-0.0068	0.2561+0.130/-0.0133	0.2592	-0.9827+0.0266/-0.0198	<-0.92	-0.9951
Union Sys	0.2561+/-0.0070	0.2561+0.0140/-0.0130	0.2804	-0.9859	<-0.92	-0.993
CMB+LSS+BAO+Union Sys	0.2561+/-0.0070	0.2561+0.0140/-0.0130	0.2577	-0.9822+0.0207/-0.0182	-0.9822+0.1217/-0.0802	-0.9989

ΛCDM	Ω_m		
	Likelihood		Best Fit
	χ²	95%	
Astier	0.2575+/-0.0064		0.2490
CMB+LSS+BAO+Astier	0.2575+/-0.0064		0.2565
Reiss06	0.2600+0.0063/-0.0061		0.2851
CMB+LSS+BAO+Reiss06	0.2599+0.0063/-0.0061		0.2598
Union NoSys	0.2590+0.0064/-0.0062	0.2590+0.0125/-0.0119	0.2883
CMB+LSS+BAO+Union NoSys	0.2590+0.0064/-0.0062	0.2590+0.0125/-0.0119	0.2600
Union Sys	0.2593+/-0.0063	0.2593+/-0.0120	0.2832
CMB+LSS+BAO+Union Sys	0.2593+/-0.0063	0.2593+/-0.0120	0.2585

Tab. 6: Detailed results for the different models

15 Discussion

We find that no matter which model is chosen, there is clearly not enough predictive power on their part to distinguish them from one another. Although some of the models do make predictions, the variation in the values of the parameters they suggest are well below the cut-off sensitivity of current generation experiments.

The results of the two high redshift SNe teams [17, 21] that the universe appears to be undergoing acceleration created waves and headlines in both the scientific and mainstream media. One of the things that need to be considered now is going beyond redshift greater than one or more. By going out to higher and higher redshifts we continuously minimize our chances of getting systematic errors. As we know that Dark Energy has only started to dominate in recent times. Matter scales as $(1+z)^3$, which means as we go further back it should be the dominant consitituent of the universe. So one should be able to see a clear turn over point. If we are to go even further we would see a decelerating universe instead of the present acceleration. Most realistic systematic effects such as evolution [25] and anomalous extinction would not show such behavior and would rather keep increasing with redshift. So probing further out into this regime will allow us to answer many questions. It might let us say something about the reliability of the cosmological parameter measurements and the effect of systematics on them. It will allow us to put better constraints on different types of models. It might solve the problem of whether it is a cosmological constant or a dynamical Dark Energy that is responsible for the current acceleration as the scaling of the two models in the past would be significantly different.

On the other hand it is also very important to take a look at the low end redshift supernovae since they work as the calibration tools. Without them we do not have much use for the high z SNe's as we would not have a way of calibrating. The study of low redshift SNe play a vital role in understanding the physics involved for a SNe. This is needed if we want to be use the observartions obtained for SNe from a fundamental theory point instead of emperically only. Studying low redshift SNe allows us to do a better spectroscopic and photometric analysis of the object, hence providing a cleaner sample to work with. Also we need to fill in the missing gap that seems to exist between the low and high redshift SNe so as to be able to make a complete analysis.

The high relative redshifts of the HST-discovered SNe Ia provide little additional power to constrain w which is fixed *a priori* to be redshift-independent. The only way to increase the precision of the constarints put on cosmological parame-

ters from SNe is by increasing their sheer numbers as the precision is dependent on the statistics with only a weak dependence on the redshift. But this is only applicable until the systematic error limit is reached.

We have seen that the errors in systematics and statistics are almost of the same order of magnitude. Hence, by increasing the sheer number of objects observed without fully understanding the systematics involved we no longer gain much. Furthermore, the larger is the number of SNe observed, the more difficult it will be to get full spectroscopic analysis for all of them resulting in lower precision and confidence in the sample's purity. It will be difficult to say that a sample was not contaminated by other sources of SNe like SNe II or SNe Ib. Under these conditions we need to ask whether increasing the number of objects observed lead to a better fit of the cosmological parameters.

We have tried to see what happens for a constant EoS but for high-precision predictions of CMB anisotropies it is better to use a scalar-field description in order to have a self-consistent evolution of the sound speed associated with the Dark Energy perturbations.

Also an indepth analysis including perturbations need to be done, as here we only run the numerical simulations for the background without taking into account the full code incorporating the perturbations.

Although it stands till today as the major observational evidence for Dark Energy and a direct probe of it, by carrying out more and more experiments for SNe observations without first finding better fundamental theories and consistent ways of measuring the light curves that all groups agree on, we see that the gain is not significant. Maybe time has come to rethink investing in SNe observations and look beyond them, as was the case with space based missions once the moon was reached. So a question that needs to be asked is how should the DETF deal with SNe and what type of budget should be allocated for it?

Since SNe alone are not enough to constrain cosmological models and we need to find better methods and techniques all the time, it might make sense to focus on the BAO. Among all the observables BAO is least likely affected by systematics. It does not go through extinction processes nor brightening and dimming, it is a fixed defined number. Yet since BAO studies are still in its infancy stages the errors associated with it are also large due to lack of understanding. More emphasis can be given on understanding what theories underlie BAO. It might be possible to make it one the most reliable observables for the future, though using it at the moment to try and constrain models other than ΛCDM and constant w [5, 6] makes little sense. Since there are many effects like correlation function

from redshift space, structure formation, matter power spectrum etc associated with BAO, systematic uncertainties need to be assigned to it carefully. But this requires a complex understanding and analysis of the original data and at the current stage results are not effected too much without it. But for the future as we get closer and closer to higher precision being able to evaluate the systematic uncertainty will become crucial.

What would be an interesting question for future is: Does a perfect SNe Ia set help distinguish between different models? Assuming we had a set of SNe data free of all systematics and also through the whole range of low redshift to high redshift with no gaps in between, do they have enough information stored in them to be able to make the subtle differences required to distinguish between different models?

Part VI. Conclusion

In this thesis we have looked extensively at what happens to different models under different data sets. We have given special emphasis on the supernovae data. We have analyzed the models using previous and present data sets of supernovae to see if indeed there is any significant change in precision or constraints by merely increasing the number of SNe and hence reducing the statistical errors. We found that it does not make a huge difference on the constraints achieved.

We took a look at the DETF report, with special emphasis being put on SNe observations and projects to be launched for that particular reason. Here it is worth noting that one needs to rethink the importance of the role of SNe data in cosmology as is already been being done by the EUCLID where in their preliinary suggestions to launch experiments dedicated to Dark Energy they suggest using BAO and Weak Lensing (WL) as alternative probes to SNe [4].

We modified the CMBEASY code and implemented the union data set into it to be able to take a look at the SNe Ia data extensively. We verified the implementation by taking the case of a simple ΛCDM model and counter checked it with results obtained by the SCP group. We also cross-referenced it with the results for the combined data set analysis including CMB, BAO and SDSS and found the results to be consistent with previous findings. After the code was double-checked we used it to implement the Union Data set to other models by making slight modifications to the code each time. The implementation was basically done by using the code provided by the SCP group to calculate χ^2 and the covariance matrices required for both systematic and nonsystematic errors [15]. The original algorithm written in FORTRAN90, was converted to a C++ format to be compatible with CMBEASY. We then used the modifed CMBEASY code and tested various Quintessence models with it. We could take this one step further and analyse for Modified Gravity and Coupled Quintessence. I am particularly interested to see how the Growing Neutrino model will behave for different values of the β coefficients. Do we have enough data and precision to get strong bounds on the mass of the neutrino will be fascinating to explore.

We found that the SNLS results contradict the results obtained from the Gold data set. This fact had been noted previously for an earlier Gold data set in [91]. However, the difference is not very large. At the 2σ level the results from both data sets are consistent with each other. The fact that the light-curve standardization of the two data sets is done using different methods, MLCS2k2 for Gold+HST and SALT for SNSL may lead to differences of up to 0.16 magnitude in the data.

The discrepancy in the cosmological results may therefore be attributed partly to the different standardization techniques. There are also possible effects from other sources in the data, such as systematic noise and K-correction.

We took a close look at what happens when we introduce systematic effects to the SNe data set and find the statistical and systematic errors are of the same order of magnitude. The Fisher information was used to create a covariant matrix to determine the systematic errors. We note that as soon as the systematics is taken into account the constraints are no longer as stringent. This once again is a strong indicator that we need to look at the systematics more carefully before we take on the daunting task of calculating spectroscopic and photometric analysis of even more SNe.

We focused mainly on Quintessence models to see how they fair now and whether it is not possible to rule them out based on current observations. We carefully analysed the Corasaniti and IPL model and its parameters. We found that the allowed parameter space for the Corasaniti model is larger than the rest in the combined plots of Ω_m, whereas it is more constrained in the IPL model. We chose these two models in particular because they can be cross-checked against each other provided the coefficients are correctly chosen. We did this and found the results to be in perfect agreement. As future work, the SUGRA model could be added to this analysis, to put further pressure on the Corasaniti model as well as the modifications to the program.

What was striking was the fact when the SNe data sets were combined with BAO, CMB and SDSS some models did not fit within the 2σ confidence region though at the 3σ level it got better. This problem was most severely noticed in the Astier data set for the IPL and Corasaniti model. Do these results provide enough for models to be disfavored or is it possible that a variation in their respective coefficients which essentially changes the slope or steepness of the potential can help overcome these narrow margins. More detailed analysis with more time invested in optimizing the values of the coefficients for the Corasaniti and the IPL model need to be done.

It seems that using just the current SNe data sets alone, a firm conclusion cannot yet be reached about the nature of Dark Eenergy. We may conclude that while the cosmological constant is more or less consistent with all data sets, evolving Dark Energy cannot be ruled out. So it was very important to have robust methods and data in place to try and constrain the cosmological parameters as much as possible. Geometric probes from the Type Ia supernovae (SN) distance-redshift relation, cosmic microwave background (CMB) acoustic peak scale shift

parameter, and baryon acoustic oscillations (BAO) angular scale serve this essential role. It was very important to combine the SNe observations to these different independent data sets. We used information on the shift parameter R from the 5-year WMAP data and the quantity A for the baryon acoustic oscillation peak from SDSS for our analysis. The results are consistent with ΛCDM but do not rule out weakly time dependent Dark Energy models. Furthermore, when a full analysis with all the combined data sets of WMAP+BAO and LSS was carried out, the results for all the of SNe data sets were strikingly similar. These data are combined by multiplying their likelihoods. When combining data sets one needs to be very careful to account for any shift in of the CMB sound horizon. It can be noted that combing these data sets make a difference to the values of the cosmological parameters. While SNe data alone is not very good at constraining w, we get fairly rigid constraints on a few percent level when used in combination with other data. As we combine data sets it gets more and more difficult to rule out the ΛCDM model though it may not seem very appealing from a theoretical perspective. We see that most observations fit the concordance model the best with Ω_m at about one-quarter of the energy density of the universe. Yet it is by no means clear that even the most classical of Quintessence models can be ruled out by present day observational values.

So in our investigation of the Reiss Gold, Astier and the Union data set in the ΛCDM, EoS, Corasaniti, and IPL model using the MCMC method adopted in the CMBEASY numerical code, we have found a various number of stiking similiraities. We have found that the value of Ω_m for the Reiss data set alone for all models, among which the Corasaniti and IPL model are investigated for the first time is almost identical. We find Ω_m for a ΛCDM has the value $0.2600^{+0.0063}_{-0.0061}$ and for the IPL it is $0.2590^{+0.0062}_{-0.0062}$ while for the Corasaniti model it is $0.2599^{+0.0083}_{-0.0083}$. We find these values to be lower than estimated by other groups which claim $\Omega_m = 0.290^{+0.050}_{-0.030}$ [15, 91, 37]. The interesting part to notice is that, this is not only true for a data set giving same results for different models. The reverse also holds. By just using different and better data sets we did not gain much in terms differentiating between models. This is clear if we look at table 6. We have found that even for newly tested models like the IPL and Corasaniti the value of Ω_m is very close to 0.26. We found $\Omega^{union}_{m_{IPL}} = 0.2579^{+0.0063}_{-0.0063}$ and $\Omega^{reiss}_{m_{IPL}} = 0.2590^{+0.0062}_{-0.0062}$ for the IPL model and $\Omega^{reiss}_{m_{corasaniti}} = 0.2599^{+0.0083}_{-0.0083}$ and $\Omega^{union}_{m_{corasaniti}} = 0.2595^{+0.0083}_{-0.0083}$ for the Corasaniti model. Including systematics as we know them today does not help to break this similarity. We also found that when the Reiss data is implemented with the WMAP 5-year data, it tends to give a much higher value of w as compared

to [37] where $w < -0.76$ at the 95% confidenc level. We claim $w < -91$ at the 95% confedence level. We saw that although the value of Ω_m is almost identical in all the cases investigated there is more variation in w over the range of data sets studied. A much lower value of w is preferred by the Astier data as compared to the others. We also found a slightly lower value than -1 can be preferred for w in the case of the Corasaniti model.

The IPL is one of the oldest models of Quintessence to date while the Corasaniti model is one of the more exciting ones. We have tested both of these extensivley. We have found that by no means can these two models be ruled out, infact they are in good agreement with observations. By choosing some old models we have proven that a much more closer look at the theory and hence systematics of the SNe needs to be taken. What are the astrophyiscal proccesses behind the SNe Ia explosions or what is the theoretical motivation behind the models etc.

We conclude by saying that more emphasis needs to be given on ways to eliminate models instead of coming up with new ones. Since even one of the very earliest and well understood models cannot be ruled out; unless there is theortical motivation on a more fundemental level the questions to be answered are: Why should $\Lambda = 0$ or how can the potentials be more fundamental motivated?

Part VII. References

[1] SNAP, G. Aldering *et al.*, (2004), astro-ph/0405232.

[2] D. Huterer and M. S. Turner, Phys. Rev. **D64**, 123527 (2001), astro-ph/0012510.

[3] Supernova Cosmology Project, M. Sullivan *et al.*, Mon. Not. Roy. Astron. Soc. **340**, 1057 (2003), astro-ph/0211444.

[4] A. Refregier *et al.*, (2010), 1001.0061.

[5] S. Rydbeck, M. Fairbairn, and A. Goobar, JCAP **0705**, 003 (2007), astro-ph/0701495.

[6] H. K. Eriksen *et al.*, Astrophys. J. **656**, 641 (2007), astro-ph/0606088.

[7] A. Gelman, ANNALS OF STATISTICS **33**, 1 (2005).

[8] J. Dunkley, M. Bucher, P. G. Ferreira, K. Moodley, and C. Skordis, Mon. Not. Roy. Astron. Soc. **356**, 925 (2005), astro-ph/0405462.

[9] W. K. Hastings, Biometrika **57**, 97 (1970).

[10] C. D. R. and S. N. H. J., Biometrika **65**, 263 (1978).

[11] SDSS, U. Seljak *et al.*, Phys. Rev. **D71**, 103515 (2005), astro-ph/0407372.

[12] The 2dFGRS, S. Cole *et al.*, Mon. Not. Roy. Astron. Soc. **362**, 505 (2005), astro-ph/0501174.

[13] The 2dFGRS, W. J. Percival *et al.*, Mon. Not. Roy. Astron. Soc. **327**, 1297 (2001), astro-ph/0105252.

[14] B. A. Bassett and R. Hlozek, (2009), 0910.5224.

[15] Supernova Cosmology Project, M. Kowalski *et al.*, Astrophys. J. **686**, 749 (2008), 0804.4142.

[16] D. Rubin *et al.*, Astrophys. J. **695**, 391 (2009), 0807.1108.

[17] A. G. Riess *et al.*, Astron. J. **117**, 707 (1999), astro-ph/9810291.

[18] B. Ratra and P. J. E. Peebles, Phys. Rev. **D37**, 3406 (1988).

[19] C. Wetterich, Nucl. Phys. **B302**, 668 (1988).

[20] P. G. Ferreira and M. Joyce, Phys. Rev. **D58**, 023503 (1998), astro-ph/9711102.

[21] Supernova Cosmology Project, S. Perlmutter *et al.*, Astrophys. J. **517**, 565 (1999), astro-ph/9812133.

[22] V. Sahni, Lect. Notes Phys. **653**, 141 (2004), astro-ph/0403324.

[23] V. Sahni, Class. Quant. Grav. **19**, 3435 (2002), astro-ph/0202076.

[24] A. H. Guth, To be publ. in Proc. of 11th Texas Symp. on Relativistic Astrophysics, Austin, Tex., Dec 13-17, 1982.

[25] I. Dominguez, P. Hoflich, O. Straniero, C. Wheeler, and F.-K. Thielemann, (1998), astro-ph/9809292.

[26] C. M. Mueller, (2004), astro-ph/0406206.

[27] L. Knox, N. Christensen, and C. Skordis, Astrophys. J. **563**, L95 (2001), astro-ph/0109232.

[28] M. Doran and C. M. Mueller, JCAP **0409**, 003 (2004), astro-ph/0311311.

[29] M. Doran, (2003), astro-ph/0310400.

[30] R. R. Caldwell and M. Doran, Phys. Rev. **D69**, 103517 (2004), astro-ph/0305334.

[31] A. Slosar and M. Hobson, (2003), astro-ph/0307219.

[32] The SNLS, P. Astier *et al.*, Astron. Astrophys. **447**, 31 (2006), astro-ph/0510447.

[33] J. Guy, P. Astier, N. Regnault, and R. Pain, To appear in the Proceedings of the 22nd Texas Symposium on Relativistic Astrophysics at Stanford University, Stanford, California, 13-17 Dec 2004.

[34] WMAP, D. N. Spergel *et al.*, Astrophys. J. Suppl. **170**, 377 (2007), astro-ph/0603449.

[35] C.-W. Chen, J.-A. Gu, and P. Chen, Mod. Phys. Lett. **A24**, 1649 (2009), 0903.2423.

[36] I. Zlatev, L.-M. Wang, and P. J. Steinhardt, Phys. Rev. Lett. **82**, 896 (1999), astro-ph/9807002.

[37] Supernova Search Team, A. G. Riess *et al.*, Astrophys. J. **607**, 665 (2004), astro-ph/0402512.

[38] R. Tripp and D. Branch, Astrophys. J. **525**, 209 (1999), astro-ph/9904347.

[39] GOODS, M. Giavalisco *et al.*, Astrophys. J. **600**, L93 (2004), astro-ph/0309105.

[40] R. J. Foley *et al.*, (2008), 0811.4424.

[41] D. A. Howell *et al.*, (2009), 0903.1086.

[42] J. A. Holtzman *et al.*, Astron. J. **136**, 2306 (2008), 0908.4277.

[43] V. Sahni and A. A. Starobinsky, Int. J. Mod. Phys. **D9**, 373 (2000), astro-ph/9904398.

[44] Archeops, A. Benoit *et al.*, Astron. Astrophys. **399**, L25 (2003), astro-ph/0210306.

[45] P. J. E. Peebles and B. Ratra, Rev. Mod. Phys. **75**, 559 (2003), astro-ph/0207347.

[46] S. Weinberg, (2001), astro-ph/0104482.

[47] J. Garriga and A. Vilenkin, Phys. Rev. D **61**, 083502 (2000).

[48] G. F. R. Ellis and H. van Elst, NATO Adv. Study Inst. Ser. C. Math. Phys. Sci. **541**, 1 (1999), gr-qc/9812046.

[49] T. Nakamura and T. Chiba, Mon. Not. Roy. Astron. Soc. **306**, 696 (1999), astro-ph/9810447.

[50] L. A. Urena-Lopez and T. Matos, Phys. Rev. **D62**, 081302 (2000), astro-ph/0003364.

[51] S. A. Pavluchenko, (2003), astro-ph/0310357.

[52] SNAP, G. Aldering *et al.*, (2002), astro-ph/0209550.

[53] M. Blomqvist, E. Mortsell, and S. Nobili, JCAP **0806**, 027 (2008), 0806.0496.

[54] T. Dahlen *et al.*, (2007), 0710.5532.

[55] L.-M. Wang, R. R. Caldwell, J. P. Ostriker, and P. J. Steinhardt, Astrophys. J. **530**, 17 (2000), astro-ph/9901388.

[56] J. V. Narlikar and T. Padmanabhan, araa **39**, 211 (2001).

[57] S. M. Carroll, M. Hoffman, and M. Trodden, Phys. Rev. D **68**, 023509 (2003).

[58] V. Sahni and A. Starobinsky, Int. J. Mod. Phys. **D15**, 2105 (2006), astro-ph/0610026.

[59] L. Amendola, M. Baldi, and C. Wetterich, Phys. Rev. **D78**, 023015 (2008), 0706.3064.

[60] J. F. Jesus, R. C. Santos, J. S. Alcaniz, and J. A. S. Lima, Phys. Rev. **D78**, 063514 (2008), 0806.1366.

[61] W. J. Percival *et al.*, (2009), 0907.1660.

[62] R. Kessler *et al.*, Astrophys. J. Suppl. **185**, 32 (2009), 0908.4274.

[63] J. M. Bardeen, P. J. Steinhardt, and M. S. Turner, Phys. Rev. **D28**, 679 (1983).

[64] P. G. Ferreira and M. Joyce, Phys. Rev. D **58**, 023503 (1998).

[65] WMAP, J. Dunkley *et al.*, Astrophys. J. Suppl. **180**, 306 (2009), 0803.0586.

[66] WMAP, M. R. Nolta *et al.*, Astrophys. J. Suppl. **180**, 296 (2009), 0803.0593.

[67] E. Jennings, C. M. Baugh, R. E. Angulo, and S. Pascoli, (2010), 1002.3255.

[68] W. J. Percival *et al.*, Mon. Not. Roy. Astron. Soc. **381**, 1053 (2007), 0705.3323.

[69] P. McDonald and D. Eisenstein, Phys. Rev. **D76**, 063009 (2007), astro-ph/0607122.

[70] J. A. S. Lima, (2007), 0708.3414.

[71] J. S. Alcaniz and J. A. S. Lima, Astrophys. J. **521**, L87 (1999), astro-ph/9902298.

[72] A. H. Guth, Phys. Rev. D **23**, 347 (1981).

[73] L. Amendola, M. Quartin, S. Tsujikawa, and I. Waga, Phys. Rev. **D74**, 023525 (2006), astro-ph/0605488.

[74] A. B. Balakin and H. Dehnen, Phys. Lett. **B681**, 113 (2009), 0910.0102.

[75] M. Amarzguioui, O. Elgaroy, D. F. Mota, and T. Multamaki, Astron. Astrophys. **454**, 707 (2006), astro-ph/0510519.

[76] H. Wei and S. N. Zhang, Phys. Rev. **D78**, 023011 (2008), 0803.3292.

[77] F. C. Carvalho, E. M. Santos, J. S. Alcaniz, and J. Santos, JCAP **0809**, 008 (2008), 0804.2878.

[78] E. Hubble, Proc. Nat. Acad. Sci. **15**, 168 (1929).

[79] B. Novosyadlyj, R. Durrer, S. Gottlober, V. N. Lukash, and S. Apunevych, (1999), astro-ph/9912511.

[80] M. S. Turner, (1999), astro-ph/9912211.

[81] The VIRGO, A. E. Evrard *et al.*, Astrophys. J. **573**, 7 (2002), astro-ph/0110246.

[82] D. W. Hogg, (1999), astro-ph/9905116.

[83] S. De and R. A. C. Croft, (2009), 0910.1310.

[84] SDSS, K. Abazajian *et al.*, Astron. J. **126**, 2081 (2003), astro-ph/0305492.

[85] A. J. Albrecht *et al.*, (2006), astro-ph/0609591.

[86] V. Sahni, T. D. Saini, A. A. Starobinsky, and U. Alam, JETP Lett. **77**, 201 (2003), astro-ph/0201498.

[87] A. Melchiorri, L. Mersini-Houghton, C. J. Odman, and M. Trodden, Phys. Rev. **D68**, 043509 (2003), astro-ph/0211522.

[88] D. Pogosyan, J. R. Bond, and C. R. Contaldi, (2003), astro-ph/0301310.

[89] D. Huterer and M. S. Turner, Phys. Rev. **D60**, 081301 (1999), astro-ph/9808133.

[90] Supernova Search Team, J. L. Tonry *et al.*, Astrophys. J. **594**, 1 (2003), astro-ph/0305008.

[91] Supernova Cosmology Project, R. A. Knop *et al.*, Astrophys. J. **598**, 102 (2003), astro-ph/0309368.

[92] B. J. Barris *et al.*, Astrophys. J. **602**, 571 (2004), astro-ph/0310843.

[93] J. Guy, P. Astier, S. Nobili, N. Regnault, and R. Pain, Astron. Astrophys. **443**, 781 (2005), astro-ph/0506583.

[94] S. Jha, A. G. Riess, and R. P. Kirshner, Astrophys. J. **659**, 122 (2007), astro-ph/0612666.

[95] A. G. Riess, W. H. Press, and R. P. Kirshner, Astrophys. J. **473**, 88 (1996), astro-ph/9604143.

[96] Supernova Cosmology Project, S. Perlmutter *et al.*, Astrophys. J. **483**, 565 (1997), astro-ph/9608192.

[97] Supernova Search Team, B. P. Schmidt *et al.*, Astrophys. J. **507**, 46 (1998), astro-ph/9805200.

[98] Supernova Cosmology Project, A. J. Conley *et al.*, Astrophys. J. **644**, 1 (2006), astro-ph/0602411.

[99] H. K. Jassal, J. S. Bagla, and T. Padmanabhan, Mon. Not. Roy. Astron. Soc. **356**, L11 (2005), astro-ph/0404378.

[100] T. R. Choudhury and T. Padmanabhan, Astron. Astrophys. **429**, 807 (2005), astro-ph/0311622.

[101] Y. Wang, V. Kostov, K. Freese, J. A. Frieman, and P. Gondolo, JCAP **0412**, 003 (2004), astro-ph/0402080.

[102] S. Lee, Phys. Rev. **D71**, 123528 (2005), astro-ph/0504650.

[103] C. J. MacTavish *et al.*, Astrophys. J. **647**, 799 (2006), astro-ph/0507503.

[104] Supernova Cosmology Project, S. Perlmutter *et al.*, Nature **391**, 51 (1998), astro-ph/9712212.

[105] J. S. Bagla, H. K. Jassal, and T. Padmanabhan, Phys. Rev. **D67**, 063504 (2003), astro-ph/0212198.

[106] D. Vanbeveren, (2003), astro-ph/0302199.

[107] B. Leibundgut, Astron. Astrophys. Rev. **10**, 179 (2000), astro-ph/0003326.

[108] P. S. Corasaniti and E. J. Copeland, Phys. Rev. **D65**, 043004 (2002), astro-ph/0107378.

[109] P. S. Corasaniti, (2004), astro-ph/0401517.

[110] P. Brax and J. Martin, Phys. Lett. **B468**, 40 (1999), astro-ph/9905040.

[111] M. Yashar, B. Bozek, A. Abrahamse, A. J. Albrecht, and M. Barnard, Phys. Rev. **D79**, 103004 (2009), 0811.2253.

[112] T. Chiba, Phys. Rev. **D81**, 023515 (2010), 0909.4365.

[113] J. Narlikar, *An Introduction to Cosmology* (Cambridge, 2008).

[114] S. Weinberg, *Gravitation and COsmology* (John Wiley, 1972).

[115] J. Bernstein, *An Introduction to Cosmology* (Prentice Hall, 1998).

[116] A. Liddle, *An Introduction to Modern Cosmology* (John Wiley and Sons, 2004).

[117] J. Peebles, *Principles of Physical Cosmology* (Princeton University, 1993).

List of Figures

1 Hubble's Law 9
2 History of our Universe from Particle Data Group 2000 12
3 Age of the Universe vs Equation of State w 17
4 Luminosity Distance vs Redshift. The luminosity distance d_L (in units of $1/H_0$) is shown as a function of cosmological redshift z for flat cosmological models with a cosmological constant. 19
5 $\Delta\theta$ *vs* z for different values of Ω_m 21
6 Pie Chart of the Universe Constituents 23
7 Density vs Redshift for an Inverse Power Law potential 37
8 Background Density for an Exponential potential 38
9 Confidence level contours of 68.3%, 95.4% and 99.7% in the $\Omega_\Lambda - \Omega_m$ plane from the Cosmic Microwave Background, Baryonic Acoustic Oscillations and the Union SNe Ia set, as well as their combination (assuming $w = -1$). Courtesy of Kowalski *et al.* [15]. 42
10 The likelihood of Ω_m for different combined data sets of various models. The specks indicate the SNe Union data likelihood. 50
11 Temperature angular power spectrum corresponding to the best-fit ΛCDM model 51
12 Total likelihood for Ω_m for different models using the Gold Sample 59
13 TotalLikelihood of Ω_m 59
14 Ω_m vs w and $\Omega_m$vs $Optdlss$ 60
15 Likelihood for Ω_m 61
16 Likelihood shown for Ω_m for the Riess data set and $\Omega_m$vs w 61
17 The Likelihood shown for the Optical depth using only Reiss data . 62
18 Likelihood for w_0 for combined data sets as well as only for Reiss data 63
19 Ω_m *vs* w_0 63
20 Ω_m *vs* $TotalLikelihood$ for different models using the Astier Data set for the SNe 64
21 Likelihood of Ω_m using the Astier data 65
22 Likelihoods for Ω_m for the combined data sets of CMB+SDSS+BAO+SNe and also for the SNe data set of Astier *et al.* or SNLS 66
23 $\Omega_m$vs w for the combined data sets. 66
24 Likelihoods of Ω_m for Astier data and the combined data sets . . . 67
25 Likelihood region of $\alpha$for an Inverse Power Law potential at the 2σ level 67

26 TotalLogLikelihood for Ω_m and w 68
27 $\Omega_m$vs w 68
28 TotalLIkelihood for Ω_m for different models taking the Union Data set into account but calculated without systematics 69
29 ΛCDM 70
30 Age of the Universe given in years. 71
31 Likelihoods for w_0 72
32 Likelihood for Ω_m 72
33 Likelihoods for Ω_m for combined data sets as well as for Union data set alone without systematics 73
34 Ω_m vs w for an IPL model using the Union SNe data set 73
35 Likelihoods for Ω_m 74
36 Likelihoods for w_o 74
37 Ω_m likelihoods for different models now including systematic errors 75
38 Likelihood for Ω_m 76
39 Age of the universe vs Ω_m and optical depth vs Ω_m 77
40 Likelihood for w 77
41 $\Omega_m - w$ plane 78
42 Ω_m vs α 78
43 $\Omega_m h^2$ vs $\Omega_b h^2$ 79
44 Likelihoods for w_0 79
45 Ω_m vs ac and Ω_m vs Totallikelihood 80

List of Tables

1 Candidates for Dark Energy 33
2 Some current and upcoming SNe surveys [39, 32, 40, 41, 42] 39
3 Current estimates on the systematic errors of $\langle w \rangle$ as measured by the major groups doing work in SNe Physics (courtesy [41]) 45
4 Parameters describing our Universe. WMAP recommended parameter values [65] from WMAP5, BAO and SNe for a ΛCDM cosmology 46
5 Other Parameters for Non-concordance models 47
6 Detailed results for the different models 81

Acknowledgment

I would like to thank first and foremost Christof Wetterich for supervising me through these years of my doctoral studies and giving his invaluable comments. I would also like to give my special thanks to Michael Doran without whom I would not have been here in the first place. Thank you for selecting me for the project.

Other than that I would like to thank all the members of the cosmology group especially David Mota who has helped me through and through with useful discussions and input and his faith in me. I would also like to thank Luca Amendola for refereeing this thesis.

I would also like to thank Rainer Ebert, Mahfuza Afroz, Mahmuda Afroz and Ashikur Rahman for proof-reading my thesis and for their advice and tremendous support.

Last but not least I would like thank you Georg Robbers for all the help he provided with the computational part of the thesis. Without it the thesis would be almost empty. He was very patient in explaining the complex CMBEASY code in a very simplified manner.